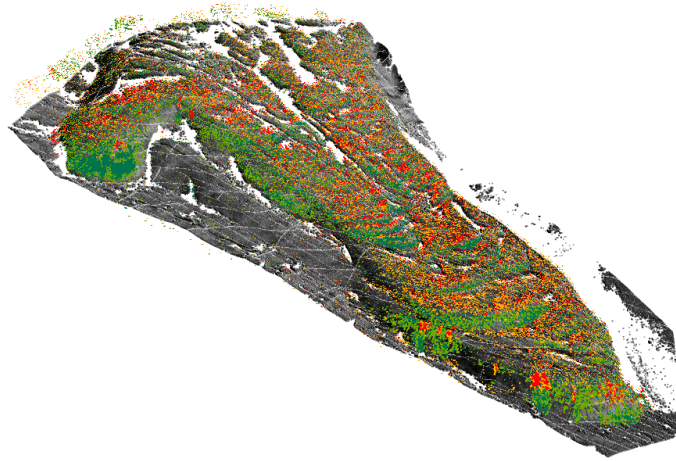


Application and Analysis of Terrestrial Laser Scanning in a Periglacial High Mountain Area

On the example of Rock Glacier Muragl, Upper Engadin, Switzerland

GEO 511 – Master Thesis



September 30, 2014

submitted by

Luca Heim

08-709-875

Supervised by

Dr. Isabelle Gärtner-Roer¹

Prof. Dr. Ross Purves¹

Johann Müller¹

Faculty member

Prof. Dr. Andreas Vieli

Glaciology and Geomorphodynamics Group – 3G
Department of Geography, University of Zurich, Switzerland

¹Department of Geography, University of Zurich, Switzerland

Preface

The main reasons why I started studying geography were my passion for mountainous regions and my interest in climate science. This interest grew in schooldays, but was strengthened during a language stay in Tasmania, Australia. During my studies, the fields of glaciology and geomorphology became my favorite topics. Beside this, I studied environmental sciences as my minor, including lectures about climate science during my bachelor's. My focus during the master's was on courses concerning geomorphodynamics, glaciology, as well as natural hazards. In addition, the field of GIScience attracted my attention during my studies as the wide range of possibilities to model and represent environmental features fascinates me. Over time it became clear that the combination of physical work, such as outdoor measurements, and GIS-related tasks, such as modeling mass movement events, comprises my most important interests. Therefore, the Master Thesis tendered by Dr. Isabelle Gärtner-Roer about the application of terrestrial laser scanning to rock glacier Muragl represented the perfect combination of my visions.

At this point I want to thank my supervisors Dr. Isabelle Gärtner-Roer and Prof. Dr. Ross Purves for the great support during my Master Thesis. Beside helpful inputs and fruitful discussions about the approach, the entire technical instruments and software needed were placed at the disposal. Furthermore, I want to thank Johann Müller for helpful assistance with technical difficulties, and for support concerning the measurement campaigns.

Hereby, I also want to thank my fellow students Daniel Kükenbrink and Christoph Rohner, who supported me by helping with difficulties in ArcGIS and Matlab as well as reading through my thesis.

Finally, a special thank-you goes to my parents who always supported me and enabled my studies in geography.

The image on the front page shows the result of annual vertical surface changes, calculated in this master's thesis, with an underlying representation of a three-dimensional point cloud.

Summary

In order to monitor variations in mass transportation in high mountain regions for geomorphologically significant forms such as rock glaciers and deep-seated slope failures, periodic measurements of the land surface form can be applied. Remote sensing techniques have become essential tools if we want to better understand variation in mass transport, and the link to process, in high mountain areas (Kääb, 2002). In addition to classical methods, such as photogrammetry, the technique of laser scanning, both airborne and terrestrial, is an established method for the purpose of geomorphological assessments (Armesto et al., 2009). This paper examines the application of terrestrial laser scanning (TLS) in a high mountain environment on the research object of rock glacier Muragl, situated in the Upper Engadin, Switzerland. The processing procedure includes the co-registration of TLS point clouds, the processing of Digital Elevation Models (DEM) with cell sizes of 1m, 0.5m, and 0.2m, the development of greyscaled Tiffs, and finally, the determination of horizontal and vertical displacement rates by application of the image correlation software CIAS (Kääb & Vollmer, 2000) and ArcGIS. The CIAS software is based on the identification of corresponding greyscale pixel values by application of a double cross-correlation function (Kääb, 2002). Based on repeated orthophotos, this method has already been applied for the Muragl rock glacier in 2000 (Kääb & Vollmer, 2000) and is now adapted with TLS data for the first time. The current study focuses on an evaluation of the resulting changes in length and height by consulting additional literature and data. Furthermore, the suitability of the TLS technique concerning the high mountain environment as well as the present procedure are assessed. The observed time span covers one year and includes four snapshots of the rock glacier's surface. Hence, the displacements are determined for three individual periods, indicating monthly (July 13 to August 13), seasonal (July 13 to October 13), and annual variations (July 13 to July 14). Distinct velocity patterns as well as vertical changes are quantified and presented with respect to permafrost-related mass movement processes.

Overall, the TLS technique can be regarded as a feasible method for the purpose of investigating or monitoring high mountain environments. Exemplarily, measured displacements of 0.5m within the area of the lower part are found to be reasonable when compared to reference data. However, specific characteristics, such as the horizontal measurement perspective or the requirement of snow-free surfaces have to be considered, as they entail the occurrence of data voids. With respect to standard deviations of around 10cm due to the co-registration process, displacements within the range of 0 and 0.1m have to be especially critically assessed.

Contents

Preface	I
Summary	III
List of Figures	IX
List of Tables	XI
1 Introduction	1
1.1 Motivation	1
1.2 Aims of the thesis	2
1.3 Structure of the thesis	2
2 Background	3
2.1 Rock glaciers	3
2.1.1 History of rock glacier research	3
2.1.2 Definition	4
2.1.3 Rock glacier classification	4
2.1.4 Rock glacier characteristics	6
2.2 Terrestrial laser scanning	9
2.3 State of knowledge	12
3 Research Questions	15
3.1 Conceptual approach	15
3.2 Suitability of data processing	15
3.3 Analysis of results	16
3.4 Suitability and limitations of TLS approach	17
4 Conceptual Approach	19
4.1 Environmental representation	19
4.1.1 GIScience	19
4.1.2 Environmental models	19
4.1.3 Object-oriented representation	21
4.2 Human cognition	23
4.3 TLS data background	26
4.3.1 Point	26

4.3.2	Point cloud	28
4.3.3	Cognition of geomorphological features	29
5	Study Site	33
5.1	Val Muragl	33
5.2	Rock glacier Muragl	35
6	Methods and Data	41
6.1	Laser scanning	41
6.2	Terrestrial laser scanning	41
6.2.1	Functionality	42
6.2.2	Accuracy and precision	44
6.2.3	Calibration and registration	45
6.2.4	Advantages and disadvantages of TLS systems	48
6.3	Data acquisition	48
6.3.1	Riegl VZ-1000	48
6.3.2	Measurement campaigns	49
6.4	Data pre-processing	50
6.4.1	Visualization of raw data	51
6.4.2	Selection of scans	52
6.4.3	Co-registration	54
6.4.4	Georeferencing	56
6.4.5	Subset of region of interest	56
6.4.6	ArcGIS	57
6.5	Displacement measurements	61
6.5.1	CIAS Feature Tracking	61
6.5.2	Input files and outcomes	62
6.5.3	Sizes of reference block and test area	63
6.5.4	Visualization of results	64
7	Results	65
7.1	Horizontal displacements	65
7.1.1	Monthly time span (July 2013 - August 2013)	65
7.1.2	Seasonal time span (July 2013 - October 2013)	69
7.1.3	Annual time span (July 2013 - July 2014)	74
7.2	Vertical surface changes	83
7.2.1	Monthly time span (July 2013 - August 2013)	83

7.2.2	Seasonal time span (July 2013 - October 2013)	85
7.2.3	Annual time span (July 2013 - July 2014)	86
7.3	Additional data	87
8	Discussion	91
8.1	Horizontal displacements	91
8.1.1	Monthly time span (July 2013 - August 2013)	91
8.1.2	Seasonal time span (July 2013 - October 2013)	93
8.1.3	Annual time span (July 2013 - July 2014)	95
8.2	Vertical displacements	99
8.2.1	Synthesis	101
9	Conclusion	105
9.1	Outlook	108
	Bibliography	109
	Appendix	121
A.1	The total of all acquired scans	121
A.2	MATLAB scripts	127
A.3	Detailed process of CIAS Feature Tracking	129

List of Figures

2.1	Two forms of rock glaciers classified by their location	5
2.2	Individual development stages of rock glaciers	7
2.3	Schematic rock glacier distribution according to the cryosphere scheme	9
2.4	Specific measurement perspectives of TLS and ALS	11
2.5	Locations of measurement points of the terrestrial geodetic network	14
3.1	Work flow with respect to the second research question	16
3.2	Work flow with respect to the third research question	17
3.3	Flow diagram representing the entire work flow	18
4.1	Vector model and raster model approaches	21
4.2	Sequence of a single measurement point, a point cloud, and a point cloud by enlarging the image section	27
4.3	A cartographic representation of Piz Muragl	30
5.1	Region of Val Muragl, Upper Engadin, Switzerland and location of rock glacier Muragl	34
5.2	Photograph of rock glacier Muragl	35
5.3	Specific borehole locations on rock glacier Muragl	36
5.4	Temperature profiles versus depth for all borholes at rock glacier Muragl	37
5.5	Measured flow velocities on rock glacier Muragl	38
6.1	TLS device with time-of-flight method	42
6.2	Scheme of TLS functionality concerning signal echoes	43
6.3	Coordinate systems incorporated in TLS instrumentation	47
6.4	Specific TLS device Riegl VZ-1000	49
6.5	Overview of measurement campaigns 2013 and 2014	50
6.6	Work flow using the software RiSCAN Pro	51
6.7	Visualization of a point cloud in RiSCAN Pro software	52
6.8	Specific locations of the target points	53
6.9	Working flow with respect to the ArcGIS software	58
6.10	Result of <i>Hillshade</i> function by using ArcGIS software	60
6.11	Principal approach of CIAS Feature Tracking with reference block and test area	62
7.1	Monthly horizontal displacements covering the entire rock glacier	66
7.2	Monthly horizontal displacements within the lower part of the rock glacier	67
7.3	Monthly horizontal displacements within the area of the rock glacier front	68
7.4	Seasonal horizontal displacements covering the entire rock glacier	70

7.5	Seasonal horizontal displacements covering the entire rock glacier, shown by arrows with specific coloring	71
7.6	Seasonal horizontal displacements within the lower part of the rock glacier . . .	73
7.7	Seasonal horizontal displacements within the area of the rock glacier front . . .	74
7.8	Annual horizontal displacements covering the entire rock glacier	76
7.9	Annual horizontal displacements covering the entire rock glacier, shown by arrows with specific coloring	77
7.10	Annual horizontal displacements within the lower part of the rock glacier	79
7.11	Annual horizontal displacements within the middle section of the rock glacier without the usage of low pass filter	80
7.12	Annual horizontal displacements within the middle section of the rock glacier by usage of low pass filter	81
7.13	Annual horizontal displacements within the area of the rock glacier front	82
7.14	Monthly vertical surface changes calculated on the basis of DEMs with cell sizes of 0.5m	84
7.15	Seasonal vertical surface changes calculated on the basis of DEMs with cell sizes of 0.5m	85
7.16	Annual vertical surface changes calculated on the basis of DEMs with cell sizes 0.5m	86
7.17	Annual horizontal displacements measured by reference points	88
7.18	Annual vertical surface changes measured by reference points	89
8.1	Combination of horizontal displacements and vertical surface changes	102

List of Tables

6.1	Specifications of laser scanner device Riegl VZ-1000	49
6.2	Scan characteristics of the selected scans acquired at the individual measurement campaigns	54
6.3	Specific standard deviations caused by procedure of co-registration including and excluding 4 July 2013.	55
6.4	Specific standard deviations caused by procedure of co-registration including the three observed time periods.	56
6.5	The total of exported txt-files from RiSCAN Pro	57
6.6	Input files for CIAS Feature Tracking software	63
7.1	Specific parameters concerning the results of horizontal displacements for the monthly period and all included figures.	65
7.2	Specific parameters concerning the results of horizontal displacements for the seasonal period and all included figures.	69
7.3	Specific parameters concerning the results of horizontal displacements for the annual period and all included figures.	75
7.4	Statistical values of the measurements concerning vertical surface changes for the several time periods.	83

1 Introduction

1.1 Motivation

In recent times, an increased number of heavy precipitation events as well as higher air temperatures have been observed in many regions of the world (Intergovernmental Panel on Climate Change [IPCC], 2007). In order to generate knowledge about influencing factors and climatic variabilities, an abundance of research has been carried out and a number of conferences have been held during the past decades (Betsill & Bulkeley, 2007). Due to their considerable climate sensitivity, high mountain environments are regarded as crucial factors in assessing the impacts on the cryosphere (Roer et al., 2008). Within these areas, rock glaciers, ice-cored moraines, or protalus ramparts represent prominent permafrost features (Maurer & Hauck, 2007). As they are strongly affected by the present climate change, the geomorphodynamic equilibriums are modified and variations in mass movement processes are forced to occur (Maurer & Hauck, 2007). As the ice contained is a crucial parameter regarding the internal stability, the ice loss due to the warming trend considerably increases the risk of natural hazards in many inhabited mountain regions (Musil et al., 2006). In order to quantify and monitor permafrost zones, rock glaciers are of particular interest, as they enable researchers to determine the lower permafrost boundary (Roer, 2005). Furthermore, these features are, due to their age of up to 10 thousand years and their strong climate dependency, considered to be evident indicators for past and present permafrost conditions (Kääb et al., 2007). Accordingly, the growing interest in rock glaciers is reflected by numerous studies which have been carried out aiming to observe and understand the related processes as well as the specific quantification of creeping rates (Roer et al., 2008).

Concerning measurement techniques, qualitative field inspections or the usage of aerial or terrestrial photographs are feasible methods (Roer et al., 2008). In addition to this, geophysical methods, such as seismic and ground-penetrating radar, are suitable for examining the internal structure (Maurer & Hauck, 2007; Musil et al., 2006), whereas horizontal velocities can be detected and quantified by means of digital orthophotos and differential GPS (Roer et al., 2008). With respect to the remoteness of features within the high mountain belt, remote sensing and photogrammetry have become essential tools, especially regarding geometric terrain information, terrain cover, and three-dimensional data (Kääb, 2002). Concerning the acquisition of digital elevation models, InSAR (airborne interferometric synthetic aperture radar) and LiDAR (airborne laser scanning) are feasible methods (Kääb et al., 2005). As a rather recent technique, terrestrial laser scanning enables the acquisition of highly accurate data without requiring direct access to the object of interest (Kääb et al., 2005). As TLS offers crucial benefits

such as the horizontal measurement perspective, the high acquisition rate, and the compactness of the measurement device, it has been increasingly applied in high mountain areas (e.g. Abellán et al., 2014; Armesto et al., 2009; Kenner et al., 2011) and for land deformation assessments (e.g. Monserrat & Crosetto, 2008; Bitelli et al., 2004; Prokop & Panholzer, 2009). Regarding the specific case of rock glacier monitoring and the quantification of movement rates, TLS has, however, rarely been used up to now (e.g. Bauer et al., 2003, 2005; Kenner et al., 2014). Measuring displacements by applying the technique of CIAS feature tracking was successfully applied to rock glacier Muragl in the year 2000, yet on the basis of digital orthophotos (Kääb & Vollmer, 2000).

1.2 Aims of the thesis

By using the TLS technique on rock glacier Muragl, four snapshot data sets are acquired, which are subsequently proceeded to DEMs. On their basis and by applying the CIAS software (Kääb & Vollmer, 2000) and ArcGIS, specific horizontal and vertical displacement rates are measured and analyzed. As that particular processing has not yet been conducted for a rock glacier surface, the main focus is on the suitability of the approach. This implies the processing from the raw data to the specific DEMs as input files for the feature tracking process as well as the reasonability assessment of the resulting displacements. Here, the abundance of data from various origins for rock glacier Muragl is considered a crucial benefit. Furthermore, this thesis aims to examine the TLS application in the particular case of a rock glacier surface, taking into account advantages and drawbacks as well as the related limitations.

1.3 Structure of the thesis

Subsequent to the introduction, a general background including rock glaciers, the technique of terrestrial laser scanning applied here, and the current state of knowledge about the object of interest is provided. In Chapter 3, the specific research questions are introduced and the entire work flow is illustrated. In the following, the raw point data is assessed with respect to a conceptual approach, and Chapter 5 provides more detailed insights in the local geography and the conditions of rock glacier Muragl. As the assessment of the applied TLS technique and the CIAS software (Kääb & Vollmer, 2000) makes up a substantial part of the thesis, in the subsequent chapter the methods and data are discussed in detail. The resulting displacements are described in the results, and an extensive assessment of its reasonability is provided in the discussion. Finally, the conclusion summarizes the most important findings, the initially defined research questions are assessed, and an outlook including future prospects is provided.

2 Background

In the following, the background of rock glaciers including their research history, their definition, their characteristics, and their appearance shall be discussed. Furthermore, the applied technique of terrestrial laser scanning is introduced, and the current state of knowledge is examined.

2.1 Rock glaciers

As seen before, permafrost and especially rock glaciers are considered as important parameters for climatic assessments today (French, 2007). However, alpine permafrost was not accepted as an ordinary feature within periglacial regions for a long time (Barsch, 1992). Today, a well-accepted definition of permafrost, approved by the international permafrost association (IPA), holds that “the ground has to remain at or below 0° C for at least two consecutive years” (Dobinski, 2011, p. 159). In order to examine the role of rock glaciers within that particular area, a brief history of research follows.

2.1.1 History of rock glacier research

A few descriptions of rock glacier features were published in the first decades of the 20th century (Roer, 2005), yet the peculiar landform was recognized by scientists even earlier (Barsch, 1996). According to Humlum (1982), the first written report of what we call a rock glacier today was probably created more than 130 years ago by Danish geologist Steenstrup in 1883, when he described the observed rock glacier features as *dead glaciers* (Barsch, 1996). Then, around the turn of the millennium, various descriptions of rock glacier features such as *a peculiar form of talus* (Spencer, 1900) (in: Barsch, 1996), or *movement of talus slopes* (Rohn, 1900) (in: Barsch, 1996) were published, even though these terms did not prevail in the literature (Barsch, 1996). Referred to by Pillewizer (1957) the term rock glacier was introduced several years later for the Rocky Mountains (Howe, 1909) (in: Pillewizer, 1957) and for permafrost features in Alaska (Capps, 1910) (in: Pillewizer, 1957). However, in Europe, the features of rock glaciers came to attention only some years later. According to Eugster (1973), the first scientist who mentioned the phenomenon was Emil Chaix in 1917, when he took into account the unknown features in the Swiss National Park. Finally, the German term “Blockgletscher” was introduced in 1920 by de Martonne (Pillewizer, 1957). Although the term “rock glacier” gradually established itself (Barsch, 1996), some confusion remained due to the addition of *glacier*, generating the wrong impression of an emergence from a true glacier (Barsch, 1996).

It was Haeberli (1985) who clarified things and argued that rock glaciers are neither a product of glaciers nor of rocks, but a consequence of creeping mechanisms within permafrost. Alongside the broad variety of terms and definitions, since the 1990s the English term “rock glacier” and the German counterpart “Blockgletscher” have been well-accepted and commonly used (Barsch, 1996).

2.1.2 Definition

For a considerable time several uncertainties about the correct definition of permafrost features existed (e.g. Barsch, 1992; Roer, 2005). A currently well-accepted definition of rock glaciers, including the processes involved, their form, and their material, is delivered by French (2007, p. 129):

“A rock glacier is a lobate or tongue-shaped body of frozen debris, with interstitial ice and ice lenses, which moves down-slope or down-valley by deformation of the ice contained within it.”

However, the actual origin of rock glaciers has been subject to debates for several years (Barsch, 1996). While numerous authors (e.g. Potter, 1972; Johnson, 1974) supposed a glacial origin, the majority of researchers argued that rock glaciers are features primarily influenced by periglacial and permafrost-related processes (e.g. Barsch, 1992; Haeberli, 2000). More recent literature states that most rock glaciers are of periglacial origin and a result of permafrost creep on relatively steep slopes by deformation of ice-rich debris under relatively warm conditions (e.g. French, 2007; Roer, 2005). Beside thermal conditions, which play a substantial role in the lasting development and existence of rock glaciers (Berthling, 2011), the kinematics also considerably influence their behaviour (Kääb et al., 2007).

2.1.3 Rock glacier classification

Classification by location

The literature principally distinguishes two different forms of rock glaciers: tongue-shaped and lobate rock glaciers (Barsch, 1992). Although the flow type is the same for both forms, they differ greatly in terms of the integrated material (Barsch, 1992). As tongue-shaped rock glaciers are rather long and distinct phenomena, they are often regarded as the typical form (Barsch, 1996). Usually they are situated below the end moraine of a glacier and, hence, transport mainly morainic or glacial debris, which leads to the nomenclature of debris rock glaciers (French, 2007). Lobate rock glaciers, on the other hand, typically develop below talus slopes

(Barsch, 1996). In accordance with the transported material, which incorporates primarily frost-shattered rock particles, they are named talus rock glaciers (French, 2007). Figure 2.1 illustrates both forms. Picture A represents a talus rock glacier developing beneath an ice-rich detritus slope, which is responsible for the debris creeping and deformation process. In contrast, the development below a glacier, consisting partly of glacier ice overrun by ablation till, shows the debris rock glacier (picture B) (French, 2007).

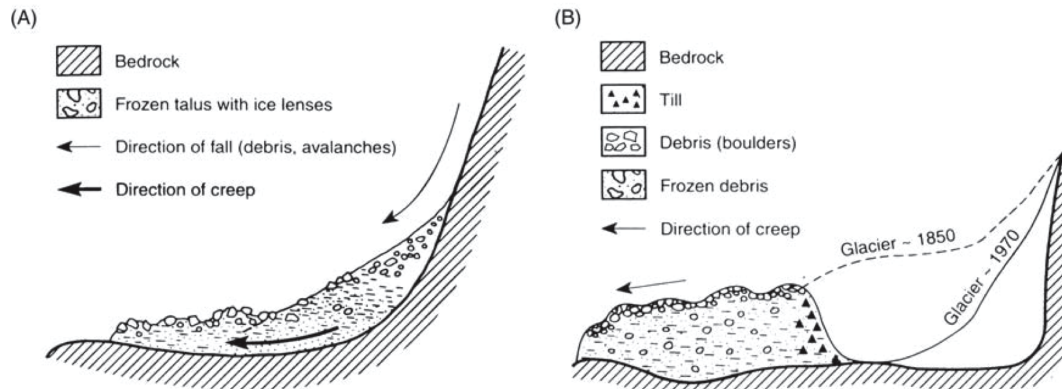


Figure 2.1: The two forms of rock glaciers, classified by their location: (A) Talus rock glacier, (B) Debris rock glacier; based on French (2007).

Classification by degree of activity

In addition to the aforementioned classification, rock glaciers may also be divided by their degree of activity (Kääb, 2013b). Barsch (1996) defined *active*, *inactive*, and *relict* types. Active rock glaciers are basically the aforementioned form, exhibiting the downward creeping due to permafrost deformation (Ikeda & Matsuoka, 2002). They consist of an ice-rich frozen debris core, the ground temperatures remain negative perennially, and the moving rates range from centimetres to metres per year (Kääb, 2013b). Furthermore, active types possess the typical steep front, where the debris is vertically sorted by grain size due to the constant debris fall driven by gravity (Kääb, 2013b). By reasons of the continuous displacements and movements of certain boulders, surfaces of active rock glaciers are nearly free of vegetation (Kääb, 2013b). Only a few highly specialized plant species and lichens are able to develop within border areas, where fine-grained soil material enables a creation of a specific micro-climate (Burga et al., 2004). In contrast, inactive rock glaciers do not possess a coherent ice core (Kääb, 2013b). Due to the absence of stress transfer, they do not reveal continuous horizontal displacement rates (Kääb, 2013b). Concerning the extent of the permafrost body and the active layer, inactive rock glaciers have a thicker active layer and a thinner permafrost body compared to active types (Kääb, 2013b). Furthermore, their stagnancy allows for more vegetation to develop,

which leads to a higher quantity of lichens (Kääb, 2013b) as well as some typical pioneer plants and several shrubs (Burga et al., 2004). Finally, relict rock glaciers do not contain ice or permafrost, nor are they subject to movement processes (Ikeda & Matsuoka, 2002). As relict rock glaciers imply a more or less stable environment, on their surface a dense vegetation with alpine grassland or subalpine shrubs can be established (Kääb, 2013b; Burga et al., 2004). Due to the strong temperature dependency, active rock glaciers imply the uppermost altitude, whereas relict types form the lowermost zone of rock glacier occurrence (Strozzi et al., 2004). However, despite the distinctive characteristics, it has to be mentioned that this classification remains a theoretical idea (Kääb, 2013b).

2.1.4 Rock glacier characteristics

Stages of development

In order to examine the specific composition of rock glaciers, the several development stages are discussed. Figure 2.2 represents the sequence from a perennially frozen talus to a protalus rampart and subsequently to a rock glacier (Kääb, 2013b). Scene 1 illustrates the typical grain-size sorting with finer material in the upper part and coarse-grained rocks in the lower part of the scree. While the higher sections become ice-supersaturated, the lower parts, which contain coarser material, are not affected by supersaturation. Consequently, the deformation rates occurring above are higher than those at the base. As debris from the headwall mainly accumulates onto the surface of the developed protalus rampart (scene 2), the material is being transported downward by creeping of the frozen body (scene 3). As a result, the blocks fall from the surface of the rock glacier front, get overridden by the moving body, and are attached to it as its subjacent basal layer. Finally, blocks falling from the body at the front are no longer overridden, but evacuated (scene 4) (Kääb, 2013b).

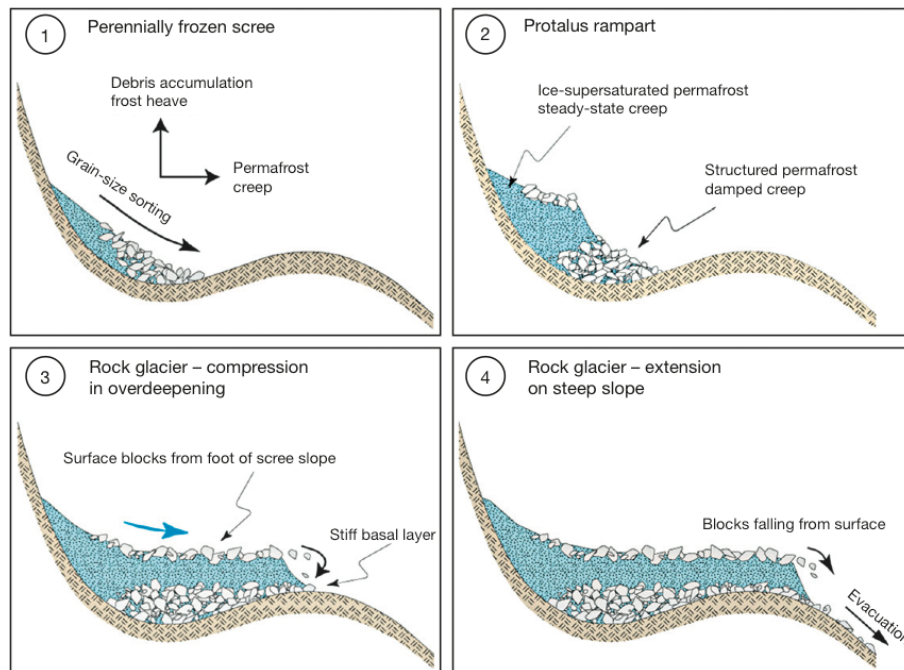


Figure 2.2: Individual development stages of rock glaciers; (Kääb, 2013b).

Rock glacier thickness

With respect to measuring rock glacier thickness, several challenges occur (Barsch, 1996). As direct observations of the actual vertical extent are typically not possible, researchers are forced to estimate or derive values (Barsch, 1996). However, by means of direct (e.g. coring) or indirect (e.g. geophysical soundings) measurement methods, it has been shown that typical values are around 50 metres, though potentially they range from 20 to 100 metres (Roer, 2005). A further challenge when estimating rock glacier thickness lies in the differentiation between the extent of the active rock glacier and that of mountain permafrost (Barsch, 1996). Here, it has to be taken into account that the specific contribution of the subjacent permafrost to the creeping of the body cannot be determined reliably (Barsch, 1996).

Deformation rates

Movement rates can vary on seasonal to millennial time scales (Kääb et al., 2007). On the temporal scale of millennia, fundamental rock glacier developments including their origin or the transition into a relict rock glacier are implied (Frauenfelder & Kääb, 2000). Regarding centuries or decades, variations are related to general boundary conditions (Kääb et al., 2007). These can be caused by changes in the supply of ice or material, variations in the thermal regime, or modifications of the terrain topography (Frauenfelder et al., 2005). Speed variations

at the perennial time scale are mainly associated with modifications in weather or climate conditions (Kääb et al., 2007). However, Roer et al. (2005) stated that rock glaciers' reaction to temperature changes is a highly complex matter and, hence, cannot be derived from basic correlations. Finally, the behaviour of climate-related changes on shorter temporal scales reveals strong dependencies on the specific internal rock glacier conditions (Kääb et al., 2007). In general, the movement rates on rock glacier surfaces range from a few millimetres to up to several metres per year (Kääb, 2013b).

Distribution

Concerning the rock glacier distribution, literature states that these features basically appear in most of the cold mountain areas of the earth (e.g. Kääb, 2013b; French, 2007). More specifically, the fundamental requirements for their existence are permafrost conditions and a sufficient supply of debris (French, 2007). According to Haeberli (1985), rock glaciers occur in cold and dry mountain areas, but not in flat lowlands nor in mountains that receive high precipitation. The potential rock glacier distribution is represented in Figure 2.3. As the equilibrium line of glaciers forms the upper limit of debris availability, zone A indicates the accumulation area of glaciers and, hence, the lack of a basic requirement for rock glacier formation (Haeberli, 1985). Zone B represents areas without continuous permafrost, which means that debris is not perennially frozen; thus, only zone C complies with the established demands (Haeberli, 1985).

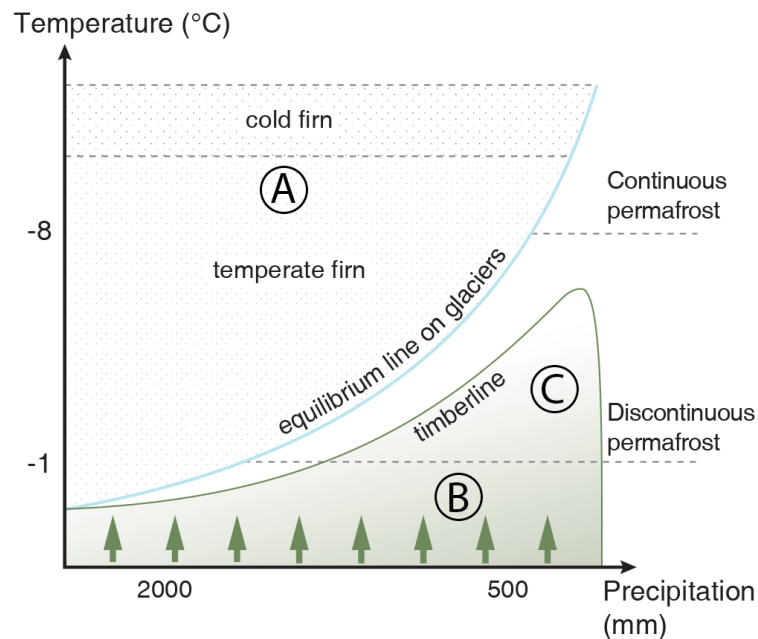


Figure 2.3: Schematic rock glacier distribution according to the cryosphere scheme; based on Haeberli & Burn (2002).

Because mountain regions often exhibit transitional climates, strict classifications of climate zones are difficult to achieve (Haeberli, 1985). Consequently, rock glaciers and glaciers can coexist or even interact with each other in certain cases (Haeberli, 1985).

2.2 Terrestrial laser scanning

In order to introduce the technique of terrestrial laser scanning, remote sensing methods in general will be briefly discussed in the following. Afterwards, the focus will be on TLS, including its functionality and several examples concerning the scope of its applications.

Remote sensing applications have become essential tools providing information about high mountain terrains (Kääb, 2002). Focussing on specific surface processes, the quality of the topographic data is a crucial factor (Tarolli et al., 2009). Due to significant improvements in measurement techniques, processing strategies, and sensor systems, the quality as well as the quantity of terrain information has been drastically increased over the past two decades (Tarolli et al., 2009).

For monitoring purposes, photogrammetry and geodetic surveys are considered to be classical methods (Avian et al., 2009). While photogrammetry delivers area-wide surface and height information (Kaufmann & Ladstädter, 2010), geodetic survey offers the advantage of lower

costs; however, it leads to lower densities of data points (Lambiel & Delaloye, 2004). Differential GPS (DGPS) provides high precision data as well, though it has the same drawback as the geodetic approach (Lambiel & Delaloye, 2004). In addition to the technique of space-borne differential synthetic aperture radar (DinSAR) interferometry, which provides highly accurate measurements (Kenyi & Kaufmann, 2003), light detection and ranging (LiDAR) has become a feasible technique (Bauer et al., 2003). Although the LiDAR technique originated in the 1970s, in the beginning it was applied especially to airborne applications, and only after 1990 was the technique integrated in geodetic instruments as well (Pfeifer & Briese, 2007). In the meantime, laser scanning, both airborne and terrestrial, has become a major technique used for fast data acquisition with high-quality demands (Ingensand, 2006).

Functionality

The fundamental principle of Laser scanning consists of capturing and recording primarily geometrical information about visible surfaces by emitting and detecting laser pulses (Vosselman & Maas, 2010). As a result, a quantitative digital 3D representation of the scanned surface including a specific measurement uncertainty is provided (Vosselman & Maas, 2010). TLS is principally based on the determination of the time delay between the moments a light signal is emitted by the source, reflected at the surface, and measured by a light detector (Bauer et al., 2005). Beside the light emitter, which delivers a bundle of laser pulses for each individual measurement unit, the main elements of a laser scanner are a receiver and a light detector system (Bauer et al., 2005). As a special feature, the horizontal measurement perspective has to be mentioned (Bauer et al., 2003). While the majority of the aerial-based methods rely on the principle of sensing the surface from almost vertical viewing angles, terrestrial laser scanners possess the principle of measuring horizontally (Bauer et al., 2003). In Figure 2.4, the resulting sampling planes are indicated by red lines and the letter A for ALS and B for TLS, respectively. The perspective is of great importance concerning the steep front and the flow lobes of rock glaciers (Bauer et al., 2003).

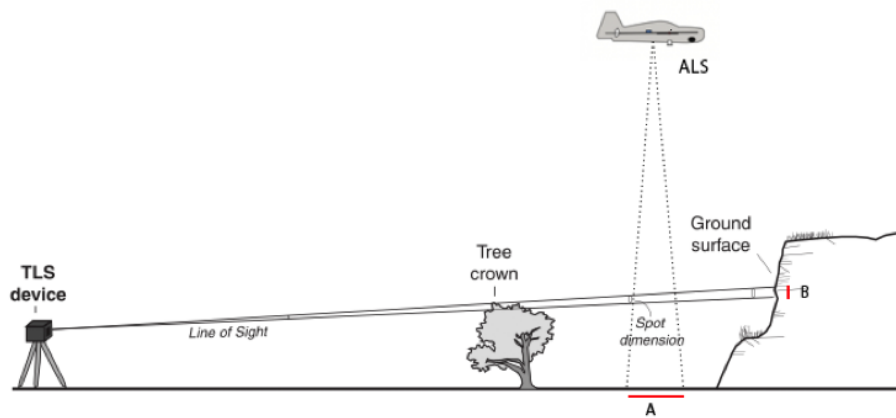


Figure 2.4: Specific measurement perspectives of TLS and ALS resulting in differing sampling planes A (ALS) and B (TLS); based on Abellán et al. (2014).

A more detailed description of the functionality is given in Chapter 7.

For the purpose of this thesis, the parameter information (i.e. X-, Y-, and Z-values) of the data points are in the centre of interest. The exact processing steps from the raw data to the input files for the displacement measurements is the subject of the methods and data chapter.

Areas of application

By reasons of the aforementioned measurement perspective and the considerably small point spacing of terrestrial laser scanning, the application areas differ from typical airborne laser scanning fields (Vosselman & Maas, 2010). While airborne-based projects focus mainly on height or area parameters, TLS enables the acquisition of very dense point clouds containing an abundance of geometric information (Vosselman & Maas, 2010). For this reason, modelling tasks in forestry are considered to be an important application area (e.g. Henning & Radtke, 2006; Watt & Donoghue, 2005). The structural composition of a forest section with detailed stem measurements is often the focus of such studies (Henning & Radtke, 2006).

Another growing field is the engineering domain (Vosselman & Maas, 2010). One reason for this is that traditional measurement techniques (e.g. leveling) are often limited by inaccessible terrain (Vosselman & Maas, 2010), which is insignificant for laser scanners, as they enable highly accurate measurements over large distances even of kilometres (Kenner et al., 2011). Regarding the lack of information between the single data points, however, challenges also exist (Vosselman & Maas, 2010). Exemplarily for the field of engineering, the study of Zogg & Ingensand (2008) shall be mentioned. By applying TLS and additional measurement techniques (i.e. leveling), the fatigue resistance of the Felsenau Viaduct of Highway 1, located

near Berne, was investigated. As an outcome, the results for vertical displacements from both methods, leveling and TLS, are in the same order of magnitude with mean residuals of less than 1.0mm (Zogg & Ingensand, 2008).

The third application field comprises investigating natural processes and phenomena at the earth's surface. In order to stick to the topic of this thesis, applications concerning geometry and stability tests of certain boulders (Armesto et al., 2009) or rock walls (Kenner et al., 2011) and a long-term rock glacier monitoring (Bauer et al., 2003) are mentioned. Here, the advantage that the observed features do not necessarily have to be accessible is highlighted (Armesto et al., 2009). Furthermore, Kenner et al. (2011), who observed destabilization processes on a recently deglaciated rock wall, concluded that TLS enables an important contribution to infrastructure planning and safety measures. A study aiming to examine land deformations with the main focus on individual processing steps, such as the actual data acquisition, the co-registration, and the assessment of the specific deformation parameters, was conducted by Monserrat & Crosetto (2008). Only recently, surface changes on rock glaciers and landslides were monitored by combining laser scanning (ALS and TLS) with digital airborne photogrammetry (Kenner et al., 2014). The study holds that the technique of laser scanning is a feasible method for surface monitoring and the precise detection of movement rates (Kenner et al., 2014).

2.3 State of knowledge

In the following, the focus will be on research carried out concerning the actual area of interest, rock glacier Muragl in the Upper Engadin, Switzerland.

Initially, it should be mentioned that, in 1996, rock glacier Muragl and the nearby Murtèl-Corvatsch were labelled the probably most investigated rock glaciers in the European Alps (Barsch, 1996). In order to obtain such a reputation, an extraordinary contribution has been yielded by Wilfried Haeberli, who laid the foundation for a modern Swiss permafrost research (Springman et al., 2012). He combined field observations (Haeberli, 1985) with measurement campaigns and interpretations (e.g. Haeberli & Hoelzle, 1995) and published numerous papers dealing with climate change and its consequences (e.g. Haeberli & Beniston, 1998; Roer et al., 2008).

For rock glacier Muragl, an abundance of differing data sets is available. Situated in the Val Muragl, it has been an object of interest for more than 60 years (Käab & Vollmer, 2000). Initially, investigations aiming at determining surface displacements were conducted by photogrammetrical and geodetic surveys (Barsch & Hell, 1975), and geomorphological mappings were done in the 1980s (Haeberli, 1993). The first high-precision aerial photography was taken

in 1981 and then subsequently recorded in nearly five-year intervals (Kääb & Vollmer, 2000). The bottom temperature of the winter snow cover (BTS) had already been measured in early years (Haerberli, 1993). By using long-term temperature loggers, which are installed in addition to the point measurements of the BTS, year-round near-surface temperatures enabled information about mean annual ground surface temperatures (MAGST) (Kneisel, 2010). Furthermore, geophysical methods have been applied to detect and characterize permafrost areas (Kneisel, 2010). In addition to the techniques of refraction seismic (Maurer & Hauck, 2007) and georadar (Musil, 2002), electrical resistivity tomography (ERT) has been used (Kneisel, 2010). For the purpose of investigating the stratigraphy and internal temperature conditions, four 70m reaching boreholes were drilled in 1999 (Vonder Mühl et al., 2003). In recent times, numerous studies aiming at determining horizontal movement rates have been conducted (e.g. Kääb & Kneisel, 2006; Debella-Gilo & Kääb, 2011). The Image Correlation Software CIAS applied here has thereby been used as well (e.g. Kääb & Vollmer, 2000; Debella-Gilo & Kääb, 2011).

As rock glacier Muragl constitutes a demonstration example of an active rock glacier (Frauenfelder & Roer, 2007), it is hardly surprising that the site is a valuable part of the Swiss Permafrost Monitoring Network (PERMOS). At present, the observation strategy of PERMOS is built on three observation elements: ground temperatures, changes in ice content, and velocities of permafrost creep (PERMOS, 2013). At rock glacier Muragl, which is classified as a temperature site, borehole measurements, aerial surveys, and terrestrial geodetic surveys are carried out. The specific locations of the measurement points included in the terrestrial geodetic network are represented in Figure 2.5. Air photos and related photogrammetric analysis enable investigations into the kinematics of rock glacier Muragl, making it a PERMOS kinematic site as well (PERMOS, 2013).

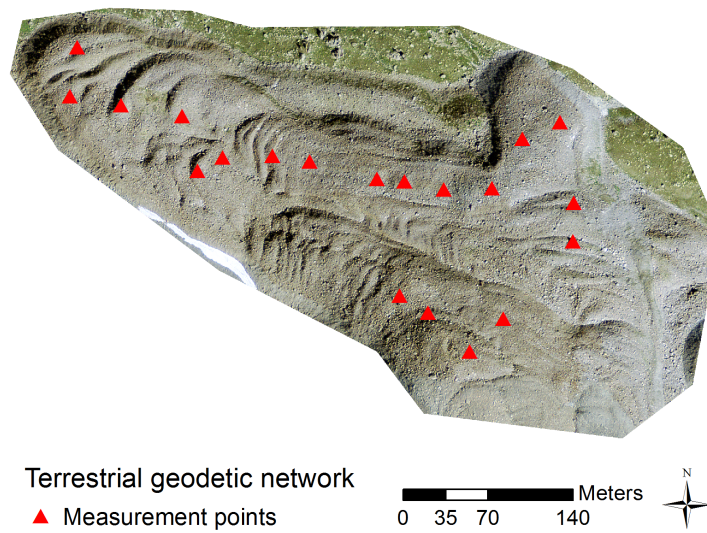


Figure 2.5: Locations of measurement points of the terrestrial geodetic network; underlying orthophoto derived from SwissImage, Swiss Federal Office of Topography (Swisstopo).

Given the number of studies and the abundance of data available, rock glacier Muragl represents an adequate site for this thesis. Concerning the application of TLS to provide georeferenced DEMs, obtaining accurate comparative data is essential for evaluation purposes. While this chapter focussed mainly on studies conducted so far, a detailed description of the study site is given in Chapter 5.

3 Research Questions

As seen before, TLS has been increasingly applied during the past decades. Nevertheless, some lack of information concerning applications in high mountain environments and especially for rock glaciers remains. Accordingly, the subsequent research questions are aimed at gaining specific knowledge.

3.1 Conceptual approach

The majority of the conducted research focussed mainly on the TLS technique itself or the results, yet rather little attention has been paid to the characteristics of the raw point data. Thus, the first research question focusses on the data background.

Based on a conceptual approach, what are the specific characteristics of an individual point, a group of points, or the entire point cloud obtained by terrestrial laser scanning?

3.2 Suitability of data processing

The second research question deals with the data processing. As Figure 3.1 indicates, the process chain includes individual operations using RiSCAN Pro and ArcGIS software. The focus here is on a suitability assessment of the TLS technique with respect to the several processing steps.

Regarding their suitability, how are the individual operations of the process chain evaluated, and is the generated Tiff-file an appropriate input for the subsequent deformation measurements?

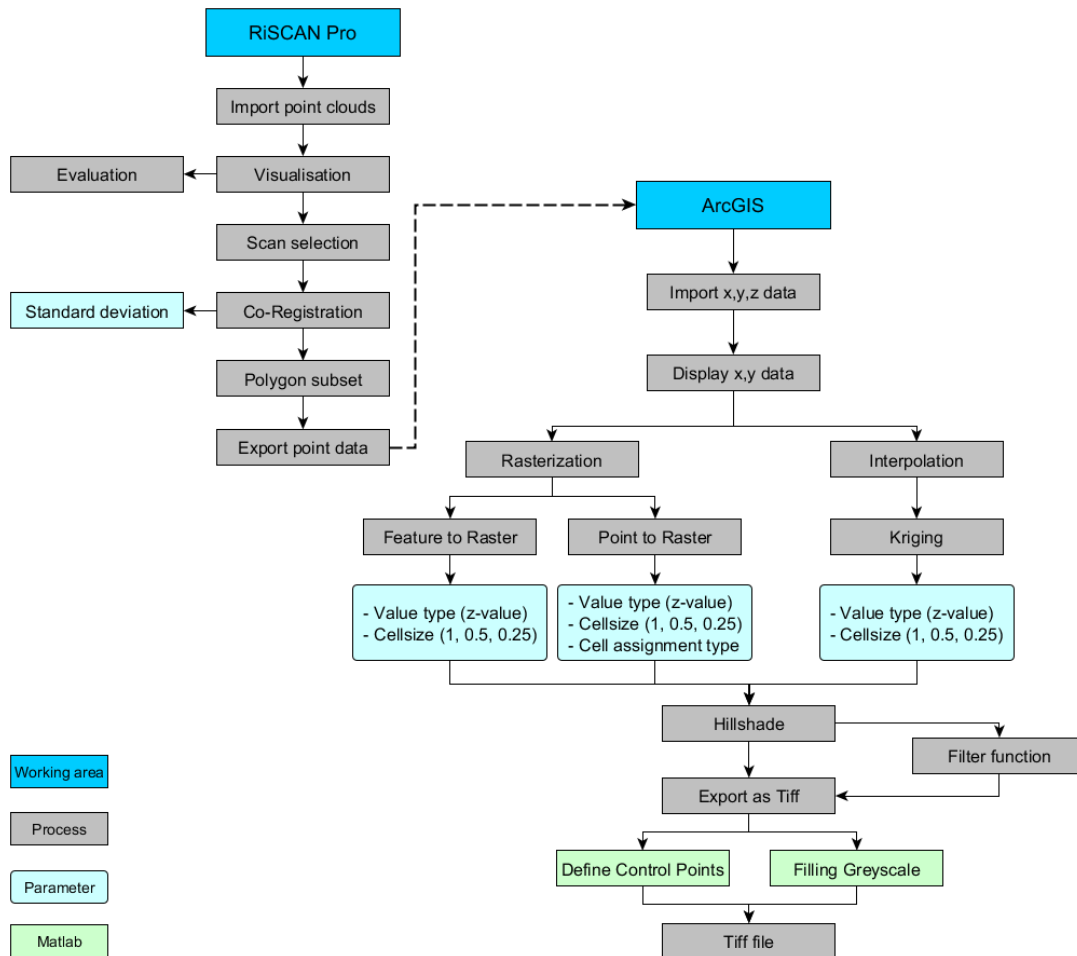


Figure 3.1: Flow diagram representing the work flow with respect to research question 2, own illustration.

3.3 Analysis of results

The subsequent research questions address the specific results of the rock glacier deformation, obtained by applying the image correlation software CIAS (Kääb & Vollmer, 2000) and ArcGIS. In order to evaluate the results, the displacements and the vertical surface changes are set in relation to findings in literature. In addition, results from terrestrial point measurements are consulted as reference data. The relevant process is represented in Figure 3.2.

On the basis of four TLS snapshot data sets within one year, what deformation patterns including horizontal displacements and vertical surface changes can be obtained?

Compared with additional data from alternative sources, how can the resulting displacements be interpreted in a geomorphological view, and are these explanations reliable?

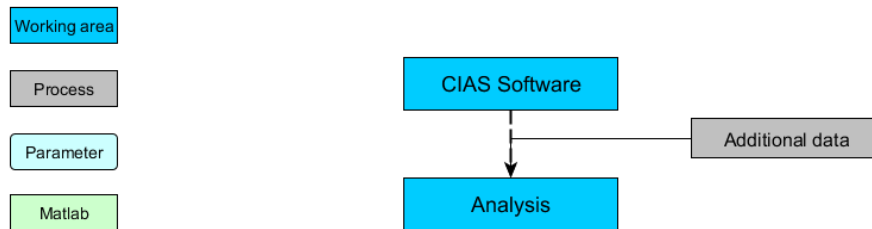


Figure 3.2: Flow diagram representing the work flow with respect to research question 3.

3.4 Suitability and limitations of TLS approach

On the basis of the previous findings, the suitability of the applied TLS approach is examined with regard to the specific case of a rock glacier surface.

With respect to the previous results, what are benefits, drawbacks and the main limitations of TLS applications concerning the specific case of a rock glacier surface in a periglacial high mountain environment?

In order to obtain an overview of the processing performed throughout this thesis, Figure 3.3 represents the entire work flow. The scheme comes along with the paper and is discussed in detail at the particular working areas.

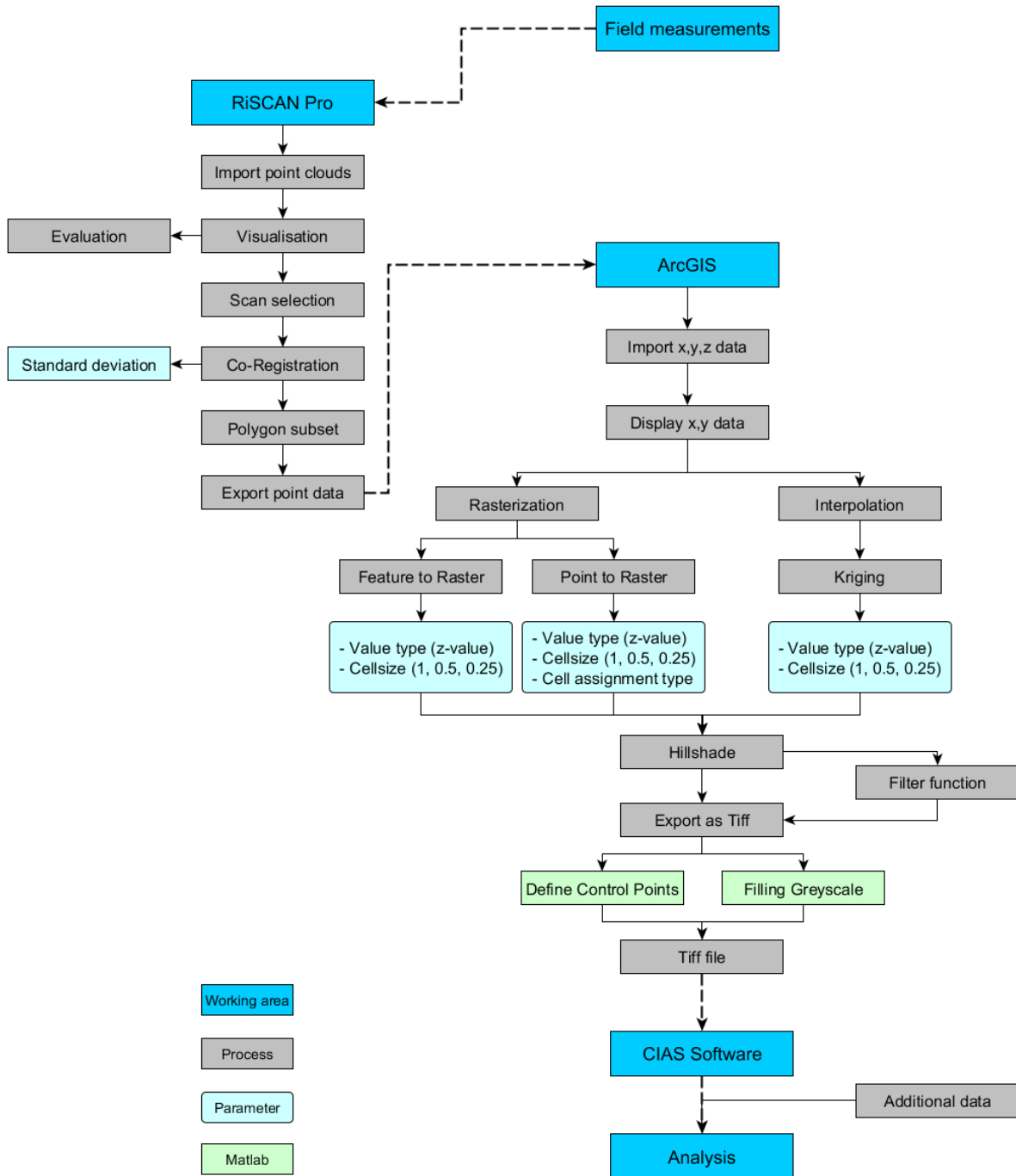


Figure 3.3: Flow diagram representing the entire work flow.

4 Conceptual Approach

In the following, fundamentals of Geographic Information Science (GIScience) and several types of representation shall be briefly discussed. In order to examine the first research question, the raw TLS data background is examined with respect to the designed theoretical approach.

4.1 Environmental representation

4.1.1 GIScience

According to Goodchild (2010), a geographic information is defined as an entity which exhibits some relationship to a location within geographic space, and which possibly entails a temporal component. Consequently, geographic information is considered to be a collection of such entities (Goodchild, 2010). A geographic information system (GIS) is a “computerized information system that contains geographic data representing various aspects of the real world categorized and described spatially” (Jones, 2012, p. 121). Concerning modern characteristics of spatial data, GIScience addresses the handling of considerable volumes of spatial data in order to analyze and represent them (Elwood, 2010). In recent times, the technical progress, resulting in increased availability of GIS applications, has expanded the user community almost to the entire public domain (Egenhofer, Max J and Glasgow, Janice and Gunther, Oliver and Herring, John R and Peuquet, Donna J, 1999). This has led to a request regarding the improvement of GIS tools in terms of user friendliness and towards a more intuitive way of problem solving (Egenhofer, Max J and Glasgow, Janice and Gunther, Oliver and Herring, John R and Peuquet, Donna J, 1999). Out of this research area has arisen a rather new subfield, concerning the interactions between human cognition of geographic phenomena and the implementation in computers, within GIScience (Montello, 2009).

In the upcoming subchapters, basic issues and individual approaches to spatial representations are discussed.

4.1.2 Environmental models

Geographical data modelling, geomorphological mapping, and the development of environmental models are merely a few of the current approaches within GIScience (e.g. Yuan, 2001; Bishop et al., 2012; Raper & Livingstone, 1995). Concerning a general standard for establishing environmental models, there is, despite the vast variety of research, still little consensus

within the scientific community (Goodchild et al., 2007). A key element of this debate is the question of which concepts of space and time are most suitable for which representation (Raper & Livingstone, 1995). Space and time are thereby both considered to be dimensions defined by the objects occupying them, which leads to the concept of *relative space* (Livingstone & Raper, 1994; Raper & Livingstone, 1995). Regarding this premise, one of the most evident illustrations is found in a note Einstein published in 1952 (in Raper & Livingstone, 1995, p. 363): “Physical objects are not in space, but these objects are spatially extended. In this way the concept *empty space* loses its meaning.” As the nature of environmental models is often determined by the representational basis of the GIS, this has led to an increased use of geometrically indexed methods for representing spatial context (Raper & Livingstone, 1995). Concerning these approaches, the characteristics of *planar enforcement* within a layer is implied (Raper & Livingstone, 1995). The term planar enforcement is described as the requirement of the representation having at every location a single value (e.g. Goodchild, 1992, 2012). As implications, overlapping features cannot be handled (Goodchild, 1992), and the representation of temporally changing phenomena is not possible (Langran, 1992). Planar enforcement is finally accompanied by a spatial interpolation, meaning the calculation procedure from a set of points to a continuous surface (Lam, 1983; Goodchild, 1996).

Field- and object-view

In principle, one of the most basic questions each researcher has to answer at the beginning of a planned representation is which of the two different views of reality, the field- or the object-view, is most suitable. The field-view reflects reality “as infinite sets of tuples approximated by regions and segments”, and the object-view as “planes littered with independent objects” (Goodchild, 1992, p. 405). While in the object-view an area or a line object can exist independently, the field-view forces a partition of the plane, resulting in the aforementioned segmentation into planar enforced layers (Goodchild, 1992). In order to refer to the Einstein statement, the object-view is able to represent empty space, whereas the field-based representation is based on the premise that every single location must contain exactly one value (Yuan, 2001). Exemplarily, spatial parameters such as elevation, temperature, or precipitation data are rather represented using the field-view, whereas discrete objects such as roads, buildings, or rivers are more suitably modelled by the object-view (Cova & Goodchild, 2002). As outcomes the raster model for either field- or object-based models (see B in figure 4.1) and the vector model for the object-based approach (see A in figure 4.1) have been established (Jones, 2014), and the term of an *object-oriented* model as a subcategory of the object approach has appeared (Goodchild, 1992).

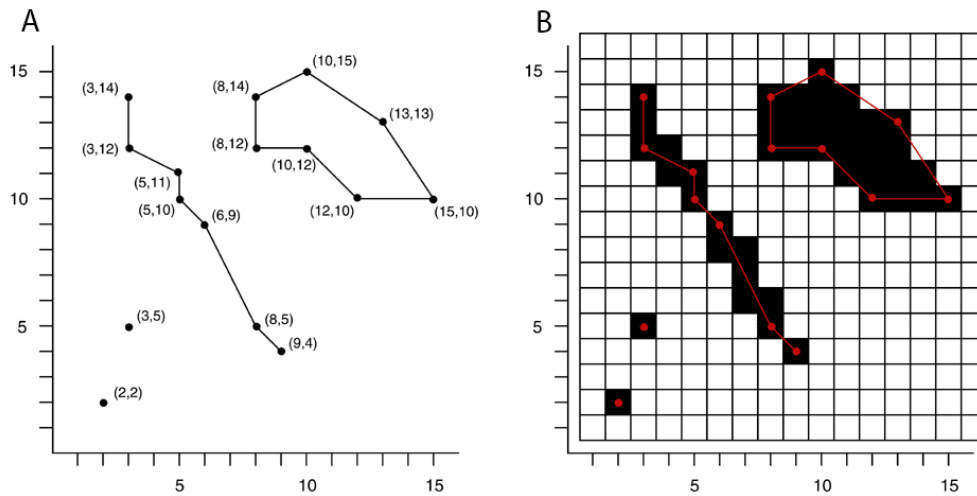


Figure 4.1: Vector model (A) and raster model (B) approach; based on Gruver (2014).

Rock glacier Muragl

The aforementioned models are examined in relation to the investigated object. Initially, rock glacier Muragl is treated as a discrete object, and hence, represented by the object-view (see A in Figure 4.1). This offers the advantages that the body can be defined at a high-spatial resolution, and that each object is able to obtain multiple attributes (Gruver, 2014). However, by partitioning the body into several sections, the question of how to merge the individual parts arises. Additionally, the information about the variation within an object is inaccessible, as objects have the property of being homogenous (Gruver, 2014). When representing rock glacier Muragl by the field-view (see B in figure 4.1), sharp boundaries occur, overlapping features cannot be handled, and planar enforcement into several layers is implied. Though, on the basis of field-based representations, digital elevation models can be easily calculated.

4.1.3 Object-oriented representation

The idea of modelling geographical features in an object-oriented way had its origins in the 1990s, even though the usage was initially limited to conventional database approaches (Goodchild et al., 2007). In the meantime, these representations have become familiar to a broader part of the scientific community and have been established as one of the software standards in terms of modelling geographic space (Bian, 2007). Due to its popularity, in 1992, the term of *objectifying* spatial phenomena had already appeared (Couclelis, 1992). The raised question of whether every environmental feature is best represented as an object, regardless of its individual characteristics, appeared again in the literature several years later (Bian, 2007).

Characteristics

The most distinct difference between geometrically indexed methods and the object-oriented approach lies in the treatment of the primary index, or in other words, the reference base of the representation (Raper & Livingstone, 1995). Concerning geometrically indexed methods, the coordinate system of the layers primarily dictates the structure of the representational frame, whereas the actual representational structure of the object-oriented approach is defined by the characteristics and behaviour of the real-world entities (Raper & Livingstone, 1995). Accordingly, the object-oriented approach focusses on the object itself, which leads to a rather knowledge-based view of how to model the perceived world (Bian, 2007). Object-oriented representations contain three parts of abstraction (Bian, 2007; Borges et al., 2001): the *object-oriented analysis* with the conceptual model of the world, the *object-oriented design* developing a formal model of objects, and the *object-oriented programming* including the implementation model. The principle of this approach is based on the two primitives objects and classes (Booch, 1991). An object is defined as a “tangible and/or entity that exhibits some well-defined behavior”, and a class is “a set of objects that share a common structure and a common behavior” (Booch, 1991, p. 79, p. 102). Concerning the APIE standard for object-oriented programming, four essential elements are coherently discussed in Kotur (2012): firstly, *abstraction* means the separation of unnecessary details from essential specifications. The second element implies *encapsulation*, which is equivalent to the process of connecting the data and functions. Thirdly, *inheritance* describes the mechanism of transferring features from one to another object, and finally, *polymorphism* means the fact that there is one interface but various implementations.

Features of spatial objects

Basically, every spatial object exhibits certain features, which construct an identity and by which it can be identified (Bian, 2007). In order to detect and categorize phenomena, probably the most manifest of these features is the *spatial scale*. Regarding scale matters, four types of spatial phenomena are defined by Zubin (1989) (in: Mark, 1989), which will be dealt with in the chapter on human cognition. Further object properties are *boundaries* or their *attributes* (Bian, 2007). Concerning the latter property, their spatial distribution is of especially great importance, as it acts as an indicator for the state of the phenomena (Bian, 2007). The *process* of a phenomenon, that equals the activity or the function, is considered to be a further fundamental property, leading consequently to a change in the state of the entity (Bian, 2007). The last property mentioned is *mobility*. While things move, they modify their attributes, behaviour, and identity; hence, mobility implies that objects are not attached to a certain location (Bian, 2007).

Benefits and drawbacks of individual approaches

With respect to the debate about representing geographic phenomena either by discrete objects or continuous fields (Couclelis, 1992) and the emergence of the object field, implying the interaction of field and object representations (Cova & Goodchild, 2002), the question of whether – and if so, why – representing geographic space has to be such a complicated matter has arisen (Goodchild et al., 2007). In order to answer this, several advantages and disadvantages of the individual approaches are discussed. Vector-based representations have the drawback of forcing the geographic space into uniform geometric objects, whilst raster-based approaches do not entirely consider the individual nature of things (Couclelis, 1992). The aforementioned predefined structure in geometrically indexed methods and the fact that the characteristics and behaviour of the real-world entities dictate the representational frame in object-oriented approaches can be viewed either as a benefit or a drawback (Raper & Livingstone, 1995). Object-oriented modelling, on the other hand, stands out in its suitability for dealing with complex geographic data (Clementini & Di Felice, 1994). Reasons for this are the modelling power, the handling of abstract data types, the object identity, and the inheritance and encapsulation (Clementini & Di Felice, 1994). An early implementation of the object-oriented approach within geomorphological research was made by Raper & Livingstone (1995), who set up a geomorphological model for coastal sand dunes. By means of this object-oriented model and the spatio-temporal data fed in, the forms and behaviour of the dunes were compared to the theoretical knowledge (Raper & Livingstone, 1995).

Despite the aforementioned differentiations, newer research especially has shown that in the meantime the object-based and the field-based approaches act rather compatibly and supportively than conflictingly (e.g. Goodchild et al., 2007; Liu et al., 2010). During this subchapter it has become clear that a multitude of approaches with an abundance of characteristics exist, making the choice of the appropriate representation difficult.

4.2 Human cognition

Driven by the technical progress and the aforementioned increasing use of GIS applications, the linkage between human cognition of geographic space and the actual model implementation has become an emerging subfield in GIScience (e.g. Bishop et al., 2012; Liu et al., 2010). The focus here lies on the handling of the enormous data volume and the increasing complexity, as well as on an attempt to improve human-interpretation capabilities (Bishop et al., 2012). The field of Cognitive Science has its origins in the 1960s and focusses on processes such as human perception or the generation of mental representations (Raper, 2000; Montello & Freundschuh, 2005). Concerning human perception, a crucial distinction exists between the

perception of a real existing object, called *materialistic metaphysic*, and the perception which is mental in origin, called *phenomenalism* (Raper, 2000).

For the majority of people the real world appears to be seen as a space littered by discrete objects which are allocated names and behaviours (Goodchild et al., 2007). In contrast, environmental properties such as atmospheric pollution or noise are rather conceptualized as continuous fields (Goodchild et al., 2007). Regarding the human perception of a geographic phenomenon, the existence of spatial patterns is of great importance as well. Patterns can vary in the entire range from locational to regional scale and, if existing, they are stored and become obvious for a human (Golledge, 1993). Nevertheless, contrary to experts, many average citizens have no need to obtain such spatial patterns and hence do not truly realize them (Golledge, 1993).

Perception of geographic phenomena

Partitioning the space into categories, so that the incorporated entities exhibit similar properties or that they are treated similarly, is one of the most fundamental steps when perceiving geographic phenomena (Mennis & Peuquet, 2000). As *spatial scale* is considered to be an essential criterion in the process of categorization, the aforementioned classification into four types of spaces, defined by Zubin (1989), is discussed (in: Bian, 2007). The first type, *A-Spaces*, comprises everyday objects with sharp boundaries that are smaller than the human body and which are able to be manipulated or moved (Couclelis, 1992; Frank, 1996). Secondly, *B-Spaces* include larger everyday features perceived as objects (Bian, 2007). As examples, an elephant or a house are mentioned (Couclelis, 1992). The third type of spatial scale, *C-Spaces*, incorporates landscapes which can be seen, yet are not directly accessible (Couclelis, 1992), and which are perceived by humans as fields (Bian, 2007). Finally, *D-Spaces* are an extension of the former type and include things which cannot be practically experienced (Couclelis, 1992). Here, an energy continuum is mentioned as an example (Bian, 2007). However, alternative literature distinguishes only two environments for human experience: small-scale spaces, including objects with sharpened boundaries (e.g. a stone), and large-scale spaces, covering objects without distinct boundaries (e.g. landscapes) (Frank, 1996).

Additionally, the aforementioned property of *boundaries* is sub-classified as well (Bian, 2007). The partitioning is based on their origins, leading to, firstly, the group of organisms and products of natural origins, and secondly, the group of boundaries projected deliberately by humans (Smith & Mark, 2003). Objects belonging to the first group reveal distinct, precise, and continuous borderlines towards the surroundings (e.g. animals or a lake) and are called *bona fide* (Bian, 2007; Smith & Mark, 2003). In contrast, boundaries that do not really exist in the physical world and that are products of artificial constructions of thoughts (e.g. profes-

sions or human ethnic groups), are called *fiat* objects (Smith & Mark, 2003).

In addition, the purpose behind the human action influences the individual conceptualization of geographic space as well (Couclelis, 1992). Exemplarily, a landmark with distinct borderlines to the surroundings is discussed (Couclelis, 1992). This environmental element can be conceptualized for the purpose of orientation or place recognition; however, it is subjectively chosen and, strictly speaking, it is not regarded as a landmark as long as someone perceives it as such (Couclelis, 1992).

Rock glacier Muragl

Relating to the aforementioned spaces, valley Muragl, in which rock glacier Muragl is embedded, is considered to be a *C-Space*. Due to the inhabited hills, streams, or permafrost feature, the perception of the landscape is rather field-like, as the features cannot be picked up and moved (Couclelis, 1992). The body of rock glacier Muragl, however, belongs to the *B-Spaces*, although it can neither be picked up nor moved. Furthermore, it is an object with rather distinct borderlines separating it from its surroundings, which makes rock glacier Muragl a *bona fide* object.

4.3 TLS data background

In the following, the first research question is examined by focussing on basic characteristics of the raw TLS data and the question of how humans perceive geographic data on different scale levels. For this, a sequence of enlarging scales showing an individual point, a small point cloud, and a point cloud representing the rock glacier front are provided (see figure 4.2).

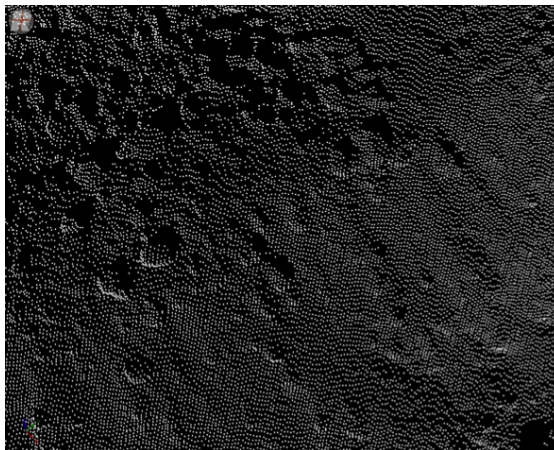
4.3.1 Point

In contrast to other subdomains of the TLS technique, rather little research investigating the actual raw data has been carried out so far. This is surprising, as the raw data points are, with exceptions of the adjustable parameters set by the researcher, acquired in a completely arbitrary manner (Bornaz & Rinaudo, 2004). Consequently, all subsequent processing steps have to be well-considered and done with special attention to the data quality (Biasion et al., 2005).

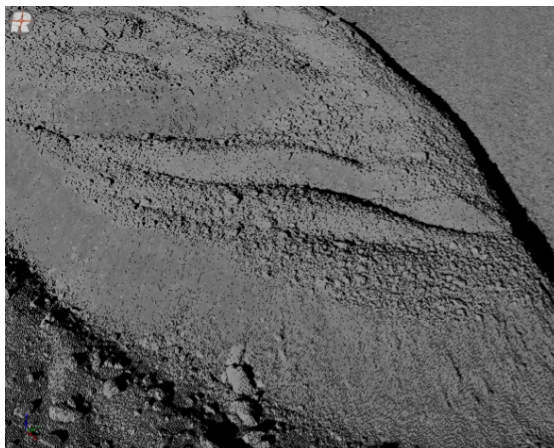
Basically, each single laser beam delivers one single point including the specific parameters $x[m]$, $y[m]$, and $z[m]$, as well as intensity values (Buckley et al., 2008). In other words, TLS results in a representation of the scanned object, implying an enormous amount of points dimensionally accurately represented in a three-dimensional space (Arayici, 2007). Investigating an individual data point, no information except the aforementioned values are included, and absolutely no structure or trend can be detected. Thus at this scale, a single measurement point does not manifest any relationship with nearby points (see (a) in Figure 4.2).



(a) Representation of a single measurement point



(b) A multitude of points creating a point cloud



(c) Representation of a point cloud including an enormous amount of points

Figure 4.2: Sequence of (a) a single measurement point, (b) a point cloud, and (c) a point cloud by enlarging the image section; own illustrations.

Concerning geomorphometric structures, a valuable contribution to the handling of single particles has been delivered by means of the so-called *Toposequenzen* in the sense of Speight (1974) (in: Rasemann, 2003, p. 34): “A Toposequenz describes the topographic sequence an imaginary particle passes through while moving downwards involving the gravitational force.” This perspective allows the detection of geomorphometric structures on various scales, such as small segments with slightly differing curvatures on a microscale, or a tributary valley on the mesoscale (Rasemann, 2003).

Depending on the scale, the nature of the scanned object, and the observer’s level of knowledge, specific characteristics, and patterns can sometimes be detected quite well (Pu & Vosselman, 2006). This is demonstrated in the following.

4.3.2 Point cloud

By enlarging the area of interest, a point cloud, including an aggregation of points, appears. Contrary to the observation of a single point, a point cloud allows geometric information to be inferred (Zeibak & Filin, 2009). However, the raw information provided by an individual point is no longer accessible, which leads to some drawbacks regarding a direct object extraction (Zeibak & Filin, 2009). In case of extracting building features, machines initially face serious troubles in directly understanding the structure of a building facade, whereas humans are able to easily detect certain elements by means of the color or position of the points (Pu & Vosselman, 2006). Exemplarily, the detection of the features *wall* and *window* are mentioned (Pu & Vosselman, 2006). While humans know that a wall usually covers the majority of a building facade and a window must be located on the wall, machines do not bring this knowledge (Pu & Vosselman, 2006). Research aiming to transfer this human knowledge to machines, which enables an automatic feature recognition from point clouds, has become a growing working area (e.g. Pu & Vosselman, 2006; Wang & Shan, 2009; Vosselman et al., 2004). In order to automatize this process, the segmentation of the point cloud, including the aforementioned spatial grouping, is one of the main tasks here (Wang & Shan, 2009). Consequently, each point in a point cloud is labelled with the certain identifier of the surface it belongs to (Pu & Vosselman, 2006).

Picture (b) in Figure 4.2 illustrates a point cloud including a multitude of data points. Contrary to the properties of an individual point, here, at least people with expert knowledge are able to assume or detect several structural features, such as a slight ridge delineating from the lower left to the upper right. Having background information about the nature or the geographical location of the object, a lobe, a specific rock glacier feature may be assumed. By further enlarging the image section, an enormous amount of data points appears, creating an almost image-like appearance of the rock glacier’s surface. As picture (c) in Figure 4.2

shows, distinct features such as lateral lobes, the steep front, and separate boulders can be observed.

Overall, it can be stated that obtaining information about geometrical location and neighbourhood of the point data is essential regarding the cognition of a rock glacier surface by means of TLS data.

4.3.3 Cognition of geomorphological features

In order to examine the human cognition of geomorphological features, the focus is on two research examples dealing with scale and cognition matters. Within the field of cognitive science, the issue of topography is a specific subfield, exhibiting a number of conceptualizations depending on the human's background (Mark & Smith, 2004): exemplarily, a topographic cartographer, a geomorphologist, or an information scientist perceives topographic features typically as fields, whereas a person from the field of aviation, anthropology, or ecology would rather conceptualize the same features as objects such as hills and valleys, or mountains and plains. This can be illustrated by concerning the topography of a mountain (Mark & Smith, 2004). Mountains do not have typical characteristics of objects, as distinct boundaries isolating them from the surroundings are absent (Mark & Smith, 2004). Hence, with respect to scale dependencies, the procedure of defining and representing mountains, and especially peaks, is a complex matter (Deng & Wilson, 2008). In case of mountain representations in cartographic maps, it is consequently up to the reader to determine the exact position of the peak or the real extent of the labelled area (Mark & Smith, 2004). Exemplarily, Figure 4.3 shows the area of Piz Muragl, which is not clearly defined, so that the map reader determines the extent of the mountain at his or her own discretion.

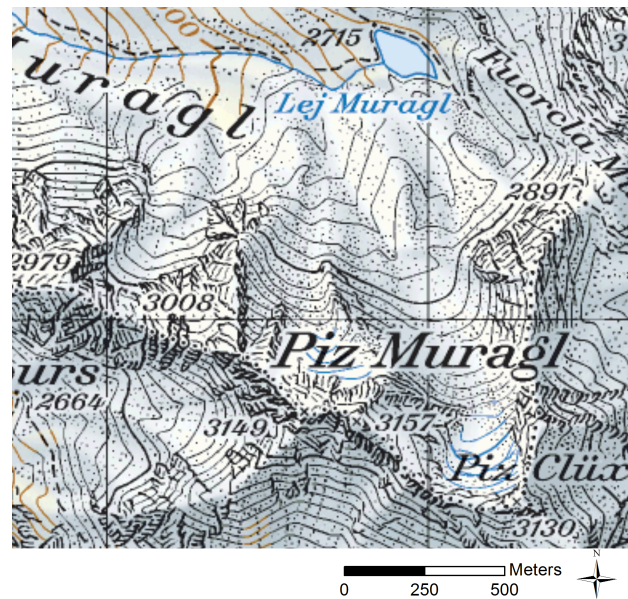


Figure 4.3: A cartographic representation of the peak of Piz Muragl in Val Muragl, Upper Engadin, Switzerland (datasource: Swiss Federal Office of Topography, Swisstopo).

Secondly, the landmark salience for human navigational purposes is discussed (Caduff & Timpf, 2008). Contrary to the traditional idea that the salience of a spatial feature is based solely upon its characteristics, Caduff & Timpf (2008) state that landmark salience depends on a number of factors: additionally to the object's properties, the observer's point of view, both physical and cognitive parameters, as well as the surroundings affects a landmark's salience. In order to be regarded as a landmark, several basic conditions have to be fulfilled. The most obvious is the requirement of being outstanding from the surroundings, either visually, semantically, or audibly. Further components are the perceptual and the cognitive salience. The perceptual salience focusses on the part perceived by the observer with respect to a certain location, whereas cognitive salience places the emphasis on the observer's experience and knowledge (Caduff & Timpf, 2008).

Rock glacier Muragl

Similar to the perceptions of mountains, rock glacier Muragl is conceptualized in various ways as well. Exemplarily, hikers probably notice the rock glacier as an ordinary feature within the landscape of valley Muragl, whereas geomorphologists or climatologists regard it as an object of investigations containing important climatic parameters. Due to the rather obvious borderlines, the body is able to be distinguished quite easily, though it is much harder to determine its subsurface extent. As rock glacier Muragl is such a distinct feature, it can be

regarded as a landmark, which is visible even from considerable distances. This leads to the following chapter discussing the study site.

5 Study Site

In the following section the study site is discussed. While the chapter on the background mainly addressed existing studies and their results, here, the focus is on the embedding into the local geography as well as on the specific characteristics of rock glacier Muragl.

5.1 Val Muragl

Geomorphology

The Val Muragl is situated above the village of Pontresina and lies within the attractive tourist region of St. Moritz in the Upper Engadin, eastern Swiss Alps (see Figure 5.1) (Maisch et al., 2003). Besides ski tourism, which is of great importance, hiking is exceptionally popular as well. Concerning inhabited landforms implying permafrost processes and glacial changes, hiking is not just hiking within this landscape. Exemplarily, Jäckli (1985, p. 37) stated: “When hiking the popular trail from Muotas Muragl through the Val Muragl to the Alp Languard, after only a short time a geological body with moving surface structures, remembering on a glacier but with coarse-grained material on the surface instead, appears”. The nearby co-existence of a glacier (i.e. Muragl glacier) and a permafrost feature (i.e. rock glacier Muragl) enables valuable information to be gained about landscape evolution during late glacial, Holocene, and present-day times (Maisch et al., 2003). Accordingly, Val Muragl is considered to be a popular *geotope-site* for all, tourists, locals, and researchers, describing following epochs (Maisch et al., 2003): the 20,000-year landscape evolution begins with the maximum glaciation, when Val Muragl was located within the accumulation zone of the Ice Age glaciers. The subsequent late glacial is characterized by a decay of surface ice including the development of distinct morainic systems (e.g. Daun-, or Egesen-stadial), followed by a series of local glacial advances and partial developments of creeping permafrost features during Holocene. Finally, in recent times, the well-known disappearance of surface ice and variations in the behaviour of periglacial permafrost features has occurred (Maisch et al., 2003).

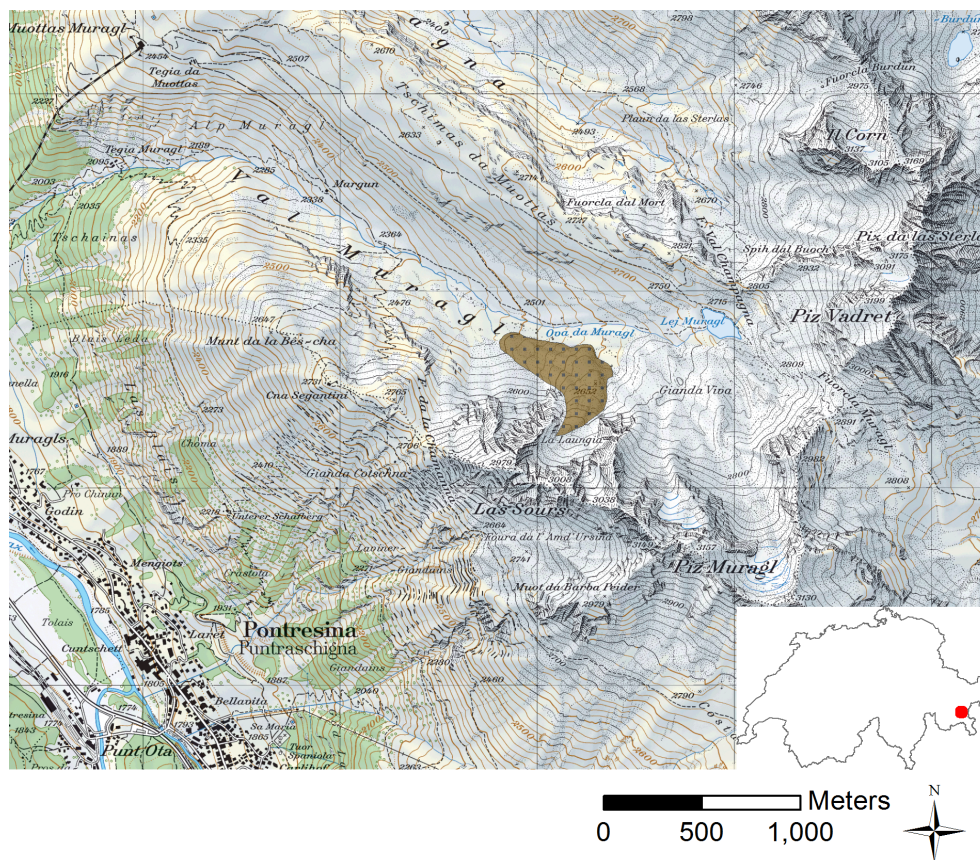


Figure 5.1: Overview of the region of Val Muragl, Upper Engadin, and the location of rock glacier Muragl shown by the polygon; (datasource: Swiss Federal Office of Topography, Swisstopo).

Meteorological conditions

From a meteorological point of view, the central alpine valleys of Grisons and Valais with limited precipitation are considered to be suitable areas for rock glacier evolution (Frauenfelder & Roer, 2007). Concerning the Val Muragl, the prevailing local climate is characterized by comparatively low precipitation and relatively high temperature amplitudes (Kneisel, 2010). According to investigations at the Muragl glacier forefield, which is adjacent to rock glacier Muragl, mean annual air temperatures (MAAT) of -2 to -4°C can be inferred within the altitudinal range of 2650m to 2900m a.s.l. (Kneisel & Käab, 2007). By means of two nearby climate stations, the overall MAAT is considered to be about -2.2°C within that area, and the typical snow height in March varies between 100cm and 300cm (Rödler & Kneisel, 2012).

5.2 Rock glacier Muragl

Extent

Rock glacier Muragl originates from the cirque La Launiga, located north of Piz Las Sours (see Figure 5.1) (Vonder Mühll, 1993). The altitudinal extent reaches from 2700m to 2480m a.s.l. (Springman et al., 2012), and the width varies between 100m and 300m (Maurer & Hauck, 2007). Furthermore, the length of the entire rock glacier is about 700m (Maurer & Hauck, 2007), and the covered area is approximately 0.12km² (Kääb & Vollmer, 2000). The steepest slopes reveal an inclination angle of 25° and are located in the upper area adjacent to the rock walls as well as at an elevation of about 2600m a.s.l. within the middle section of the rock glacier (Kääb & Vollmer, 2000). The average inclination angle is 15°, and the aspect is west-southwest (Springman et al., 2012). According to Vonder Mühll (1993), the entire body can be divided into three different zones: the uppermost area including the origin, the middle section, and the lowermost zone. The specific characteristics of those zones are discussed in the section on appearance.



Figure 5.2: Photograph of rock glacier Muragl; own photograph.

Thermal regime and composition

In order to investigate thermal properties of rock glaciers, borehole drilling represents a complicated and costly, yet also feasible method (Vonder Mühll et al., 2003). At rock glacier

Muragl, the drilling sites were first chosen to be in the lower part, where compressive flow entails the formation of transverse ridges and furrows (Arenson et al., 2002). Secondly, the sites were selected according to areas where ground ice was expected (Springman et al., 2012). The specific borehole locations are visible in Figure 5.3. While boreholes 2/1999 (2538m a.s.l.), 4/1999 (2549m a.s.l.), and 3/1999 (2558m a.s.l.) were drilled in an almost parallel line onto the body, borehole 1/1999 (2536m a.s.l.) is located at the edge of the geomorphologic borderline of the rock glacier (Vonder Mühl et al., 2003).

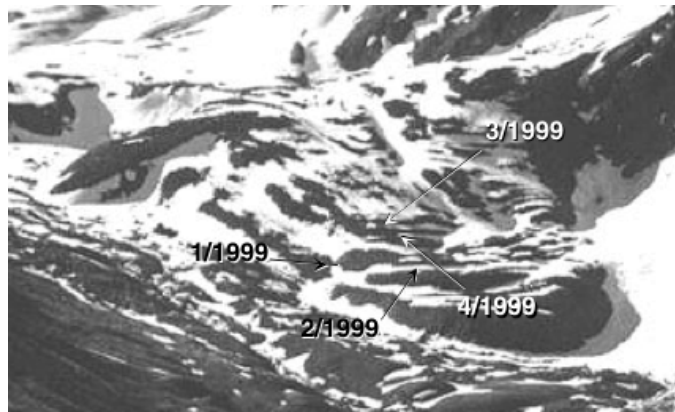


Figure 5.3: Locations of the drilled boreholes on rock glacier Muragl; (Arenson et al., 2002).

The borehole measurements by Vonder Mühl et al. (2003) revealed the following characteristics: The thermal regimes of boreholes 2, 3, and 4 were almost identical, revealing ice particles in the cores up to a depth of about 18m. At approximately 25m, a distinct escape of air was observed, and the bedrock followed in a depth between 30m and 38m. In accordance with previous seismic measurements, at the site of borehole 1 no permafrost was expected and found, and the bedrock was encountered at a depth of about 50m. Within this borehole, temperatures were all above 0° C, and negative temperatures occurred only near the surface, as temperatures underlie seasonal shifts (see Figure 5.4).

According to boreholes 2, 3, and 4, the active layer has an extent of about 3m, and the permafrost body reaches a depth of maximally 20m. Concerning a thermal trend, however, it has to be mentioned that the coldest measured temperature is 0.5° C (in borehole 4 at a depth of 10m), and that the temperatures are only marginally below 0° C (see Figure 5.4). The incorporated thermal regime appears to be regulated by diffusive processes, and it exhibits a logarithmic amplitude decrease (Vonder Mühl et al., 2003). Overall, it can be stated that rock glacier Muragl reveals a comparatively low ice content, a considerable amount of coarse rock fragments, a relatively high air-void ratio, and temperatures only slightly below 0° C (Vonder Mühl et al., 2003; Arenson et al., 2002).

Concerning the general geological composition within the observed area, the predominant features of underlying rocks and the rock wall are layered paragneisses containing minerals such as plagioclase, quartz, apatite, or biotit (Springman et al., 2012).

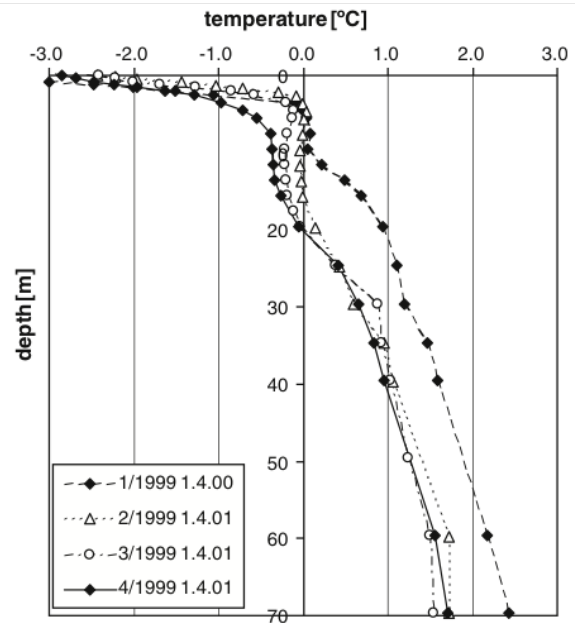


Figure 5.4: Temperature profiles versus depth for all borehole locations at rock glacier Muragl; (Vonder Mühl et al., 2003).

Deformation rates

Rock glacier deformation is determined mainly by atmospheric temperature, bedrock and surface slopes, and the conditions of the subsurface ice (Arenson et al., 2002). Accordingly, the aforementioned characteristics of rock glacier Muragl become crucial when assessing flow velocities. As seen before, the thermal conditions of the incorporated ice is close to 0°C , and compared to other rock glaciers (e.g. rock glacier Murtèl), the slopes are slightly steeper (Arenson et al., 2002). The combination of gravity-driven forces (i.e. slope) and degradation processes (i.e. relatively warm temperatures) leads to high velocities measured at rock glacier Muragl (Arenson et al., 2002). According to Kääb & Vollmer (2000), who investigated the period from 1981 to 1994, the flow velocities range between 0.01ma^{-1} to maximum values of up to 1ma^{-1} , even if strong seasonal variations are observed. More recently, the PERMOS report revealed certain flow velocities even reaching up to 1.5ma^{-1} in the period of August 2009/2010 (PERMOS, 2013). As Figure 5.5 indicates, the largest horizontal deformations are detected on the central lobe (red circle) and on the outbreaking lobe (yellow circle). The yellow dots represent the network of the terrestrial survey (PERMOS, 2013).

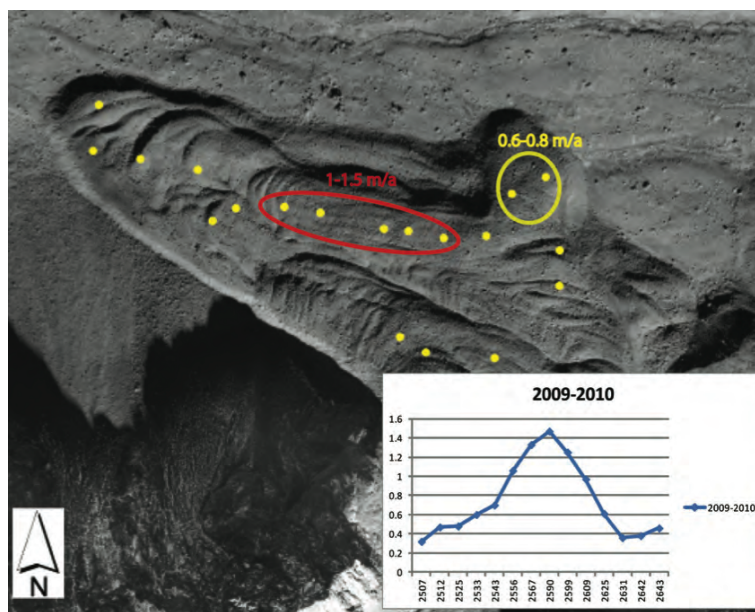


Figure 5.5: Measured flow velocities on rock glacier Muragl; (PERMOS, 2013).

Specific appearance

A valuable contribution to the material on the specific appearance of rock glacier Muragl was made by the study of Vonder Mühll (1993), which the following refers to. Here, one of Muragl's most distinctive characteristics shall be discussed: its form. Contrary to typically rather linear shapes, rock glacier Muragl exhibits a drastic change in its direction. While the initial movement is oriented north-northeast, after approximately half the distance it separates into two individual parts. The main part thereby flows in direction of north-northwest, whereas the outbreking lobe moves towards the north (see Figure 5.5). Concerning the individual parts mentioned earlier, within the uppermost zone a lot of perennial snow patches occur and no vegetation is observable. Accordingly, within this area (to 2670m a.s.l.) the coarse-grained debris and the lack of vegetation exhibit the typical appearance of an active rock glacier. The middle section reaches to an altitude of 2560 m a.s.l. and includes two differing parts. The orographically left side reveals similar characteristics to the upper part, whereas in the opposite area the boulders are intensely covered by lichens and humus. The lowermost zone shows a denser coverage of lichens and even some continuous grass patches occur. As the front is partially planted, it is presumed that rock glacier Muragl is slowly developing towards the transition to becoming inactive (Vonder Mühll, 1993).

As Figure 5.2 shows rock glacier Muragl in its full extent, the distinct flow lobes within the middle section and the lower part are clearly visible. According to Maurer & Hauck (2007), the transverse furrows and ridges are likely to have originated from repeated mass movements. Consequently, it is probable that the present-day topography represents several stages in the development of rock glacier Muragl (Maurer & Hauck, 2007).

6 Methods and Data

In this chapter, laser scanning in general and the applied TLS technique including its characteristics are discussed. Subsequent to a theoretical part, the actual data acquisition with instrumental specifications and measurement details are examined. Furthermore, the actual measurement procedures for determining horizontal displacements using the CIAS software (Kääb & Vollmer, 2000), as well as for calculating vertical changes by means of ArcGIS, are specified. The several processing steps shall be accompanied by the scheme of the work flow.

6.1 Laser scanning

The LiDAR technique, which had its beginnings in the 1970s, represents a crucial component in the development of laser scanning (Zogg & Grimm, 2008). The actual operational start of laser scanning for the purpose of surface reconstructions was then in the mid-1990s (Pfeifer & Briese, 2007). In the following years, this technique could be implemented in geodetic devices by means of enormous technical progress in fields such as computer technology or regarding optical elements (Zogg & Grimm, 2008). The fundamental measurement principle is based on capturing and recording primarily geometrical information of visible surfaces (Vosselman & Maas, 2010). As a result, a quantitative 3D representation (e.g. a point cloud) of the scanned surface is provided (Vosselman & Maas, 2010). In order to classify optical 3D measurement techniques, the literature proposes several approaches (Fröhlich & Mettenleiter, 2004; Vosselman & Maas, 2010). However, a broadly accepted classification distinguishes between the following methods: interferometry, time-of-flight (TOF), and triangulation methods (e.g. Vosselman & Maas, 2010; Zogg & Grimm, 2008). Concerning these techniques, laser scanning, both airborne and terrestrial, is based mainly on the TOF measurement method (Vosselman & Maas, 2010). In order to trace the ground, the data acquisition is reached by combining a laser source with the known propagation velocity of light (Vosselman & Maas, 2010).

6.2 Terrestrial laser scanning

Subsequent to the general information about laser scanning, the specific technique of terrestrial laser scanning is in the focus. This includes a discussion of the functionality, an examination of accuracy matters and registration procedures, and an analysis of advantages and disadvantages.

6.2.1 Functionality

The basic principle of measuring a time delay between the moments a light signal is emitted by the source, reflected at the surface, and measured by a light detector enables an appropriate method for evaluating distances (Vosselman & Maas, 2010). However, before lasers emerged in the 1950s, radio waves were used for TOF measurements, establishing the nomenclature of radar (radio detection and ranging) (Vosselman & Maas, 2010). The transition from radio waves to light then enabled measurements with much higher angular and range resolution (Vosselman & Maas, 2010).

The light emitter, as a crucial component, delivers a bundle of laser pulses for each single measurement unit (Bauer et al., 2003). Additional main elements of a laser scanner device are the receiver, and the light detector system (see Figure 6.1)(Vosselman & Maas, 2010). The emitter thereby encloses the information for determining the time needed from the transmitter to the object (Zogg & Grimm, 2008). The reflected return signal is subsequently analyzed by a processor and translated into a single distance measurement (Bauer et al., 2003).

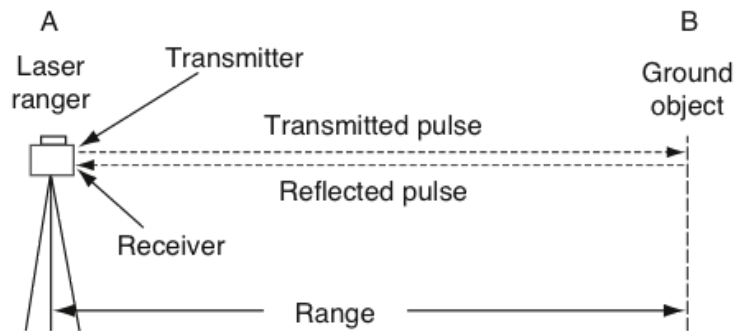


Figure 6.1: Terrestrial laser device (A) with the main elements measuring based on TOF method; (Shan & Toth, 2009).

In other words, by multiplying the detected time of the signal with the velocity of light, the double distance is determined (Zogg & Grimm, 2008). More quantitatively, the functionality is summarized in the following formula (Vosselman & Maas, 2010):

$$\rho = \frac{c}{n} \cdot \frac{\pi}{2} \quad (6.1)$$

where ρ is the range between the laser device and the scanned surface (see Figure 6.1), c is the speed of light in a vacuum (current accepted value equals 299 792 458 m/s), and π the round-trip. Depending on air temperature, pressure, and humidity, the value of c has to be

adjusted according to a correction factor n ($n \approx 1.00025$) (Vosselman & Maas, 2010, p. 3). The specific implications of environmental influences are discussed in the section on calibration.

Measurement modes

The wavelength of the laser beam lies either in the spectrum of optical or near infrared, so that the scanned object is directly affected by the incident ray (Armesto et al., 2009). Depending on site characteristics, a number of signal returns may be measured, leading to multiple pulse echoes (Vosselman & Maas, 2010). Due to the bundle of laser pulses, which are emitted for each single measurement, different types of pulses such as *first pulse*, *last pulse*, or *strongest pulse* exist (Bauer et al., 2003). On the basis of these individual pulses, the so-called pulse method is enabled as an alternative to the common wavelength method (Abellán et al., 2014). Both methods are shown in Figure 6.2, where several pulses result from the echoes of the tree and from the ground surface, respectively (Abellán et al., 2014). The different measurement modes allow satisfying results to be reached even in difficult weather situations and on challenging surfaces (e.g. vegetated or moist terrain) (Bauer et al., 2005).

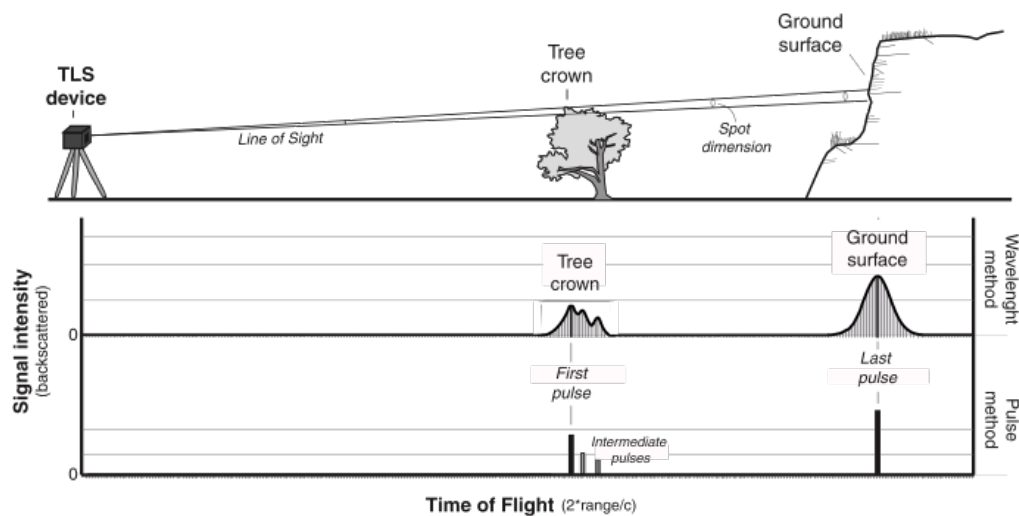


Figure 6.2: Scheme of TLS functionality concerning signal echoes; (Abellán et al., 2014).

Perspective

As already mentioned in Chapter 2, the measurement perspective represents a specific characteristic of the TLS technique (see Figure 2.4). While the majority of aerial-based methods reveal almost vertical viewing angles, terrestrial laser scanners possess a horizontal measurement perspective (Bauer et al., 2003; Abellán et al., 2014). Accordingly, aerial-based applications are usually faced with challenges in investigating steep slopes, whereas this problem does not occur when applying terrestrial laser scanning (Oppikofer et al., 2009). In the case of investigating a rock glacier surface, most remote sensing methods are consequently afflicted with a crucial disadvantage, as the steep front is considered to be one of the most distinct features of rock glaciers (Bauer et al., 2003).

6.2.2 Accuracy and precision

Accuracy

In the domain of remote sensing, the accuracy is subclassified into location and thematic accuracy (Congalton & Green, 2008). Location accuracy describes how accurately acquired data points are represented with respect to their *true* position on the surface, whereas thematic accuracy indicates the accuracy of a reflected condition of the surface (e.g. spectral information) (Congalton & Green, 2008). Concerning TLS applications, several accuracies are defined (Abellán et al., 2014). Initially, the *range accuracy* specifies the exactness of a measurement to the real range (Abellán et al., 2014). The resulting error depends strongly on the instrument, the properties of the target's surface, and the tested range, and varies between millimetres and centimetres. Further, the *instrument accuracy* is influenced mainly by ambiguous conditions such as rainy or foggy weather or low reflectivity of the scanned object (Abellán et al., 2014). Finally, the *angular accuracy* includes any errors caused by the rotating device, by which the emitted laser pulse is deflected and consequently sent to the object (Boehler et al., 2003). Generally, the overall measurement accuracy reveals a decrease with increasing distance, surface complexity, and incidence angle (Abellán et al., 2009).

With respect to the type of range, long or short, different accuracy values are expected (Shan & Toth, 2009). Concerning a range of 50m (i.e. short range), the accuracy varies between 4mm and 15mm (Shan & Toth, 2009), whereas long-range applications with a range of up to 1500m possess an accuracy in the order of centimetres (Schulz & Ingensand, 2004).

Resolution

Basically, the resolution dictates the level of detail which can be represented by TLS (Abellán et al., 2014). Pesci et al. (2011) provide a coherent description of the term resolution and

distinguish the following types for TLS devices: the *range*, the *angular*, and the *intensity resolution*. The range resolution “accounts for its ability to differentiate two objects on the same LOS (lines-of-sight)” (Pesci et al., 2011, p. 169). This type is influenced by the pulse length and, concerning long-range devices, usually 3 to 4mm. The angular resolution is defined as the “ability to distinguish two objects on adjacent LOSs” (Pesci et al., 2011, p. 169). This resolution is determined by the width of the laser beam and the point spacing, and entails a spatial resolution of ~ 10 to 15mm at a distance of 50m. Finally, the intensity resolution describes the “ability to differentiate adjacent areas, having similar but not equal reflectance” (Pesci et al., 2011, p. 169). More generally, point spacing, determined by the range and the angular spacing between the LOSs, is usually considered to be the resolution (Abellán et al., 2014).

In order to assess TLS accuracy for applications in alpine environments, several approaches exist (Kenner et al., 2011). Exemplarily, Rabatel et al. (2008) calculated the total uncertainty by the quadratic sum of the individual errors, which occurred during processing. Another assessment approach consists of a comparison of the results with existing findings gained by single point measurements (e.g. snow depth measurement) (Prokop et al., 2008).

6.2.3 Calibration and registration

Considering the quality of the acquired data, two of the main influencing parameters are discussed in the following: calibration and registration.

Calibration

For the purpose of maximizing data accuracy, the process of calibration implies that systematic error sources, which are implicitly related to TLS measurements, are identified, modelled, and determined (Vosselman & Maas, 2010). Yet, as LIDAR calibration is, contrary to photogrammetric methods, considered to be a nontransparent process, that means that the calibration process is strongly dependent on the specific system (Shan & Toth, 2009). Accordingly, no adjustment procedure exists, by which the acquired data can be manipulated in a general manner (Shan & Toth, 2009). Due to the lack of a prevalent and approved procedure to assess and control the quality, LIDAR systems are typically regarded as *black boxes* (Shan & Toth, 2009).

Concerning systemic errors, Reshetyuk (2006) defined the following coherent classification of potential error sources when applying terrestrial laser scanning: instrumental, object-related, environmental, and methodological sources of errors. Instrumental errors are related to the scanner and its specific technical elements, and include both random and systematic errors.

Due to the treatment as *black boxes*, systematic errors need to be handled with special attention. Object-related errors imply, as the name suggests, errors occurring due to objects' characteristics. Here, the most obvious is the reflectance of the object surface, which depends on various factors such as material properties (e.g. electric permittivity), surface color and roughness, or the specific surface temperature. Environmental errors appear because of external factors including ambient temperature, pressure, illumination, or relative humidity, and result in modification of the laser beam propagation. These effects include a distortion of the returned laser pulse or an attenuation due to scattering and absorption. Finally, methodological errors originate from the applied survey methodology and imply potential errors such as the determination of the sampling resolution, or the applied georeferencing approach (Reshetyuk, 2006).

Registration

In case of extraordinarily large or complex investigation areas, the coverage by an individual scan position is commonly not possible; hence several scans are recommended (Reshetyuk, 2006). Similarly, a multitude of individual scans is acquired when applying a snapshot survey of the object of interest, as it is done in this thesis. As terrestrial laser scanners acquire the point cloud on the basis of their scanner's own coordinate system, the individual scans have to be adjusted afterwards (Vosselman & Maas, 2010). The first step consists of the transformation of the scans into a common coordinate system (Reshetyuk, 2006). Concerning this procedure, called *registration* (or *co-registration*), typically one of the individual point clouds provides the reference base, by which the unregistered scans are transformed (Reshetyuk, 2006). Although the several point clouds are registered in a common internal system now (i.e. project coordinate system), they are still not compatible with external spatial data (Vosselman & Maas, 2010). The related procedure, transforming the registered point clouds from the internal into an externally defined coordinate system, is called *georeferencing* (Reshetyuk, 2006). The individual coordinate systems, included in a TLS instrumentation, are illustrated in Figure 6.3, where SOCS implies the scanner's own coordinate system (red), PRCS the project coordinate system (blue), and GLCS the external global coordinate system (black).

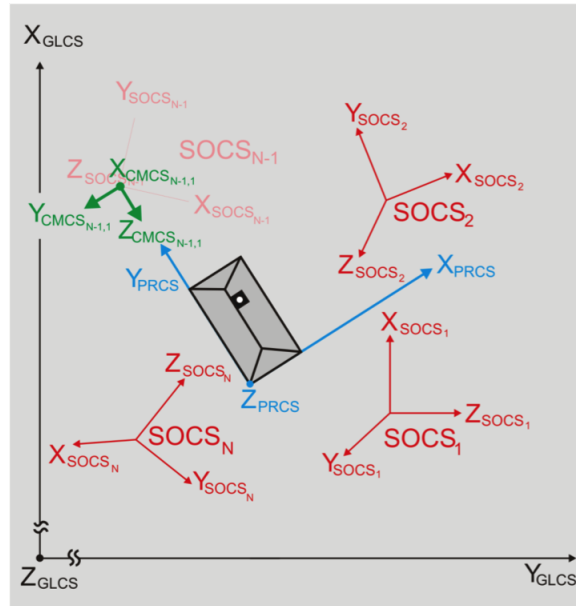


Figure 6.3: Coordinate systems incorporated in TLS instrumentation with SOCS (scanner's own coordinate system), PRCS (project coordinate system) and GLCS (global coordinate system); (RIEGL Laser Measurement Systems GmbH, 2012b).

Methods for registration

For the purpose of registering several TLS point clouds, generally two different approaches are applied (Kenner et al., 2011): ICP (iterative closest point) algorithm and target-based registration (e.g. Kenner et al., 2011; Vosselman & Maas, 2010). Registration based on ICP algorithm consists of progressive point adjustments within two overlapping point clouds on the basis of stable regions (Abellán et al., 2014). Although this referencing technique is considered to be a flexible, independent, and very accurate method, the use is potentially challenging in mountainous terrain considering the requirement of stable surfaces (Kenner et al., 2011). The target-based registration employs targets (also *tie-points*) with known locational correspondence, which are mounted within the scanner's view (Vosselman & Maas, 2010). As tie-points either special targets or common environmental features are posed, the determining criteria here are that they are able to be detected in each overlapping scan, and that their reflectivity differs sufficiently from the surroundings (Reshetyuk, 2006). Concerning the applicability of the described methods, the process of target-based registration can be characterized as time-consuming, as the placing of the targets may be a difficult task (Pfeifer & Briese, 2007). In contrast, the fact that ICP algorithm can be run entirely automatically is considered to be an advantage of the ICP method (Pfeifer & Briese, 2007).

6.2.4 Advantages and disadvantages of TLS systems

To complete this section, several advantages and disadvantages of TLS systems are discussed. Concerning applications in high mountain environments, the horizontal measurement perspective has already been mentioned as a crucial benefit. This is of great importance, as mountain areas incorporate peaks, vertical rock walls, or features including steep slopes (Armesto et al., 2009). A further benefit of alpine applications and especially regarding related natural hazards is the ability to measure remotely in safe areas (Prokop et al., 2008; Rub & Zogg, 2008). Relatively short acquisition times, millimetre to centimetre accuracy, and the high spatial resolution are further advantages appearing frequently in the literature (e.g. Abellán et al., 2014; Armesto et al., 2009; Lichti et al., 2005; Abellán et al., 2006). Contrary to traditional measurement techniques (e.g. levelling), which deliver very accurate yet spatially limited measurements, TLS is, due to the aforementioned properties, considered to be comparatively cost-effective (Lichti et al., 2005).

Despite the aforementioned cost efficiency, the relatively high initial costs for a TLS device, compared to traditional surveying instrumentations (e.g. theodolites or total station), has to be mentioned as a drawback (Rub & Zogg, 2008; Shan & Toth, 2009). An additional disadvantage concerning cold mountain environments is the restriction to snow-free surfaces of most TLS devices, which reduces the potential period of application during the year drastically (Kociuba et al., 2013). With respect to the laser's wavelength and the laser beam propagation, poor weather conditions such as fog can also render reliable measurements impossible (Reshetyuk, 2006; Prokop et al., 2008).

6.3 Data acquisition

The current chapter deals with the actual data acquisition including specifications of the used TLS device as well as information concerning the individual measurement campaigns.

6.3.1 Riegl VZ-1000

For this study the laser scanner Riegl VZ-1000 from manufacturer Riegl in Austria was used. According to the producer, this device is distinguished by properties such as a very long range of up to 1400m, a wide field of view, high accuracy and precision, and high-speed data acquisition (RIEGL Laser Measurement Systems GmbH, 2014). The most important attributes are summarized in Table 6.1, and Figure 6.4 beside represents a photograph of Riegl VZ-1000.

Table 6.1: Specifications of laser scanner device Riegl VZ-1000; (RIEGL Laser Measurement Systems GmbH, 2014).

Range performance	Specification
Max. measurement rate	122,000 meas./sec.
Max. measurement range	1,400 m
Accuracy	8 mm
Precision	5 mm
Min. range	2.5 m
Laser wavelength	near infrared
Beam divergence	0.3 mrad
Scan performance	
Scan angle vertical	total 100° (+60°/-40°)
Scan angle horizontal	max. 360°
General technical data	
Weight	approx. 9.8 kg



Figure 6.4: Specific TLS device Riegl VZ-1000; (RIEGL Laser Measurement Systems GmbH, 2014).

The beam divergence of 0.3mrad is equivalent to an increase of 30mm of beam diameter per 100m distance (RIEGL Laser Measurement Systems GmbH, 2014). Due to the included WLAN antenna, the device offers the possibility of managing the measurement setup remotely via laptop or smartphone (RIEGL Laser Measurement Systems GmbH, 2014).

6.3.2 Measurement campaigns

The field measurements cover the time span of an entire year. In order to assess the research questions, the dates of the measurement campaigns represent snapshots establishing a monthly, seasonal, and annual period (see Figure 6.5). The first data acquisition took place on the 4th and the 5th of July in 2013, the second on the 23rd of August, and the last measurements in 2013 were carried out on the 7th of October. The first campaign in 2014 could be executed only on the 25th of July 2014, due to the long-lasting snow cover in the Upper Engadin. Figure 6.5 illustrates the field measurement campaigns including the several periods in between.

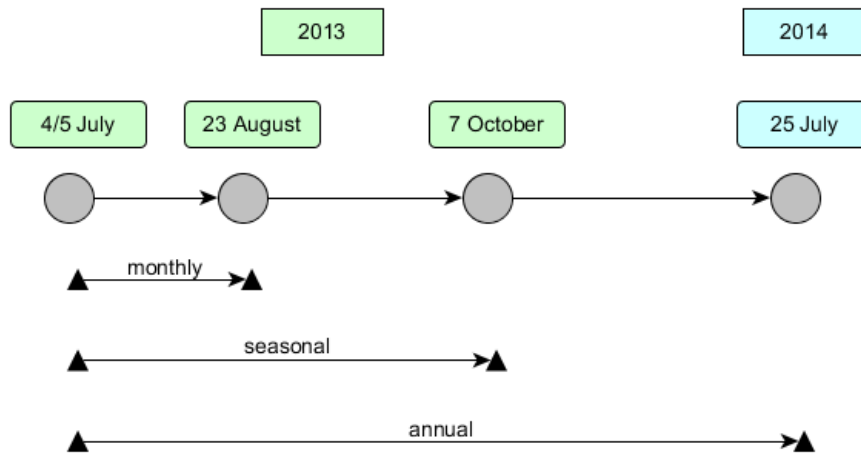


Figure 6.5: Overview of measurement campaigns conducted in 2013 and 2014; own illustration.

6.4 Data pre-processing

The subsequent processing after data acquisition comprises the input of the gained scans in the RiSCAN Pro software, which is provided by the laser's manufacturer RIEGL GmbH. Among others, this software offers the possibility of viewing the point clouds, possesses an abundance of manipulation tools, and enables the procedure of co-registration. In the following, the related processing steps including the data import, the visualization, the determination of the selected scans, and the registration and georeferencing processes are examined. To refer to the schema of the work flow, Figure 6.6 shows the individual processing steps.

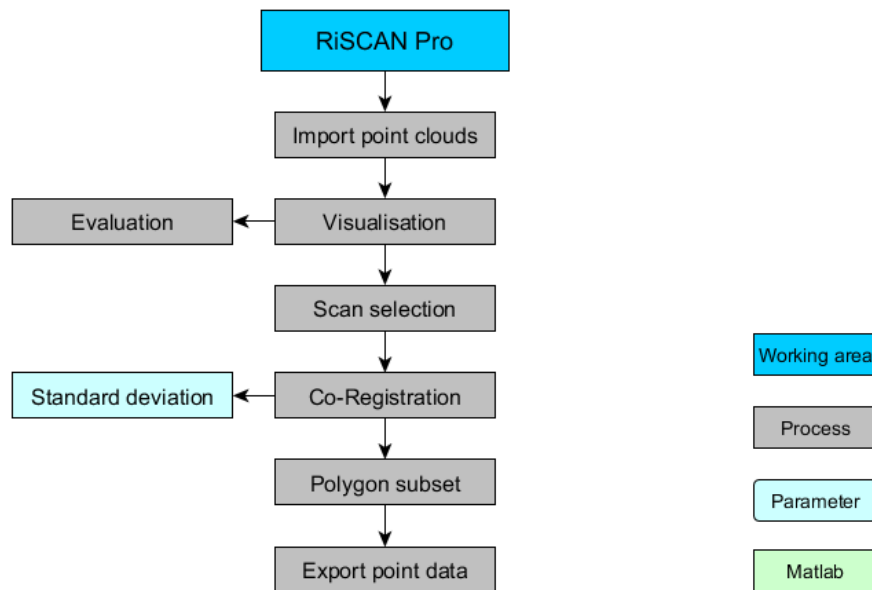


Figure 6.6: Flow diagram representing the processing using RiSCAN Pro software; own illustration.

6.4.1 Visualization of raw data

As all scans have been imported in RiSCAN Pro, initially, the focus is on providing an overview of the point clouds regarding its characteristics. This implies the visualization of each single scan, and an assessment of its sizes, coverages, and qualities. According to those findings, the scans are selected in the subsequent processing step. In order to illustrate how a raw point cloud appears in RiSCAN Pro, Figure 6.7 represents the point cloud of 5 July 2013.

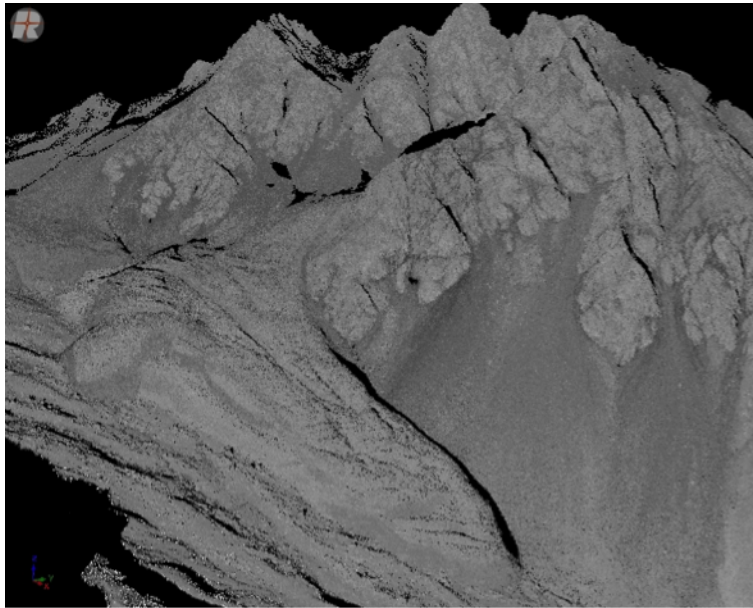


Figure 6.7: Visualization of the point cloud of 5 July 2013 in RiSCAN Pro software; own illustration.

6.4.2 Selection of scans

As mentioned above, the specific scans that will be included in further processing are determined according to the size (MB), the amount of coverage, and the quality of the point clouds. The assessment of the coverage also includes the sight of the fixed target points, due to its great importance concerning the subsequent co-registration procedure. These targets consists of aluminum disks with a prism lamination and a diameter of 35cm. Their exact locations were calibrated by total station in 2013. Figure 6.7 indicates the exact locations of the four targets. The total of all scans acquired during the measurement campaigns is provided in the Appendix A.1.

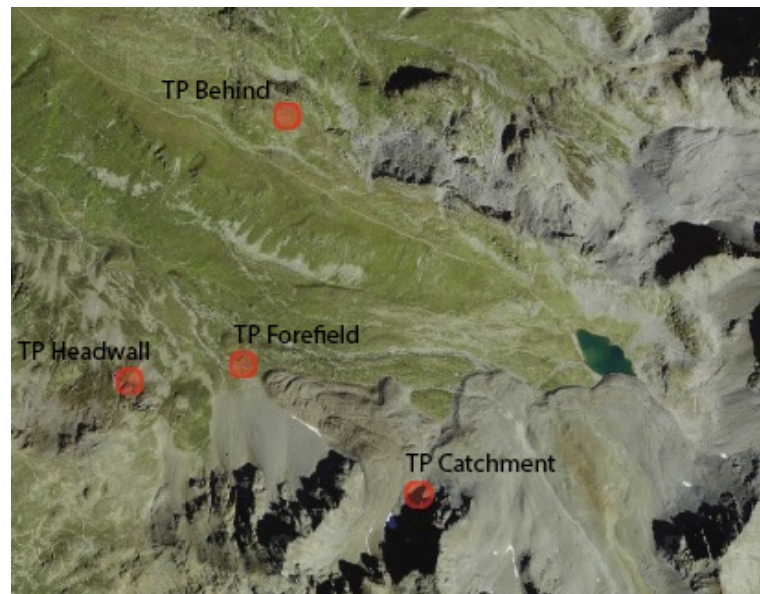


Figure 6.8: Specific locations of the target points; underlying aerial imagery derived from Swiss Federal Office of Topography (Swisstopo).

The finally determined scans are summarized in Table 6.2. In addition to the measurement date and the name, the applied measurement program, the resolution, the size, the coverage, and the related tie points (i.e. targets) are also indicated. Regarding the tie points, it is distinguished between those that were automatically found and those that needed to be added manually. The last line reveals special remarks about the specific scan. At this point it has to be mentioned that the measurements of 4 July 2013 did not provide any reliable results, as this day was used for establishing a suitable measurement setup for the subsequent campaigns. Accordingly, those point clouds were excluded for the following processing steps and the deformation analysis.

Table 6.2: Scan characteristics of the selected scans acquired at measurement campaigns of 5 July 2013, 23 August 2013, 7 October 2013, and 25 July 2014.

Date	5 July 2013	23 August 2013
Name	121146	110056
Program	1400m (70kHz)	1400m (70kHz)
Resolution	0.001 [m]	0.001 [m]
MB	529	894
Coverage	Entire rock glacier, rock wall, headwall partly	Entire rock glacier, rock wall, headwall
Tie points (auto.)	TP Catchment, TP Forefield, TP Headwall	TP Headwall, TP Forefield
Tie points (man.)	-	TP Catchment
Remarks	TP Behind not visible	False TP found, high resolution
Date	7 October 2013	25 July 2014
Name	133236	113645
Program	1400m (70kHz)	1400m (70kHz)
Resolution	0.001 [m]	0.001 [m]
MB	700	504
Coverage	Entire rock glacier, rock wall, headwall	Entire rock glacier, rock wall, headwall
Tie points (auto.)	TP Catchment, TP Forefield, TP Headwall	TP Catchment, TP Forefield, TP Headwall
Tie points (man.)	-	-
Remarks	TP Behind not visible, high resolution	TP Behind not visible

6.4.3 Co-registration

As the previously selected point clouds are still referenced with respect to their acquired scanner's own coordinate system (SOCS), the adjustment into a common project coordinate system (PRCS) is the subject of the current processing step. For this, various approaches have been tested in order to find the one obtaining the most accurate results. In a first attempt, the three selected and, at this time, available scans (5 July, 23 August, 7 October 2013) were included and registered one after the other. Due to the three tie points found automatically, the point cloud of 7 October 2013 was elected as reference scan, and the scans of 5 July and 23 August were registered individually to the previously registered. This procedure led to standard deviations within the range of less than 1cm to up to 20cm. In an alternative

approach, the individual scans were registered with respect to all previously registered scans (i.e. the point cloud of 23 August 2013 was registered with the scan of both 7 October AND 5 July 2013). Although this approach delivered slightly better results (see Table 6.4), the results were not consistent overall. Furthermore, this procedure did not suit the logical structure, as the subsequent analysis follows a pairwise approach. In order to demonstrate the implications of a low-quality scan, the point cloud of 4 July 2013 was included. As Table 6.4 indicates, here, considerably larger standard deviations occurred, which is hardly surprising considering the quality, the coverage, and the fact that only one tie point was found automatically.

Table 6.3: Specific standard deviations caused by procedure of co-registration including and excluding 4 July 2013.

	Including 4 July 2013	Excluding 4 July 2013
Scan position	Standard deviation [m]	Standard deviation [m]
4 July 2013	0.2431 / 24.31 cm	
5 July 2013	0.0519 / 5.19 cm	0.00374 / 3.74 cm
23 August 2013	0.1110 / 11.1 cm	0.0307 / 3.07 cm
7 October 2013	0.0846 / 8.46 cm	0.0120 / 1.20 cm
TPL (PRCS)	0.1997 / 19.97 cm	0.1190 / 11.9 cm

Eventually, the attempt described first was considered to be the most accurate approach. This is due, on the one hand, to the reliable standard deviations, and on the other hand to its suitability to the subsequent intention. As the deformation analysis compares point clouds originating from two snapshot data sets (e.g. 5 July and 23 August), the aforementioned procedure implies the most natural method of co-registration. The resulting standard deviations of the co-registration for the several periods range between 2.16cm and 3.62cm and are represented in Table 6.4. In addition to the total standard deviation, the averaged radial deviation, the theta deviation indicating the vertical alignment, and the phi deviation specifying the horizontal alignment are provided (RIEGL Laser Measurement Systems GmbH, 2012a). Furthermore, the standard deviations occurring during the georeferencing process, which is treated in the subsequent chapter, is shown in the bottom line.

Table 6.4: Specific standard deviations caused by procedure of co-registration including the three observed time periods.

Time period	July 13 - August 13	July 13 - October 13	July 13 - July 14
Standard dev. [m]	0.0362 / 3.62 cm	0.0232 / 2.32 cm	0.0216 / 2.16 cm
Avg. radial dev. [m]	-0.0141	-0.0076	-0.0079
Avg. theta dev. [m]	0.0005	0.0004	-0.0006
Avg. phi dev. [m]	0.0053	0.004	0.0031
TPL (PRCS)	0.1180 / 11.80 cm	0.1339 / 13.39 cm	0.1332 / 13.32 cm

6.4.4 Georeferencing

Since the exact location of the TLS device is not gathered during data acquisition, the point clouds do not reveal a linkage to common external data yet. Accordingly, the previously co-registered point clouds need to be transformed into an external global coordinate system (GLCS). This is done by referencing on the exact location of the highly reflective targets (i.e. in coordinate system CH1903 LV03). The related coordinates are imported in RiSCAN Pro, and subsequently, after being renamed in *TP Headwall*, *TP Catchment*, *TP Forefield*, and *TP Behind*, registered with the tie points of the project coordinate system (PRCS). At this point it has to be mentioned that *TP Behind* could unfortunately not be included in the registration procedure, because the scans did not cover this area, as scan duration and the related size would have soared drastically. Referring to Table 6.4, the resulting standard deviations including the entire co-registration and georeferencing procedure range between 11.8 and 13.32cm.

6.4.5 Subset of region of interest

Having the specific point clouds adjusted, the adjacent work step includes subsetting the region of interest from the entire point cloud. This is of great importance concerning the rasterization procedure in ArcGIS that follows later, as a smaller observation area enables the determination of smaller cell sizes. Furthermore, this procedure reduces the file sizes, hence decreasing subsequent processing times. By means of user-defined polygons, three individual regions of interest are established, namely: the entire rock glacier, half the rock glacier, and the lower part focussing on the rock glacier front. These particular areas are subsetting for all four relevant point clouds.

Data export

With respect to the further processing in ArcGIS, all relevant snapshot data sets including the previously subsetted regions are individually exported. As data format, txt-files are chosen in order to preserve the complete geometrical information contained in the individual point data. The total of exported txt-files used for further processing is summarized in Table 6.5.

Table 6.5: The total of exported txt-files from RiSCAN Pro including all subsetted regions of interest.

Snapshot	txt-files		
5 July 2013	5July13_EntireRG	5July13_HalfRG	5July13_RGFront
23 August 2013	23Aug13_EntireRG	23Aug13_HalfRG	23Aug13_RGFront
7 October 2013	7Oct13_EntireRG	7Oct13_HalfRG	7Oct13_RGFront
25 July 2014	25July14_EntireRG	25July14_HalfRG	25July14_RGFront

6.4.6 ArcGIS

The following section focusses on the processing steps realized by using the ArcGIS software. To provide an overview, Figure 6.9 represents the flow diagram including the individual operations and processes.

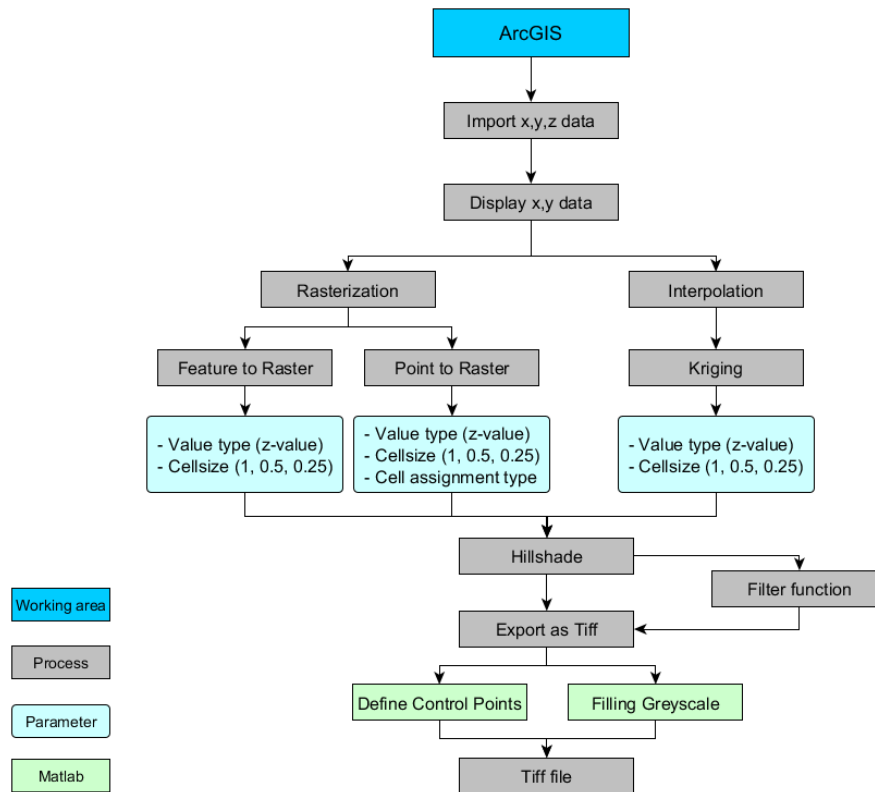


Figure 6.9: Flow diagram representing the processing in ArcGIS software, own illustration.

Data import and visualization

As Figure 6.9 indicates, the initial task implies the import of the previously produced txt-files in ArcGIS. The present files contain an ID as well as values for the relevant parameters $X[m]$, $Y[m]$, and $Z[m]$. In the adjacent work step, the individual points are displayed, and the certain coordinate system is specified (i.e. CH1903 LV03).

Point conversion

With respect to the greyscale Tiffs, which are subsequently required for the deformation measurements, the point data need to be converted into raster representations. On the basis of single points, various rasterization methods are applicable, which are individually tested out in order to find the most suitable approach. The related methods include *Feature to Raster*, *Point to Raster*, and the interpolation method *Kriging*. Although *Feature to Raster* and *Point to Raster* methods follow similar procedures, the latter method offers the opportunity to specify the handling if more than one point falls within a cell. Here, the maximum value of the attribute (i.e. height parameter) of the points within the relevant cell is determined as default.

Concerning the procedure, additional settings such as the output cell size (i.e. 1m, 0.5m, 0.2m) and the relevant processing extent are specified. The alternative approach of applying the interpolation method *Kriging* serves a satisfying raster; however, it is not regarded as absolutely coherent for the current purpose. There are two reasons for this lack of coherence: firstly, the possible interpolation methods implicitly incorporate some degree of blurring, secondly, the considerable amount of contiguous voids within the data set results in big euclidian distances between data points, thus increasing the uncertainty of the interpolated values.

After evaluating the results and the impacts of the various rasterization methods, *Point to Raster* is, with respect to the current purpose, considered to be the most appropriate approach. Consequently, the alternative methods are not further pursued.

Hillshade function

In order to generate single channel images (i.e. greyscale), the subsequent processing step implies the application of the *Hillshade* function. For the purposes of better exploiting the various shadows and testing their implications, two hill shades with differing altitude angles of the light source are generated for each individual raster. The altitude angle is expressed in positive degrees, where 0° implies the source of light at the horizon, and 90° directly overhead (ArcGIS Resources, 2012b). For the first produced hill shade, the default angle of 45° is used, whereas the second hill shade is calculated by means of an angle of 90° . Exemplarily, a result of the *Hillshade* function using the default angle is illustrated for the date of the 5th of July 2013 in Figure 6.10.



Figure 6.10: Result of the *Hillshade* function for the data set of the 5th of July 2013 with a DEM possessing a cell size of 1m.

As an additional operation, both a low and a high pass filter are applied to the raster data sets. While the low pass filter smooths the surface by reducing the local variation, the high pass filter sharpens the edges (ArcGIS Resources, 2012a). These filters are applied mainly for the purpose of comparing their implications regarding the subsequent displacement measurements.

Export and stretching

In the last work step using ArcGIS, the produced greyscale images are exported as Tiff-files. Subsequently, the exported files are stretched by a MATLAB script (see Appendix A.2) in order to obtain images exhibiting the full greyscale range from 0 to 255. As the CIAS software (Kääb & Vollmer, 2000) considers differences in overall grey values, this stretching is not necessarily needed, though it is done for comparison and the assessment of potential implications. By establishing an additional MATLAB script (see Appendix A.2), a number of randomly distributed points (i.e. *control points*), which are subsequently used as measurement points for the displacement measurement, are extracted.

The individual Tiff-files now fulfil the requirements of the CIAS Feature Tracking software (Kääb & Vollmer, 2000), which is introduced in the following section.

6.5 Displacement measurements

The final section in the chapter of methods and data focusses on the applied technique for measuring the horizontal displacements. Initially, the functionality of the CIAS software (Kääb & Vollmer, 2000) is introduced, followed by a discussion of requirements and input files. Subsequently, the determination of various measurement setups is examined, and, finally, ways of visualizing the results are described.

6.5.1 CIAS Feature Tracking

The method of CIAS Feature Tracking is based on normalized double cross-correlation, and computes displacements between two georeferenced images (Kääb, 2013a). The related function of double cross-correlation is showed in Formula 6.2 (Kääb & Vollmer, 2000):

$$\Phi(i, k) = \frac{\sum_j \sum_l s((i + j, k + l) - (\frac{T_{test}}{N})) * m((j, l) - (\frac{T_{ref}}{N}))}{\sqrt{\sum_j \sum_l s^2((i + j, k + l) - (\frac{T_{test}}{N})) * \sum_j \sum_l m^2((j, l) - (\frac{T_{ref}}{N}))}} \quad (6.2)$$

where the parameters imply the following (Kääb & Vollmer, 2000, p. 318): the coordinates within the test and reference blocks are represented by (i, k) and (j, l). While s is the spatial grey value function of the test block, s(i, k) is the corresponding grey value at location (i, k). Similarly, m is the spatial grey value function of the reference block, m(j, l) the corresponding grey value at location (j, l). The sum of grey values of the test or reference block and the number of pixels of the test or reference block are represented by T and N, respectively ($N_{ref} = N_{test}$). Due to the T/N terms, the grey values are normalized, so that differences in overall grey value do not affect the correlation process (Kääb & Vollmer, 2000).

The approach includes two individual steps (see Figure 6.11) (Kääb & Vollmer, 2000): Initially, the pixel size of a reference block in the image of the first time stamp is determined. Secondly, the pattern of the specified reference block is then searched within the predefined test area in the image from the later date (Kääb & Vollmer, 2000). With respect to the known coordinates, the shift of the central pixels directly determines the horizontal displacement (Kääb & Vollmer, 2000). As the choice of pixel sizes for the reference block and the test area strongly influences the measurement, it is discussed separately later on.

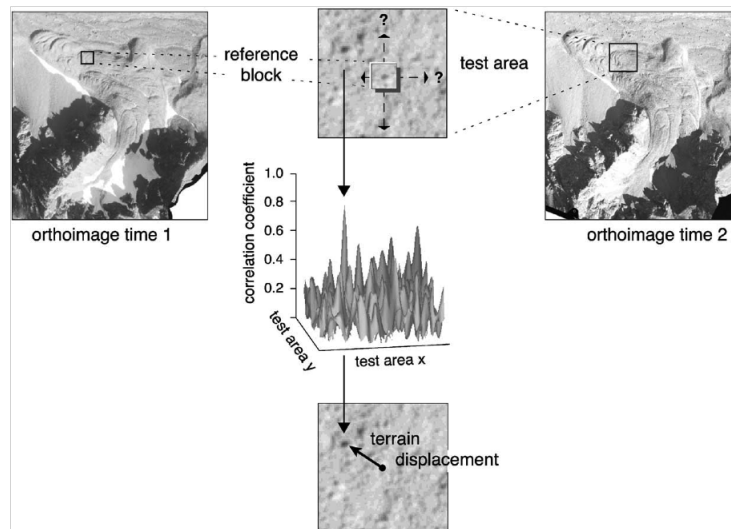


Figure 6.11: Principal approach of CIAS Feature Tracking with reference block and test area; (Kääb, 2002).

6.5.2 Input files and outcomes

According to the software requirements, the images need to be precisely co-registered and in the format of geotiff or Tiff-world (Kääb, 2013a). Furthermore, both images must have the same resolution and, as aforementioned, need to be greyscale images (Kääb, 2013a). The output of the procedure is an ASCII list including offsets in cartesian and polar coordinates, as well as certain correlation coefficients (Kääb, 2013a). A detailed description including all individual work steps is given in the Appendix A.3.

Table 6.6 provides the total of all used input files concerning an observed time period. Besides the previously produced Tiff-files and the txt-files containing the *control points*, additional txt-files for the Helmert transformation are established. For this, 10 points, which remain as stable as possible in the images of both time stamps, are determined. Due to that transformation, the coordinate systems of the two images can be aligned accurately (Vollmer, 1999). In Table 6.6 the input files for the monthly displacement measurement for the subsetted region of the rock glacier front are specified. This table can be transferred to the several periods and to each individual region of interest.

Table 6.6: Input files for CIAS Feature Tracking software concerning the monthly period, including Tiffs and txt-files for the Helmert transformation and the definition of control points; Hillshade is hereinafter referred to by abbreviation HS.

Tiff	Helmert function	Control points
5July Hillshade Cell1	Helmert 10 Points Cell1	10,000 Points Cell1
5July HS Angle90 Cell1		
5July HS Cell0.5	Helmert 10 Points Cell0.5	10,000 Points Cell0.5
5July HS Angle90 Cell0.5		
5July HS Cell0.2	Helmert 10 Points Cell0.2	
23Aug HS Cell1		
23Aug HS Angle90 Cell1		
23Aug HS Cell0.5		
23Aug HS Angle90 Cell0.5		
23Aug HS Cell0.2		
5July HS Cell1 LowPass	Helmert 10 Points Cell1	10,000 Points Cell1
5July HS Cell1 HighPass	Helmert 10 Points Cell1	10,000 Points Cell1
5July HS Cell0.5 LowPass	Helmert 10 Points Cell0.5	10,000 Points Cell0.5
5July HS Cell0.5 HighPass	Helmert 10 Points Cell0.5	10,000 Points Cell0.5
23Aug HS Cell1 LowPass		
23Aug HS Cell1 HighPass		
23Aug HS Cell0.5 LowPass		
23Aug HS Cell0.5 HighPass		

6.5.3 Sizes of reference block and test area

In order to obtain best possible correlation results, the choice of reference block and test area sizes is a crucial factor. According to Käab & Vollmer (2000), the reference block size has to be determined regarding the specific textural properties of the observed surface. If chosen too large, calculating time increases vastly; if chosen too small, Φ does not obtain a distinct maximum (Käab & Vollmer, 2000). Regarding the determination of the test area size, Formula 6.3 specifies the related parameters (Vollmer, 1999). The factor 2 in the numerator implies the quadratic expansion of the test area from the block centre (Vollmer, 1999).

$$\text{Test area} = \frac{(\text{Time difference} * \text{max. velocity} * 2)}{\text{Cell size}} \quad (6.3)$$

Exemplarily, the specific input values for the annual time period are provided: The time lapse between the measurements is one year (i.e. 1), the maximum velocity of rock glacier Muragl

is specified as 2ma^{-1} (i.e. 2), and the cell sizes vary between 1, 0.5, and 0.2m (e.g. 0.2). Accordingly, the size of the test area should be chosen as 20 pixels in that certain case.

6.5.4 Visualization of results

The CIAS software (Kääb & Vollmer, 2000) offers the possibility of displaying the resulted displacements instantly. Yet the enormous amount of measurement points leads to rather overloaded and unclear representations. Besides this, the resulting ASCII files can also be imported as point data in ArcGIS. Here, the displacements can either be visualized as graduated dots or as arrows indicating the specific length values and its directions.

7 Results

7.1 Horizontal displacements

In order to gain systematic findings, the results will be discussed in separate subchapters. Initially, horizontal displacements, calculated by using the CIAS Feature Tracking software (Kääb & Vollmer, 2000), are in the focus. The displacement rates for the specific time span (i.e. monthly, seasonal, and annual) are examined separately. In the subsequent part, the vertical surface changes, which are obtained by applying the ArcGIS software, are described for the aforementioned periods as well.

7.1.1 Monthly time span (July 2013 - August 2013)

The first observed time span includes monthly variations between the beginning of July 2013 and the end of August 2013. The previously described measurement process was conducted with all input files proceeded, summarized in Table 6.7. Though, for enabling a subsequent discussion of the resulting displacements, a selection of significant results is provided in the following. In order to avoid redundancy and to deliver the best possible overview, the important parameters of each result are summarized in a table at the beginning of each time period. These tables include information about the measurement setup (i.e. cell sizes, reference block size [RBS], test area size [TAS], and input type for the determination of the measurement points), statistical values (i.e. mean and standard deviation), and for the illustration excluded values (i.e. maximum correlation coefficient as well as minimum and maximum length values).

Table 7.1: Specific parameters concerning the results of horizontal displacements for the monthly period and all included figures.

	Figure 7.1	Figure 7.2	Figure 7.3
Cell size [m]	0.5	0.5	0.2
RBS [pixels]	4	4	4
TAS [pixels]	6	6	6
Meas. points	Txt-file	Polygon	Man. selected
Mean [m]	0.34	0.43	0.61
St. deviation	0.29	0.3	0.19
Max. corr. Coeff.	< 0.8	< 0.8	-
Min. length [m]	< 0.1	< 0.1	-
Max. length [m]	> 2	> 2	-

Figure 7.1 shows the result of the displacement measurement covering the area of the entire rock glacier. The displacements are represented by means of graduated symbols and the coloring and the break values of the classes are chosen as follows: dark green indicates small displacements between 0.10 and 0.50m, light green from 0.51 to 1.00m, yellow between 1.01 and 1.50m, and orange indicates the largest displacements within the range of 1.51 to 2.00m. While the break values remain equal for all subsequent results, the type of representation varies between graduated symbols (i.e. dots) and arrows, which represent the incorporated directions. As base maps the DEMs covering the entire rock glacier and that including half the rock glacier, which both possess a cell size of 1m, are used in the subsequent figures.

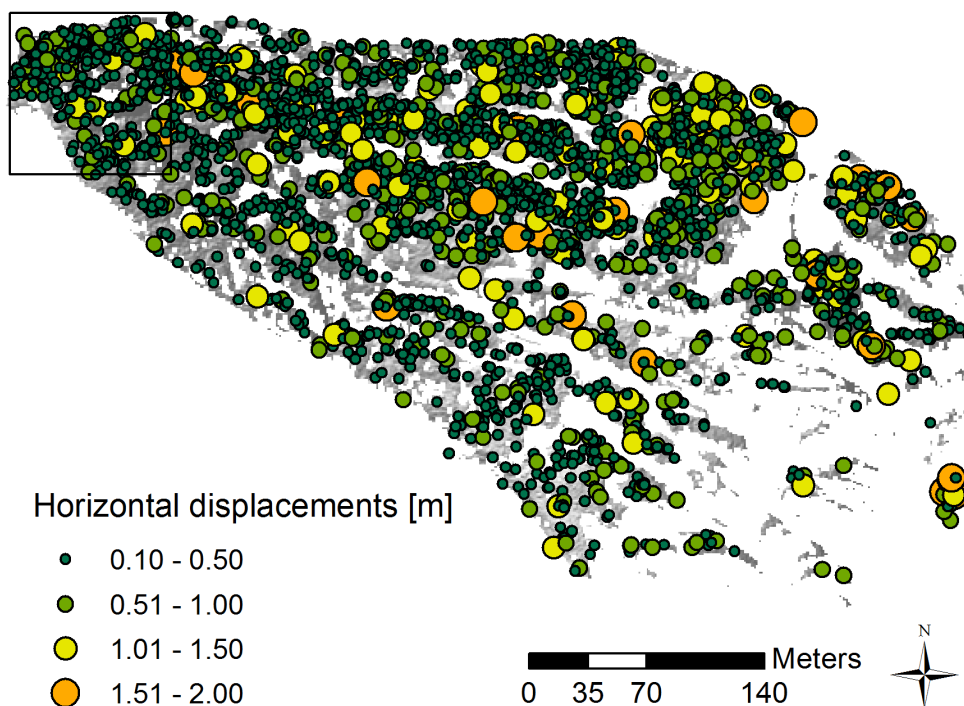


Figure 7.1: Horizontal displacements concerning the monthly time span and the entire rock glacier, shown by graduated symbols, DEMs possess a cell size of 0.5m. The rectangle to the upper left marks the section depicted in Figure 7.2.

At first glance it seems that Figure 7.1 contains only a mix-up of different-colored and -sized points. However, two observable types of patterns should be mentioned. Initially, it appears that the major part of the dots is dark greenish, indicating that the displacements are predominantly within the range of 0.1 to 0.5m. This is congruent with the mean value, which is about 0.34m. The second observable pattern concerns the areas of the middle section and the small

break-out zone. Within those regions, an accumulation of rather larger displacements ranging from 1.0 to 1.5m, or even up to 2.0m, appears. Besides these areas, the remaining parts of the rock glacier rather show displacements within the two smallest categories.

In Figure 7.2 an enlarged view of the lower part of the rock glacier is shown (see rectangle to the upper left in Figure 7.1). Instead of graduated symbols, the monthly displacements are here represented by arrows, which are colored according to their length variation.

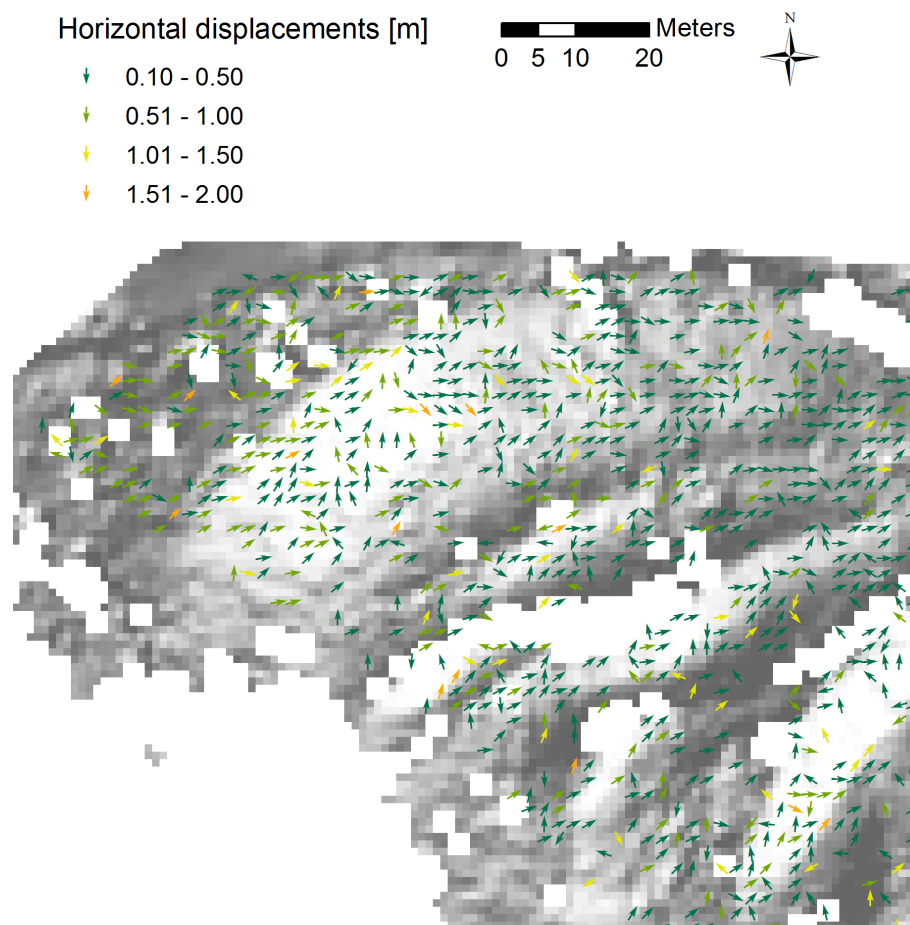


Figure 7.2: Horizontal displacements concerning the monthly time span and the lower part, shown by arrows colored according to their length change, DEMs possess a cell size of 0.5m.

Investigating Figure 7.2, the impressions gained in Figure 7.1 can be confirmed. Besides the fact that the majority of the arrows appear to be greenish (i.e. within the range of 0.1 to 1.0m), the current result implies displacements with mostly differing directions. However, several small aggregations of adjacent arrows form at least some type of contiguous movement, which

is, however, positioned rather towards the north-northeast.

Figure 7.3 represents the area of the rock glacier front and shows the result of manually selected points. Although the type of representation is chosen similarly to before, it has to be mentioned that the smallest displacement is about 0.19m, thus the smallest class starts at 0.19m instead of the common 0.1m.

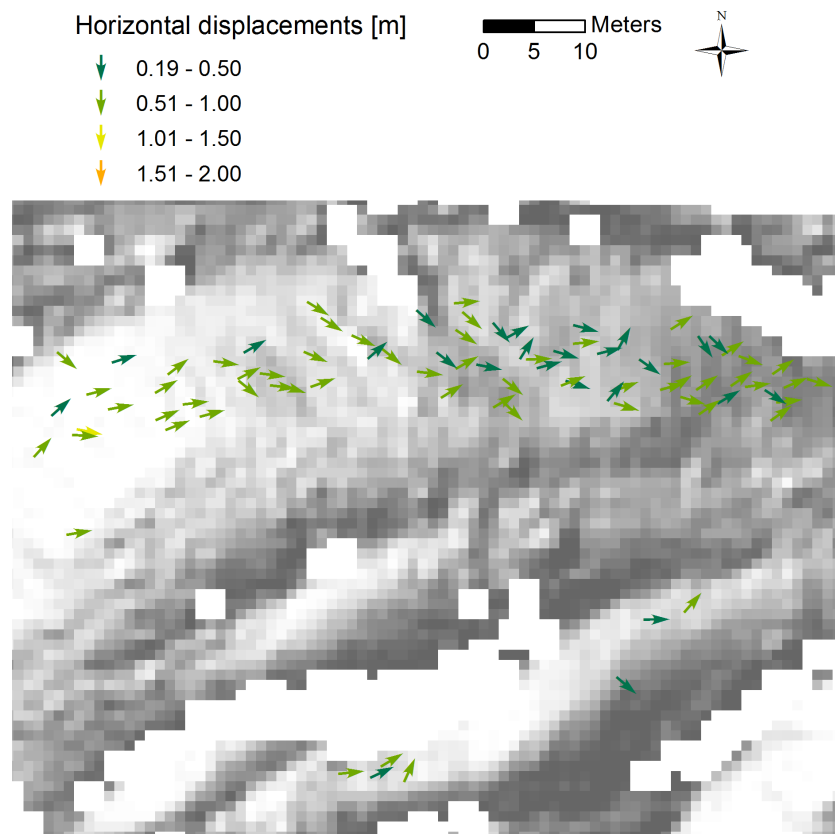


Figure 7.3: Horizontal displacements concerning the monthly time span and the front area, measurement by manually selected points, DEMs possess a cell size of 0.2m.

Except for one individual displacement, all resulting movements are within the range of 0.1 to 1.0m. In addition, the majority of the arrows are positioned nearly linearly, revealing an orientation towards the northeast or the southeast, as was already mentioned in the previous result.

7.1.2 Seasonal time span (July 2013 - October 2013)

The second time period includes seasonal displacements between the beginning of July 2013 and the beginning of October 2013. Similarly to the previous period, the first figure shown represents the result covering the entire rock glacier. In order to provide the best possible comparison, in Figure 7.4 the displacements are represented by means of graduated symbols again. The important parameters concerning the results are summarized in the subsequent table.

Table 7.2: Specific parameters concerning the results of horizontal displacements for the seasonal period and all included figures.

	Figure 7.4	Figure 7.5	Figure 7.6	Figure 7.7
Cell size [m]	0.5	0.5	0.5	0.2
RBS [pixels]	4	4	4	5
TAS [pixels]	6	6	6	10
Meas. points	Txt-file	Polygon	Polygon	Man. selected
Mean [m]	0.41	0.48	0.53	0.3
St. deviation	0.31	0.3	0.35	0.17
Max. corr. Coeff.	< 0.8	< 0.8	< 0.7	-
Min. length [m]	< 0.1	< 0.1	< 0.1	-
Max. length [m]	> 2	> 2	> 2	-

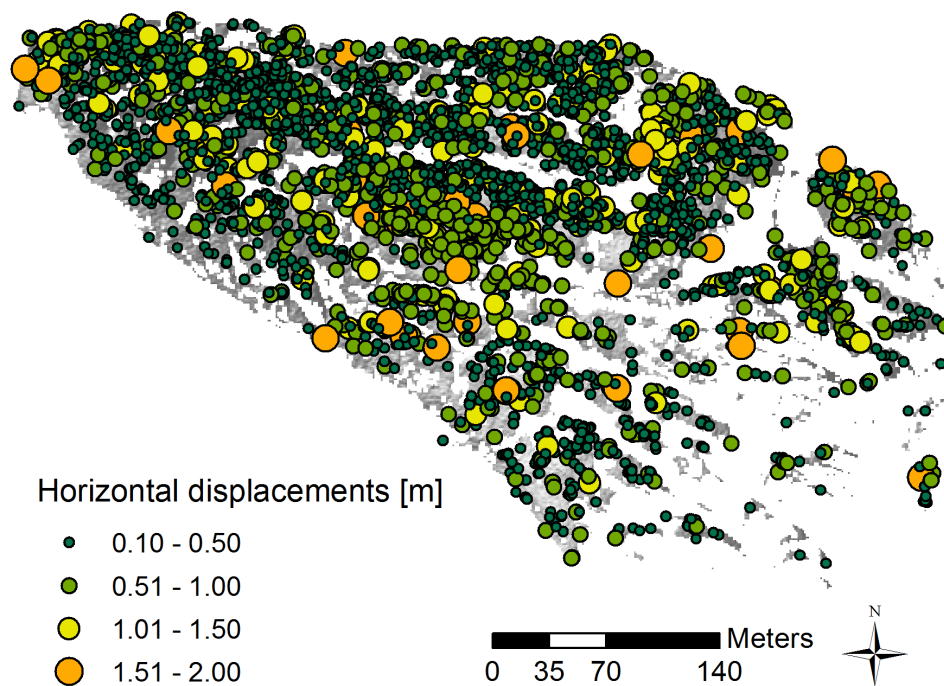


Figure 7.4: Horizontal displacements concerning the seasonal time span and the entire rock glacier, shown by graduated symbols, DEMs possess a cell size of 0.5m.

When examining Figure 7.4, it is conspicuous that the dark green dots are not equally predominant anymore, compared to Figure 7.1. Instead, several small-scale patterns are observable: In the area on the orographically right side within the lower part, small displacements between 0.1 and 0.5m seem to prevail, whereas the middle section shows an accumulation of light green dots, indicating displacements between 0.5 and 1.0m. Adjacent to this region on the orographically right side, smaller displacements within the range of 0.1 to 0.5m occur. Similarly to the findings of the monthly period, the break-out zone, and especially its frontal part, is characterized by rather larger displacements between 1.0 and 1.5m. The uppermost part of the rock glacier reveals moderate changes between 0.1 and 1.0m.

The subsequent Figure 7.5 shows an additional result covering the entire rock glacier, yet the displacements are indicated by arrows with the commonly used length-specific coloring.

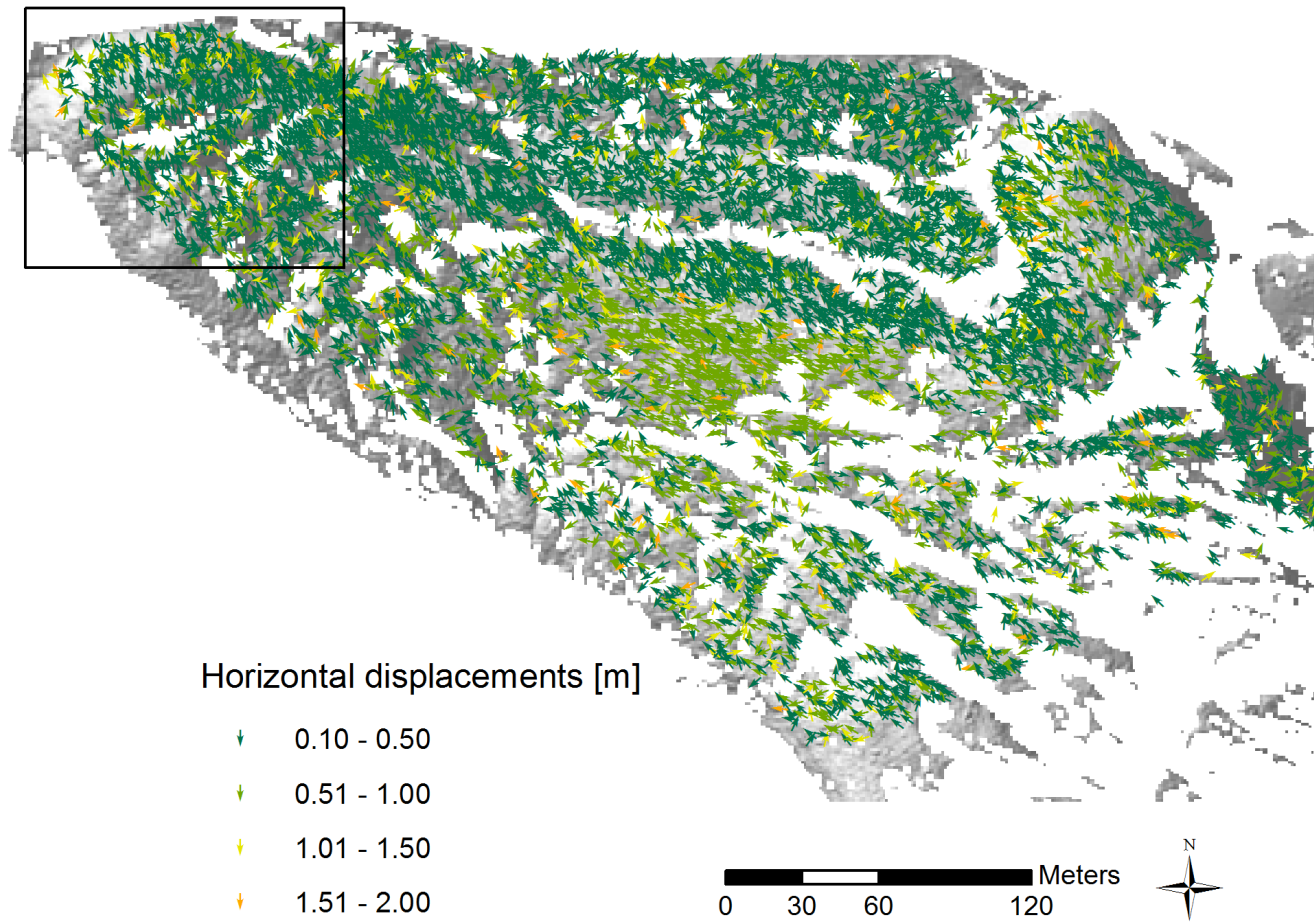


Figure 7.5: Horizontal displacements concerning the seasonal time span and the entire rock glacier, shown by arrows colored according to their length change, DEMs possess a cell size of 0.5m. The rectangle to the upper left marks the section depicted in Figure 7.6.

In Figure 7.5, many of the aforementioned arrangements and patterns reappear. Initially, the middle section is mentioned, where light green arrows are predominant, indicating displacements between 0.51 and 1.0m. In that particular area the arrows are positioned mainly linearly to the northwest. Northerly of that area an accumulation of smaller displacements is observable. Here, dark green arrows imply horizontal changes within the range of 0.1 and 0.5m. Concerning both the lowermost and the uppermost part, representatives of the two smallest classes mainly occur. However, it has to be noted that displacements covering the entire range are represented within these areas as well. Again, the break-out zone is characterized by differing displacements between 0.1 and 2.0m. With respect to the flow movement, the general direction of adjacent arrows seems to be more or less linear, and the major orientation points north (e.g. break-out zone) or northwest (e.g. middle section). The only area where no directional pattern is observable consists of the region on the orographically right side beside the rock glacier body. Instead of a contiguous flow movement, a clutter of differing directions occurs within this area.

Figure 7.6 shows an enlarged view of the lower part of the rock glacier (see rectangle to the upper left in Figure 7.5), and includes the same type of representation as before.

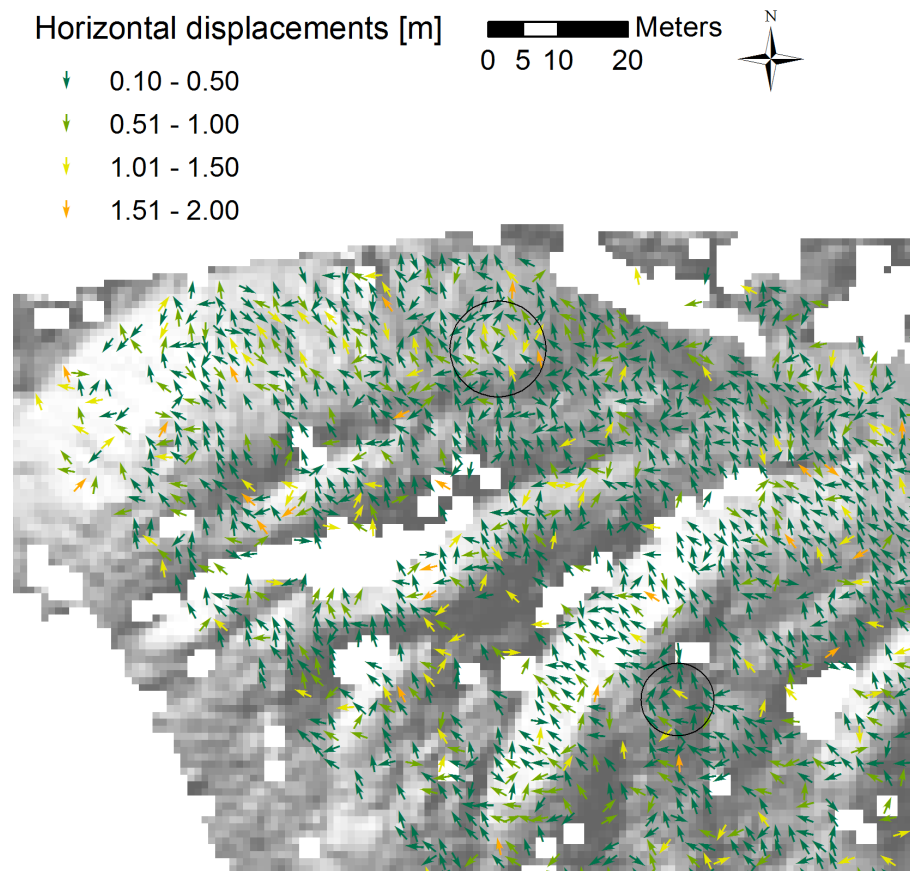


Figure 7.6: Horizontal displacements concerning the seasonal time span and the lower part of the rock glacier, shown by arrows colored according to their length change, DEMs possess a cell size of 0.5m, circles indicate locations of curls.

Investigating the figure above, a conspicuous flow movement pointing to the front is visible, which is mainly established by the dark green arrows. Accordingly, the main displacements range here between 0.1 and 0.5m. However, in between, larger displacements of the remaining classes also occur. As noticeable features, the developing curls have to be mentioned (see circles).

Similarly to Figure 7.3, the subsequent Figure 7.7 represents displacements at the rock glacier front, measured by manually selected points. Considering the modified order of magnitude, the break values of the individual classes have been adjusted and now range between 0.10 and 1.14m.

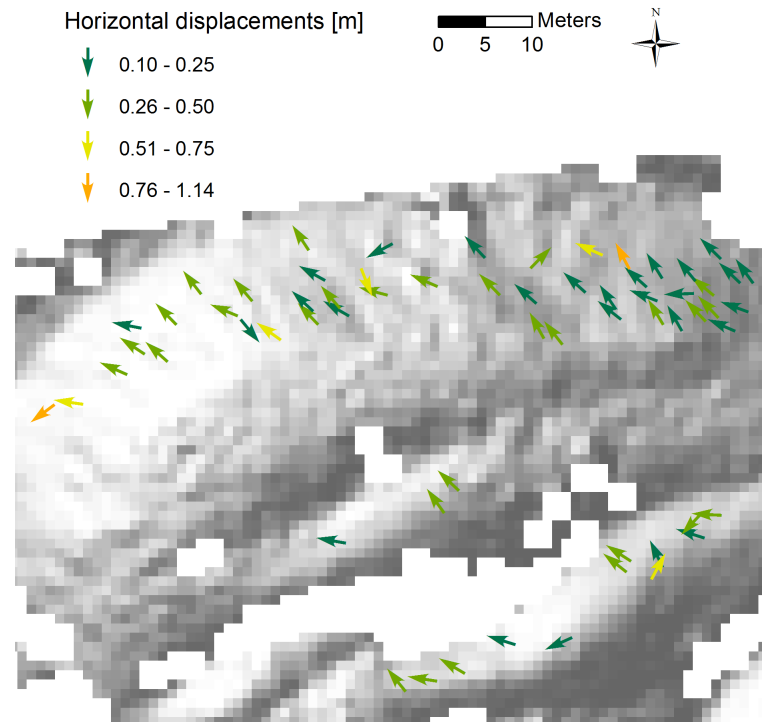


Figure 7.7: Horizontal displacements concerning the seasonal time span and the rock glacier front, shown by arrows colored according to their length change, measurement by manually selected points, DEMs possess a cell size of 0.2m.

Overall, the existing displacements range between 0.1 and 1.14m. A slight tendency of rather small displacements in the eastern part and fairly larger length changes in the western part is observable. With respect to the flow direction, the existing displacements reveal a fairly consistent direction to the north-northwest. However, a few outliers pointing to differing directions occur as well.

7.1.3 Annual time span (July 2013 - July 2014)

The third observed time span covers an entire year and includes displacements between the beginning of July 2013 and the end of July 2014. Similarly to Figures 7.1 and 7.4, Figure 7.8 shows the result for the entire rock glacier by representing the displacements as graduated symbols. As the actual period is considerably longer, the specific pixel sizes (i.e. RBS and TAS), determined by Formula 6.3, were modified (see Table 7.3). Furthermore, the threshold for the maximum values was enlarged to 3m, as displacements possibly exceed 2m. Similar to the previous periods, the subsequent table provides an overview of the important parameters used for the results.

Table 7.3: Specific parameters concerning the results of horizontal displacements for the annual period and all included figures.

	Figure 7.8	Figure 7.9	Figure 7.10
Cell size [m]	0.5	0.5	0.5
RBS [pixels]	5	5	5
TAS [pixels]	10	10	10
Meas. points	Txt-file	Polygon	Polygon
Mean [m]	0.74	0.9	1.03
St. deviation	0.54	0.61	0.65
Max. corr. Coeff.	< 0.8	< 0.8	< 0.7
Min. length [m]	< 0.1	< 0.1	< 0.1
Max. length [m]	> 3	> 3	> 3
	Figure 7.11	Figure 7.12	Figure 7.13
Cell size [m]	0.5	0.5	0.2
RBS [pixels]	5	5	15
TAS [pixels]	10	10	20
Meas. points	Polygon	Polygon	Man. selected
Mean [m]	1.03	1.27	0.3
St. deviation	0.65	0.73	0.14
Max. corr. Coeff.	< 0.7	< 0.7	< 0.3
Min. length [m]	< 0.1	< 0.1	< 0.1
Max. length [m]	> 3	> 3	-

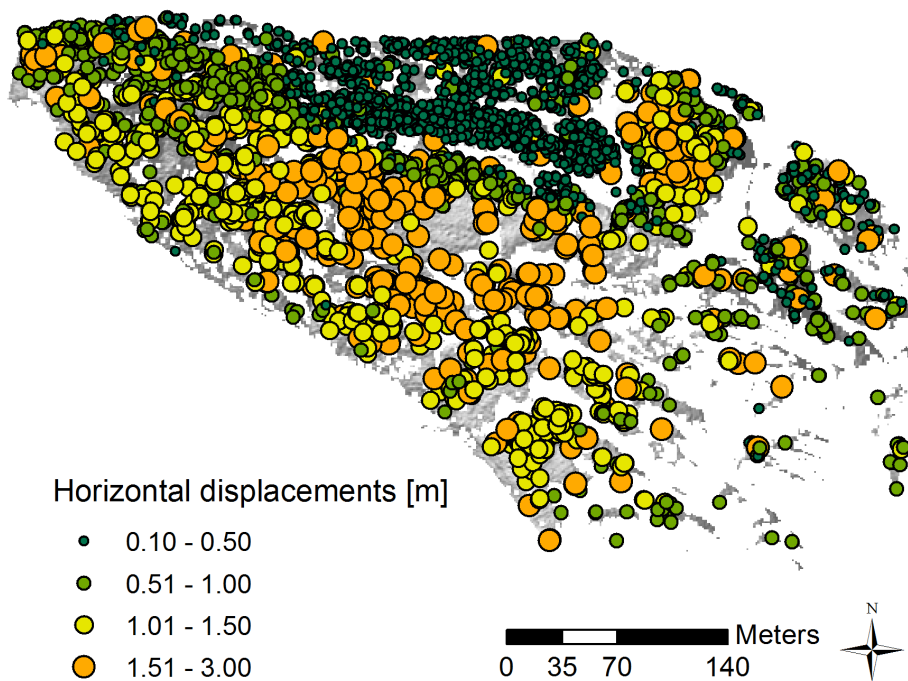


Figure 7.8: Horizontal displacements concerning the annual time span and the entire rock glacier, shown by graduated symbols, DEMs possess a cell size of 0.5m.

Investigating Figure 7.8, it is conspicuous that individual regions reveal distinct patterns. Overall, it can be stated that the displacements are in a larger order of magnitude, compared to the equivalent figures of the previous periods. With respect to the considerably larger time lapse, though, this is hardly surprising. An area showing a fairly distinct pattern is the region beside the actual rock glacier, where displacements mainly between 0.1 and 0.5m occur. An additional evident trend is visible within the middle section, which includes an accumulation of orange dots (i.e. 1.51 to 3.0m). The lower part is characterized mainly by displacements ranging from 0.51 up to 1.5m, yet in between larger displacements from 1.51 to 3.0m also appear. The area of the break-out zone includes, again, displacements covering the entire range. Finally, the zone behind that area shows rather smaller length changes between 0.51 and 1.0m, whereas the uppermost area of the rock glacier includes displacements mainly within the range of 0.51 and 3.0m.

The subsequent Figure 7.9 covers the area of the entire rock glacier and represents the displacements by means of arrows with length-specific coloring, similarly to Figure 7.5.

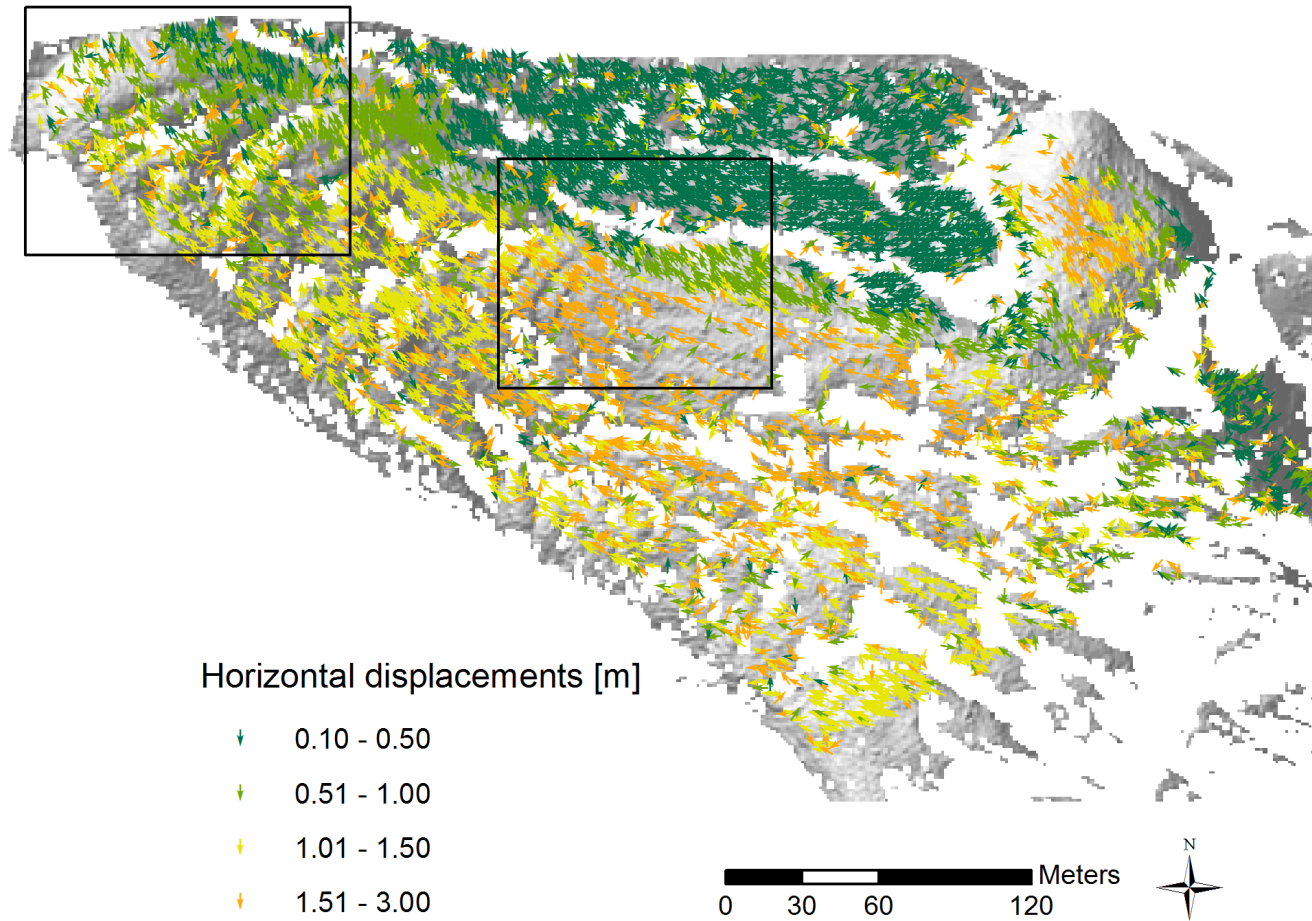


Figure 7.9: Horizontal displacements concerning the annual time span and the entire rock glacier, shown by arrows colored according to their length change, DEMs possess a cell size of 0.5m. The rectangle to the upper left marks the section depicted in Figure 7.9, the rectangle in the center marks the section depicted in Figures 7.11 and 7.12.

By investigating Figure 7.9, the several patterns mentioned in Figure 7.8 become even more distinct: the area beside the rock glacier is now clearly predominated by displacements within the range of 0.1 to 0.5m. The border region at the orographically right side of the lower part shows a pattern of displacements between 0.1 and 1.0m, whereas the counterpart on the orographically left side rather includes larger changes between 1.01 and 1.51m. Furthermore, the aforementioned large displacements within the middle section (i.e. 1.51 to 3.0m) are observable again, and the adjacent area to the north reveals a clear decrease of displacement rates (i.e. 0.51 to 1.0m). Similarly to the previous result, the break-out zone is characterized by large displacements in the range between 1.01 and 3.0m. Finally, the zone behind that area includes displacements from 0.1 to 1.0m, and the uppermost zone reveals rather large changes between 1.01 and 1.5m. Concerning the directional pattern of the flow movement, the arrows point mainly to the northwest.

Figure 7.10 represents an enlarged view of the lower part (see rectangle to the upper left in Figure 7.9). The displacements are illustrated by the same type of representation as before.

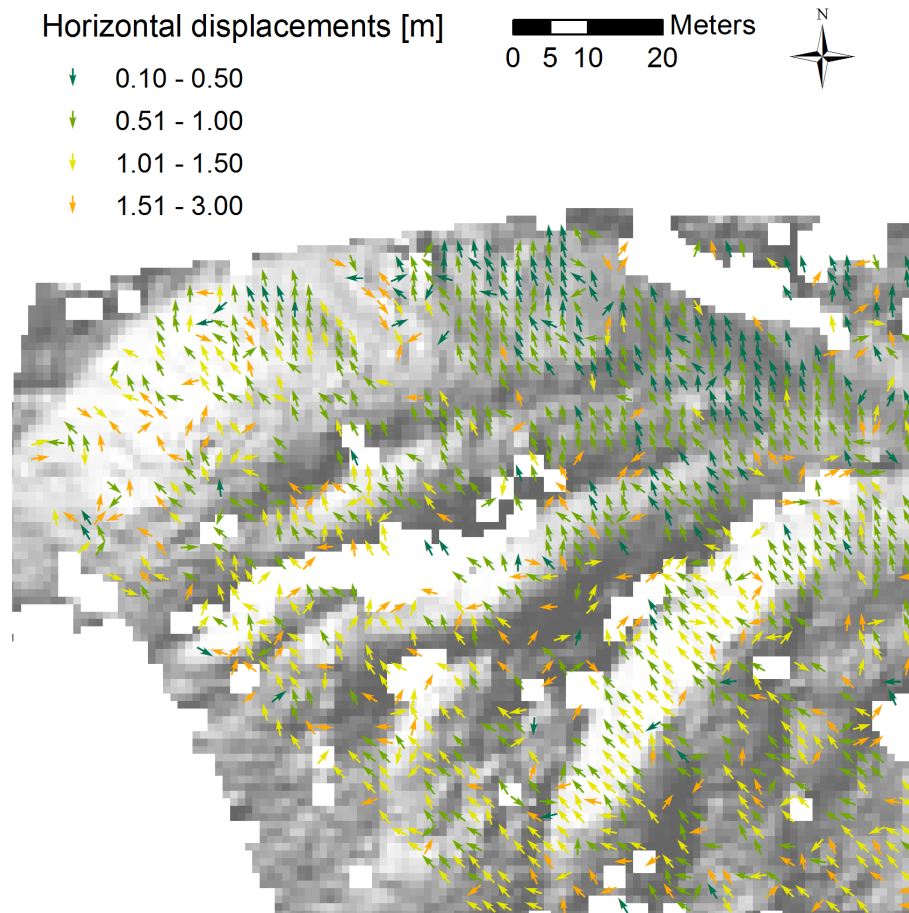


Figure 7.10: Horizontal displacements concerning the annual time span and the lower part of the rock glacier, shown by arrows colored according to their length change, DEMs possess a cell size of 0.5m.

The majority of the arrows in Figure 7.10 point northwest, establishing a distinct pattern of flow movement. Besides this, two of the aforementioned patterns reappear: firstly, the area on the orographically right side within the lower part is characterized mainly by small displacements between 0.10 and 1.0m. Secondly, the counterpart on the left side reveals comparably larger displacements ranging from 1.01 to 3.0m. Furthermore, the curls, which were observed in Figure 7.6, have almost vanished in the actual result.

As mentioned in the chapter on methods and data, low pass filtering was applied in order to investigate its implications compared to the common DEMs. Exemplarily, Figures 7.11 and 7.12 show the result for the middle section of the rock glacier (see rectangle in the center in Figure 7.9).

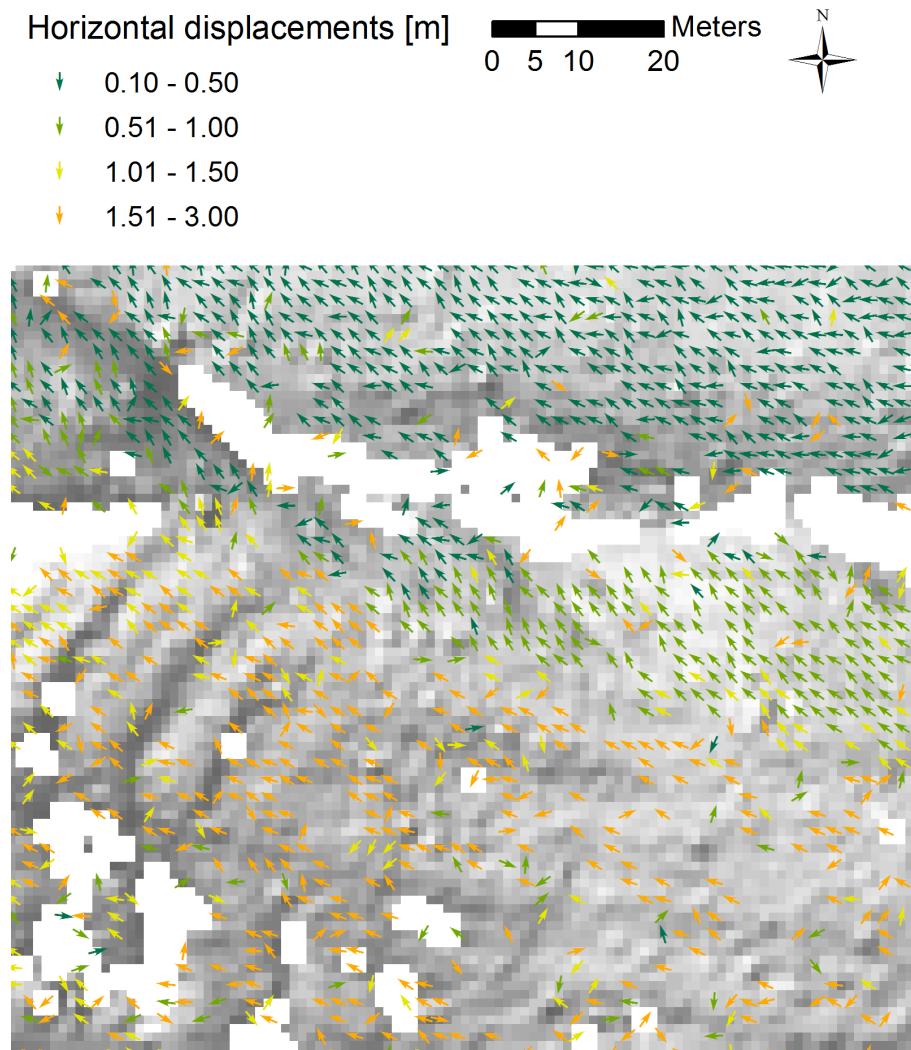


Figure 7.11: Horizontal displacements concerning the annual time span and the middle section, shown by arrows colored according to their length change, DEMs possess a cell size of 0.5m.

Considering the following Figures 7.11 and 7.12, the focus is on specific movement patterns of several areas. In Figure 7.11 a fairly ordered flow movement pointing northwest occurs within the area beside the rock glacier in the north. The flow pattern within the adjacent border area of the rock glacier points rather north-northwest, whereas within the area in front of the middle section, a flow movement pointing northwest is detectable again. In contrast, the middle section does not provide a contiguous directional pattern concerning the flow movement.

As mentioned above, Figure 7.12 shows the same area of interest as Figure 7.11, yet the measurement was conducted on the basis of low pass filtered DEMs.

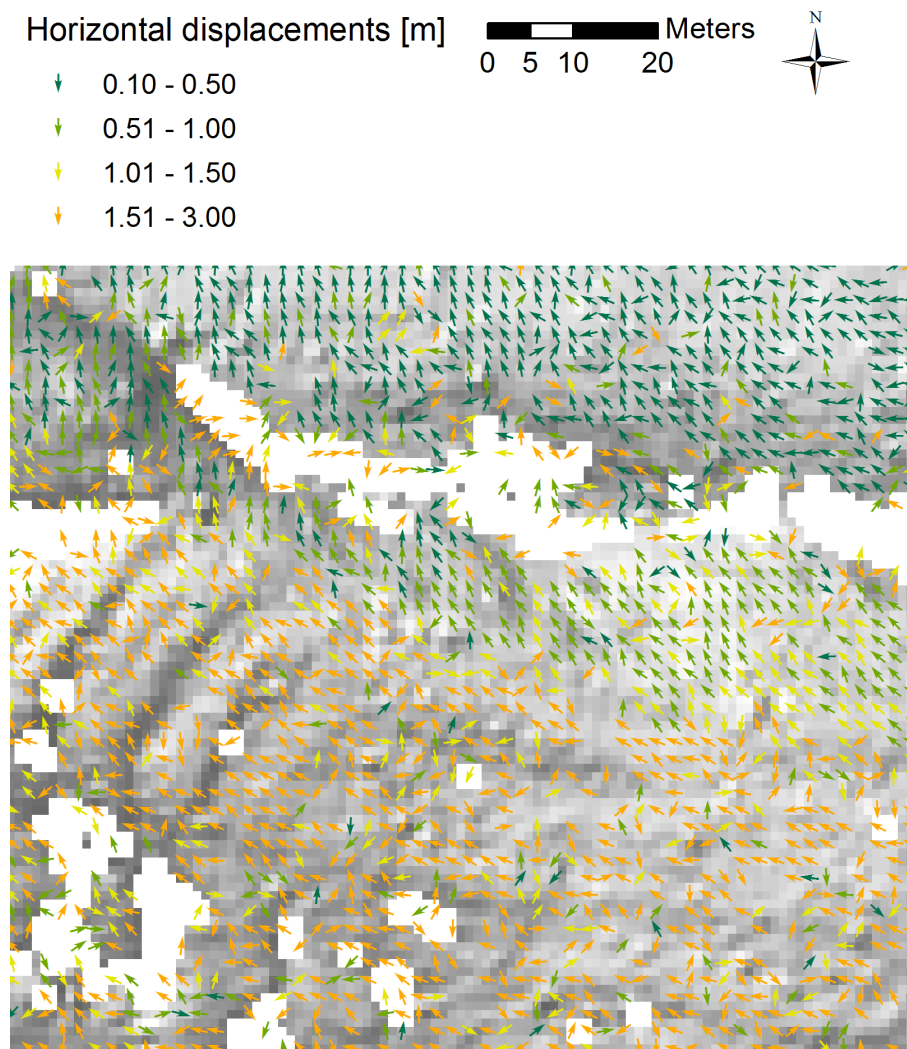


Figure 7.12: Horizontal displacements concerning the annual time span and the middle section, shown by arrows colored according to their length change, DEMs possess a cell size of 0.5m and a low pass filter was applied.

The previously discussed patterns are resumed by examining the result of the low pass filtered DEMs (Figure 7.12) and comparing that to the outcome of the common DEMs (Figure 7.11): the flow movement within the area beside the rock glacier body appears a little less structured, and the direction has changed to rather north-northwest. The adjacent border area remained more or less stable concerning both results, whereas in front of the middle section

a more regular flow pattern is visible in Figure 7.12. However, the area within the middle section has modified even more drastically. While in the previous result no contiguous pattern could be described, a rather coherent flow movement pointing northwest is detectable in the actual outcome. Possible reasons for these findings are provided in the discussion.

Concluding the section of horizontal displacements, Figure 7.13 represents the result for manually selected points at the rock glacier front. Similar to the relevant results of the previous periods (Figures 7.3 and 7.7), the break values were adjusted according to the actual order of magnitude and range between 0.10 to 1.00m.

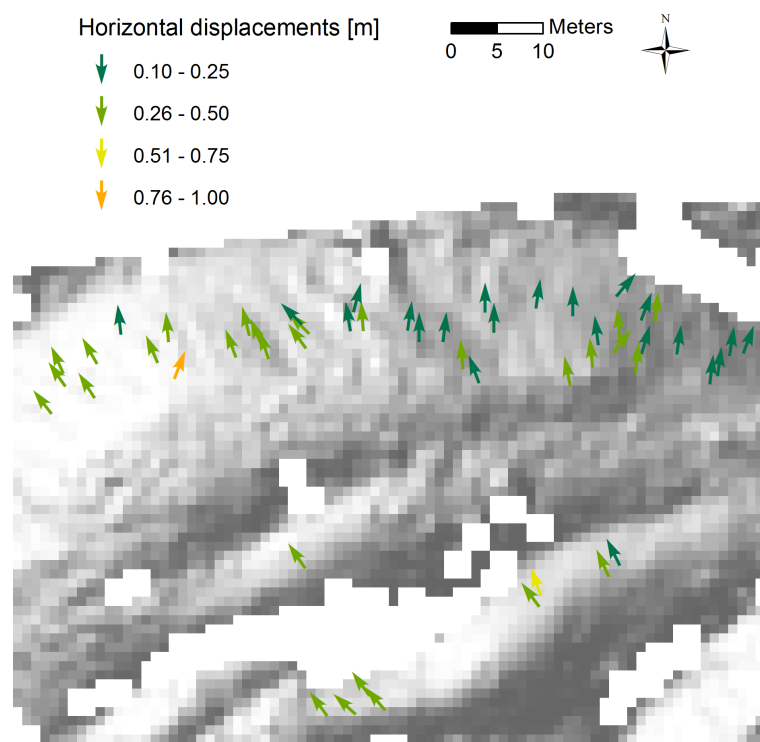


Figure 7.13: Horizontal displacements concerning the annual time span and the rock glacier front, shown by arrows colored according to their length change, measurement by manually selected points, DEMs possess a cell size of 0.2m.

Overall, the resulting displacements range between 0.1 and 1.0m. Furthermore, a slight shift from rather small displacements within the area on the right side (i.e. 0.1 to 0.5m) to larger displacements on the left side is observable (i.e. 0.5 to 1.0m). Concerning the direction of the arrows, the latter area includes mainly movements pointing north or northwest, whereas the counterpart on the right side rather reveals north and northeast as directions. Finally, the

individual lobes reveal moderate displacements within the range between 0.1 and 0.75m.

7.2 Vertical surface changes

In addition to horizontal displacements, vertical surface variations occurring during the various time periods are examined in the following. For this, the particular DEMs of the periods are deducted from each other by the application of the *Minus* function in ArcGIS. This processing is done with DEMs possessing both a cell size of 1, and 0.5m, respectively. Due to the increased accuracy and degree of detail incorporated in 0.5m DEMs, subsequently, those results are provided exclusively. On the basis of the histogram and the revealed Gaussian distribution, distinct outliers are excluded, so that the majority of the values can be treated in more detail. In order to allow the best possible comparison of the individual outcomes, equal break values of the classes are determined for each result. With respect to the standard deviations of the co-registration between 0.118 and 0.134m, a class is defined between -0.15m and +0.15m, including the range of uncertainty and indicating stable areas. The remaining classes range between -1.0 and -0.31m, -0.30 and -0.16m, +0.16 and +0.3m, and +0.31 and +1.0m. Regarding the coloring, greenish colors indicate increases in height, whereas reddish colors show height decreases. Lastly, no color is assigned to the class in between, as this allows for a better separation of stable areas and uncertain results.

Similarly to the section before, the individual time periods are examined separately. Furthermore, a table summarizing the specific statistical information of the results is provided subsequently.

7.2.1 Monthly time span (July 2013 - August 2013)

Table 7.4: Statistical values of the measurements concerning vertical surface changes for the several time periods.

Period		Min. [m]	Max. [m]	Mean [m]	Standard dev.
Monthly	Figure 7.14	-4.33	+3.06	+0.09	0.17
Seasonal	Figure 7.15	-4.63	+2.36	-0.07	0.13
Annual	Figure 7.16	-4.65	+2.91	0	0.23

Figure 7.14 represents the result of the vertical surface changes concerning the monthly period.

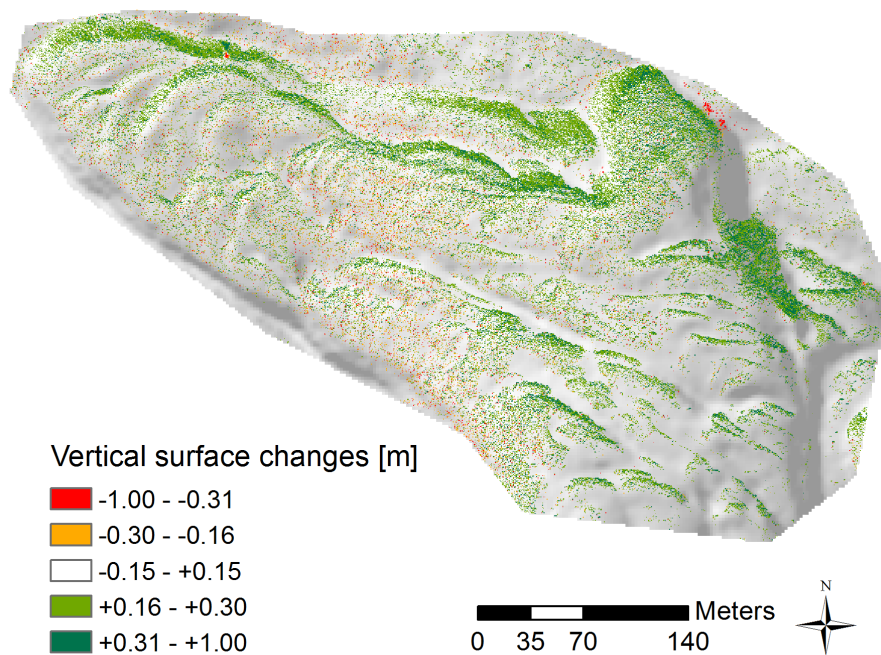


Figure 7.14: Vertical surface changes concerning the monthly time span and the area of the entire rock glacier with a cell size of 0.5m, underlying base map from SwissALTI3D, Swiss Federal Office of Topography (Swisstopo).

Considering the result of the monthly period, it is noticeable that the majority of the measured vertical changes lies within the range of -0.15 and +0.15m. Besides this, a distinct tendency of a slight height increase (i.e. +0.16 to +0.3m) is indicated by the light greenish pixels. These are accumulated exceptionally at the rock glacier snout, the frontal parts of the lobes, the border areas, the region behind the break-out zone, and within the uppermost area. The complement class, indicating vertical changes between -0.16 and -0.3m, is very weakly represented; only a few accumulations are visible within the middle section and the area on the orographically left side at higher altitudes. Similarly, the most negative (i.e. -0.3 to -1.0m) and the most positive (i.e. +0.3 to +1.0m) surface changes constitute the minority; however, a conspicuous feature is observable at the orographically right side of the rock glacier front. Here, a distinct decrease in height at the top of the front is adjacently balanced by an evident height increase at the bottom. An additional accumulation of strong negative surface changes is detectable northeasterly of the break-out zone.

7.2.2 Seasonal time span (July 2013 - October 2013)

The vertical surface changes measured during the seasonal time period are shown in Figure 7.15.

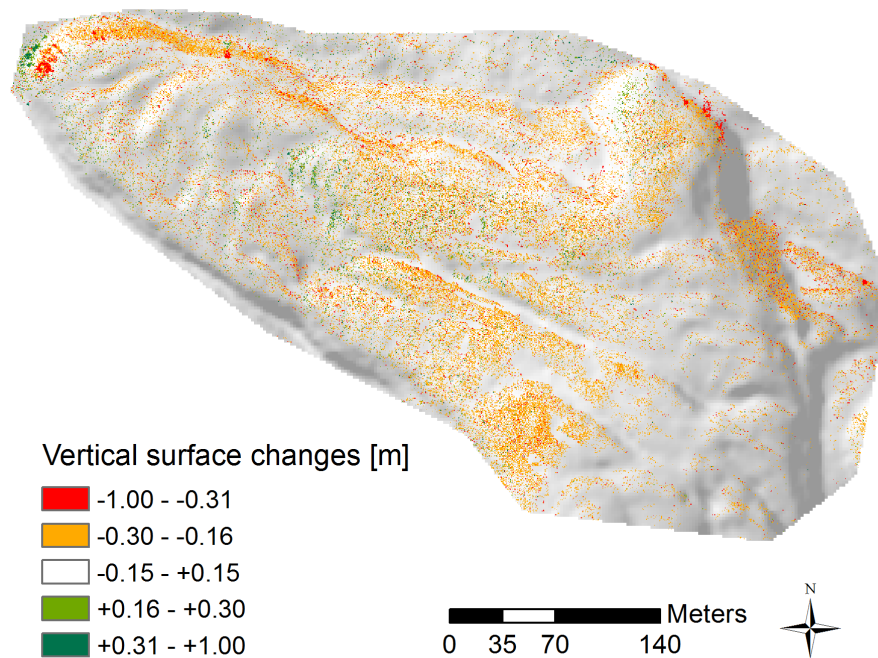


Figure 7.15: Vertical displacement measurement concerning the seasonal time span and the area of the entire rock glacier with a cell size of 0.5m, underlying base map from SwissALTI3D, Swiss Federal Office of Topography (Swisstopo).

The overall appearance of the existing height variations has changed drastically, compared to the monthly time span. Instead of the previously described tendency of a slight height increase, the actual result reveals a contrary general trend of a weak height decrease within the range of -0.16 to -0.3m. Considering the individual mean values of +0.09m (i.e. monthly period) and -0.07m (i.e. actual period), this finding is confirmed. However, it has to be stated that most of the areas of the rock glacier surface still represent changes between -0.15 and +0.15m, and hence indicate stable or uncertain zones. Some slight trends of height increases are visible at the front of the individual lobes within the area of the middle section as well as at the frontal part of the break-out zone. Lastly, the aforementioned feature of contiguous height decreases and increases at the rock glacier front appears again. Additionally, similar features are detectable within the western part of the front.

7.2.3 Annual time span (July 2013 - July 2014)

The resulting vertical surface changes within the annual period are represented in the subsequent Figure 7.16.

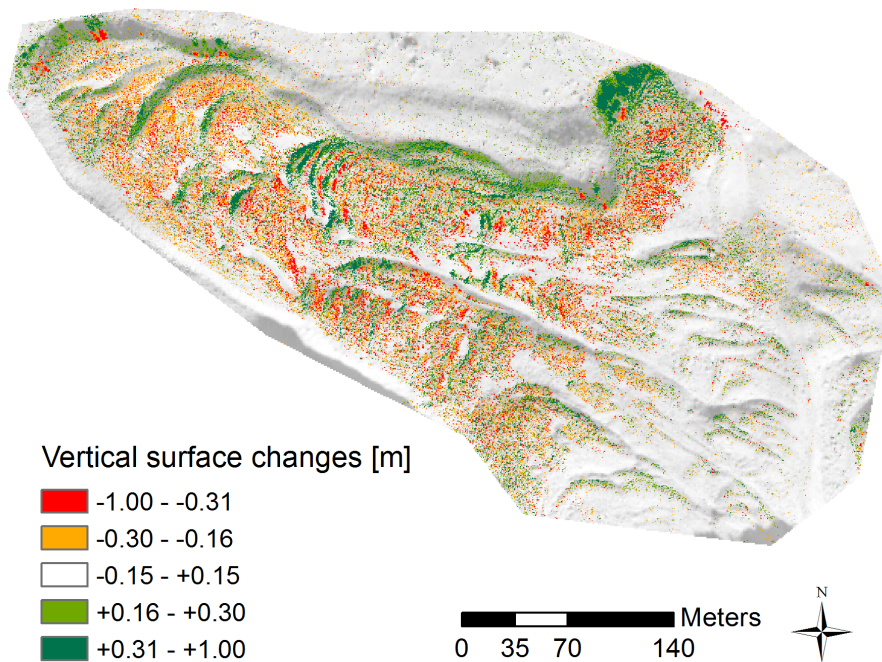


Figure 7.16: Vertical displacement measurement concerning the annual time span and the area of the entire rock glacier with a cell size of 0.5m, black dots indicate reference points, underlying base map from SwissALTI3D, Swiss Federal Office of Topography (Swisstopo).

Contrary to the previous results, in the actual outcome no overall tendency of height changes is observable, which is confirmed by the mean value of 0m. Instead, a highly detailed representation of small-scale variations including all existing classes is provided. As a considerable part of the rock glacier body incorporates surface changes smaller or larger than -0.15 and +0.15m, the actual body can be clearly distinguished from the surroundings. Exemplarily, the northerly region beside the rock glacier is almost free of colored pixels, which indicates a stable or uncertain zone, whereas the adjacent rock glacier surfaces reveal highly significant surface variations. The individual small-scale patterns are examined subsequently.

Beginning with the rock glacier front, the aforementioned evident height decreases and increases appear again, and similar features occur in the northeasterly part of the front as well. Within the area behind the rock glacier front the individual lobes can be detected easily, as their faces indicate evident increases in height between +0.16 and +1.0m. The surfaces adja-

cent to those faces are characterized by rather moderate height decreases within the range of -0.16 to -0.30m. The existing ridges and furrows in front of the middle section exhibit similar patterns, though here, the relating increases and decreases have magnitudes of mainly +0.31 to +1.0m and -0.31 to -1.0m, respectively. The overall appearance of the middle section reveals highly varying surface changes, which cover the entire range. On the surface of the break-out zone a sequence of rather strong height decreases and increases is observable, whereas its frontal part is evidently characterized by maximum height increases between +0.31 and +1.0m. Lastly, the uppermost part of the rock glacier incorporates primarily surface variations between -0.15 and +0.15m. The question of whether this is due to extraordinarily stable conditions or because of the occurrence of data voids is the subject of the subsequent discussion.

7.3 Additional data

In the chapter on the state of knowledge, the additional data for the purpose of evaluating the results have been mentioned. These data sets are subsequently presented and examined, similar to the previous approach.

Figure 7.17 shows horizontal displacements for specific measurement points and the period of an entire year (5 July 2013 and 25 July 2014). The measurements were carried out by means of terrestrial point measurements (see Figure 2.5). In order to enable a comparison, the coloring has been chosen similarly to the previous results of the horizontal displacements. The actual mean value is 1.04m.

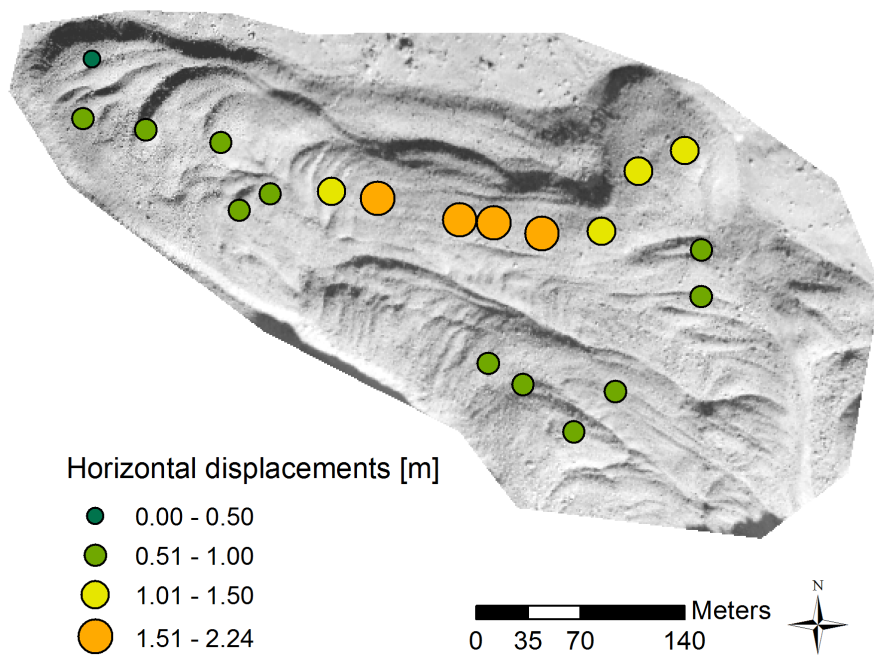


Figure 7.17: Horizontal displacements between 5 July 2013 and 25 July 2014, shown by points with specific coloring and sizes; underlying orthophoto from 2007, proceeded by I. Gärtner-Roer.

The figure above indicates the following movement patterns: smallest displacements between 0 and 0.5m are measured within the area of the lower part. Behind this region and higher up, the displacements increase and reach their maximum of up to 2.24m in the area of the middle section. Behind that and in the area of the break-out zone, rates in the range of 1.01 and 1.5m are registered. Finally, the area behind the break-out zone and the uppermost part of the rock glacier are characterized by displacements in the range of 0.51 to 1.0m.

Figure 7.18 represents the same reference points as before, yet here, vertical surface changes are shown. The coloring and the break values are chosen as follows: dark green (-0.10 to -0.30m) and light green (-0.31 to -0.50m) indicate small and moderate changes, while orange (-0.51 to -0.70m) and red (-0.71 to -0.90m) represent larger variations.

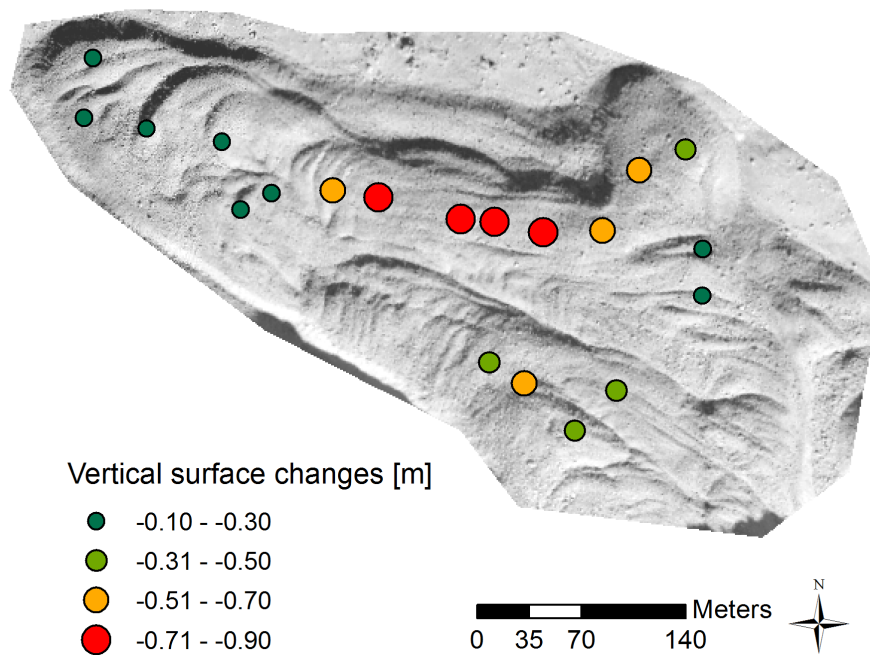


Figure 7.18: Vertical surface changes between 5 July 2013 and 25 July 2014, shown by points with specific coloring and sizes; underlying orthophoto from 2007, proceeded by I. Gärtner-Roer.

In Figure 7.18 the following patterns are observable: first, the lower area of the rock glacier is characterized by small height changes in the range of -0.10 to -0.30m. Larger variations in height are measured within the area of the break-out zone as well as in the uppermost region of the rock glacier. Here, vertical changes between -0.31 and -0.70m are revealed. While the area behind the break-out zone shows variations between -0.10 and -0.30m, the middle section is characterized by maximum displacements within the range of 0.71 to -0.90m. Just in front of that area, the orange measurement point indicates vertical changes between -0.51 and -0.70m.

8 Discussion

In the subsequent discussion the reasonability of the results is evaluated by consulting findings in literature and additional data. In other words, the research questions dealing with the analysis of the results are considered. The initial part focusses on the horizontal displacements occurring within the individual time spans. The various periods are discussed separately, and the specific findings are subsequently compared and evaluated. The second part includes the examination of the vertical surface changes. This section pursues the same approach and involves an assessment and a comparison of the results.

8.1 Horizontal displacements

8.1.1 Monthly time span (July 2013 - August 2013)

The individual results of the monthly period reveal a few conspicuous characteristics: overall, it can be noted that the major part of the measured displacements appears to be in the smallest class within the range of 0.1 and 0.5m. With respect to the considerably short time lapse, this fact can be regarded as positive. Furthermore, the slight tendency of apparently larger displacements within the area of the middle section is noteworthy. According to PERMOS (2013), who bore maximum displacement rates of 1.5ma^{-1} within that particular area, the observed trend can be considered reasonable. Another area including a broad range of displacements is the break-out zone. With respect to the previous data set of PERMOS (2013), which revealed displacements between 0.6 and 0.8ma^{-1} , it appears that this detected tendency can be evaluated as faithful as well. With respect to the measurement by manually selected points (see Figure 7.3), solely small displacements between 0.19 and 1m occurred within the part of the snout. Compared to measured displacements in literature (i.e. around 0.25ma^{-1}) (e.g. Käab et al., 2005), this result seems, at least partly, acceptable. Yet, an established assessment concerning the magnitude of these outcomes is not possible, as the length of the actual time span has not been the subject of investigations so far. In addition, the orientation of the flow movement shall be discussed. Considering the resulting directions, it should be stated that the individual orientations differ significantly, and, thus, no contiguous movement pattern is observable. In contrast, the result of the manually selected points reveals fairly linearly arranged displacements, though, pointing northeast or even southeast. With respect to the confirmed downslope movement of rock glacier Muragl (e.g. Käab et al., 2005), this movement pattern needs to be falsified. Besides the aforementioned tendencies, the actual results do not allow for detailed statements about distinct patterns neither concerning displacement

rates nor regarding movement patterns.

Potential problems

The main issue of the observed period becomes obvious consulting Formula 6.3. By inserting the specific values for the time difference (i.e. 0.15 year), the maximum displacement rates (i.e. 2ma^{-1}), and the several cell sizes (i.e. 1, 0.5, 0.2m), test area sizes of 0.6, 1.2, and 3 pixels are returned. According to the premises that the test area should be at least larger than the reference block size, and that input values smaller than two pixels are inadequate (Kääb & Vollmer, 2000), the uncertain outcomes become explicable. Consequently, the actual time lapse between the measurement dates has to be considered too short, with respect to the available cell sizes. An additional disturbing factor is the standard deviation, which developed during the co-registration (i.e. here 11.8cm). Although excluding length values smaller than 0.1m tried to eliminate this error, it still entails some uncertainties to the measurement. This is mainly due to the small displacements, which are assumed to appear during the actual period. In addition, the considerable standard deviations, which arose during the measurements, have to be examined. Except for the result of the manually selected points, these values are regarded as significant, compared to the related mean values. Possible reasons for these errors are firstly the occurrence of data voids, and secondly the uncertainty due to the inappropriate input values.

In the chapter on methods and data it was mentioned that the DEMs were stretched by a MATLAB script in order to obtain the full range of greyscale values. For the purpose of an evaluation of possible implications, the results of both unstretched and stretched DEMs were compared. As an outcome, it can be stated that absolutely no differences occurred between these approaches. Accordingly, the measurement process of the CIAS software (Kääb & Vollmer, 2000) does fully consider existing differences in the DEMs concerning the range of the greyscale values.

Findings

Overall, it can be noted that at least a few tendencies are observable. With respect to measured annual displacement rates between 0.01ma^{-1} (Kääb & Vollmer, 2000) and 1.5ma^{-1} (PERMOS, 2013), though, especially displacements larger than 0.5m need to be interpreted with caution, bearing in mind the noticeably short time lapse. Furthermore, the direction of the flow movement is considered to be false, as the rock glacier in reality moves downwards, pointing to north-northwest (e.g. Kääb & Vollmer, 2000; Kääb et al., 2005). In summary, the actual time period appears to be too short for this type of measurement, especially concerning the coincidence of inadequate input values and applied cell sizes.

8.1.2 Seasonal time span (July 2013 - October 2013)

Considering the seasonal period, the general appearance is slightly modified compared to the previous period, and a number of small-scale patterns are detectable. Overall, it seems that the group of the smallest displacements does not constitute the major part anymore. Instead, the category including displacements between 0.5 and 1.0m is even predominantly represented in several areas. The most obvious of these regions is the middle section of the rock glacier (see Figures 7.4 and 7.5). Consulting the aforementioned report of PERMOS (2013), and concerning the similar finding of the previous period, this detected tendency of rather large displacements within that area can be regarded as reasonable. Additionally, strong seasonal variations of the flow speed at Muragl rock glacier need to be considered (Kääb & Vollmer, 2000). While minimum rates of about 0.01ma^{-1} were measured in spring and early summer, the highest displacements of up to 1ma^{-1} were detected in late autumn (Kääb & Vollmer, 2000). Accordingly, the actual resulting displacements between 0.51 and 1.0m within the middle section can be further confirmed. An additional distinct pattern appears at the orographically right side within the lower part of the rock glacier. Considering Figures 7.5 and 7.6, mainly displacements between 0.1 and 0.5m were measured here. In order to assess this outcome, results from borehole measurements are consulted (see Arenson et al., 2002). The relevant borehole (borehole 1/1999) is situated adjacent to that border area and does not contain ice at present (Arenson et al., 2002). Accordingly, the correspondent region is considered to be within a currently less active zone of the rock glacier (Maurer & Hauck, 2007). This finding is supported by means of geoelectric and seismic measurements, by which a degraded permafrost body was detected in the ground at the location of borehole 1/1999 (Maurer & Hauck, 2007). With respect to these prevailing conditions, the measured displacements between 0.1 and 0.5m can be regarded as realistic. Furthermore, the break-out zone is examined. Similarly to the result of the monthly period, a rather wide range of displacement is observable here. Even if PERMOS (2013) bore fairly large displacements between 0.6 and 0.8ma^{-1} , at least the measured length changes larger than 1m are regarded as clearly overestimated. Considering the uppermost region of the rock glacier, rather small displacements within the range of 0.1 and 0.5m were measured (see Figures 7.4 and 7.5). As the reference points reveal displacements between 0.51 to 1.0m, and additional literature yielded displacements around 0.5m within that area (Kääb et al., 2005), this outcome is deemed to be reasonable. With respect to the manually selected points at the rock glacier snout, a slight tendency of rather small displacements in the eastern part and fairly large displacements in the western area appears. Examining this pattern, firstly, the currently less active state of the rock glacier at the orographically right side is mentioned. Secondly, decreasing flow speeds lead to an actual horizontal flow compression within that area and, hence, to the development of the evident ridges and furrows (Kääb et al., 2005; Kääb

& Vollmer, 2000). Consequently, at least the tendency of smaller displacements in the eastern part appears explicable. Overall, the existing order of magnitude at the rock glacier front is considered to be reasonable, as Käab et al. (2005) refer to maximum length changes of up to 0.45ma^{-1} for that particular area.

A further conspicuous pattern involves the orientation of the flow movement. While the directions in the monthly period established an unordered appearance, here, a partly contiguous flow movement pointing north (e.g. break-out zone) and northwest (e.g. middle section) is detectable. Consulting findings in literature (e.g. Käab et al., 2005; Debella-Gilo & Käab, 2011), these particular motional patterns agree quite well. Nevertheless, the appearing curls have to be taken into account (see Figure 7.6). These features indicate potential problems during the process of finding corresponding points, and are mainly due to ambiguous conditions such as strongly undulated surface properties, shadows, or the occurrence of snow patches (Käab & Vollmer, 2000).

Potential problems

Reviewing the aforementioned outcomes, the resulting displacements are quite often overestimated. In order to provide a possible reason, Formula 6.3 is consulted and the specific input variables are examined: the time difference is calculated as 0.3 year, the maximum annual displacement remains 2ma^{-1} , and the cell sizes are still 1, 0.5, and 0.2m. Accordingly, specific test area sizes of 1.3, 2.6, and 6.6 pixels should have been applied for the measurements. Because at least the pixel sizes of 1.3 and 2.6 are not in an adequate order of magnitude, this must be considered to be a potential source of problems. Similarly to the previous period, further potential errors lie in the process of co-registration. Although the standard deviation is about 13.4cm for the actual time span, its implication is diminished, compared to the monthly time span. This is due primarily to the fact that displacements are now likely to be larger than 0.1m. Furthermore, results smaller than 0.1m were excluded anyway, as in the monthly period. In addition, the measurement-related standard deviations are regarded as indicators for potential measurement uncertainties. Considering the actual period, the values are even larger than concerning the previous time span, though this is likely due to the significantly wider range of displacements. An exception exists in the manually selected points, where the particular standard deviation decreased. Accordingly, the actual result is regarded as more reliable than that of the monthly time span.

Findings

Considering the existing results, the major part of the displacements appears to be more or less consistently arranged, which allows for specific spatial characteristics to be observed.

Some of the detected areas with distinct displacement patterns can be reasonably confirmed by consulting reference data or findings in the literature, whereas other areas do not reveal congruent magnitudes of displacements. With respect to the orientation of the flow movement, the existing patterns provide rather natural appearances. While the outcomes of the monthly period did not reveal a contiguous flow, here, the displacements build a fairly distinct network of downward movements.

A further noticeable characteristic is the fact that generally the results become more detailed and reliable by shrinking the applied cell sizes. However, considering the equation for the determination of the test area size, this is hardly surprising. Accordingly, DEMs with a cell size of 0.2m provide tolerably reasonable input values for the observed time lapse. Hence, the achievement of more faithful results can, at least partly, be explained by the more suitable input parameters. Overall, it has to be stated that a considerable part of the existing displacements appears to be overestimated.

8.1.3 Annual time span (July 2013 - July 2014)

On the basis of the existing annual results, a few of the aforementioned findings can be recognized and confirmed. Additionally, further evident patterns of displacement rates and flow movement directions appear. Initially, the specific mean value of 0.74m for this period is mentioned (see Figure 7.8). Compared to the previous time spans, which revealed a mean value of 0.41m (i.e. seasonal) and 0.34m (i.e. monthly), this general enlargement seems plausible.

In order to assess the reasonability of the results, appearing patterns are examined. Beginning with the area northerly of the rock glacier body, a distinct accumulation of smallest displacements is observable (see Figure 7.8 and 7.9). As the same tendency already emerged in the results of the previous periods, and due to the fact that this area beside the actual rock glacier body is not affected by permafrost occurrence (Maurer & Hauck, 2007), this outcome is regarded as faithful. Nevertheless, several larger displacements appear within this area as well, which have to be considered outliers and mismatches. The area on the orographically right side within the lower part is characterized by displacements between 0.51 and 1.0m. With respect to the aforementioned temperature conditions at the adjacent borehole 1/1999 (Arenson et al., 2002), the existing order of magnitude is regarded as relatively high. On the left side within the lower part, larger displacements between 1.01 and 1.5m constitute the major part. Considering the reference points (i.e. 0.35 to 1.0m), and according to findings in literature (i.e. $< 0.5\text{ma}^{-1}$) (Kääb et al., 2005), these resulting displacements are rather overestimated. However, the existing surface inhomogeneity (Kääb & Vollmer, 2000) and the fact that inactive layers are bound to be overridden by active lobes within that area (Kääb et al., 2005) have to be taken into account. Due to the occurrence of that rough small-scale topography, inaccurate or

outlying results are likely to emerge, especially concerning the still short observed time period (Kääb & Vollmer, 2000). The described tendency of enlarging displacements from the eastern part to the western area already appeared in the previous periods, and can be explained by the currently less active state of the rock glacier within the eastern part (Musil et al., 2006). Furthermore, a significant accumulation of displacements ranging from 1.01 to 1.5m appears between the lower part and the middle section. According to the reference points (i.e. 1.01 to 1.5m) and the measured displacements around 1.0m by the PERMOS network (PERMOS, 2013), these length changes are absolutely congruent. In order to examine specific thermal properties within that area, borehole 2/1999 is consulted (see Arenson et al., 2002). Here, the so-called *zero-curtain* effect emerges, which implies uniform temperatures of just below 0°C and, consequently, that this region is close to melting (Arenson et al., 2002). However, the largest displacements of 1.51 to 3.0m appear within the middle section (see Figure 7.9 and 7.10). As the reference points indicate displacements between 1.51 and 2.24m, an agreement between both results is reached. For justifying the existing order of magnitude, actual thermal conditions at boreholes 3/1999 and 4/1999 are consulted. According to Arenson et al. (2002), here, permafrost conditions are discovered, yet, the volumetric ice content of the frozen layers is comparatively low (i.e. 40 to 70% by volume) and heterogenous. Consequently, the coincidence of the creep of warm ice (i.e. just below 0°C), and the temperature-related reduction of shear resistance is considered to be the main reason for the high velocity rates (Arenson et al., 2002). Shear resistance bears strong influences, as borehole measurements provided that 77% (Borehole 3) and 82% (Borehole 4) of the total surface deformation occurs within the shear zone (Arenson et al., 2002). Considering the ice found within the middle section, Hoelzle (1996) indicated that this was probably generated initially higher up, as the lower part of the rock glacier does currently not reveal favourable climatic conditions for permafrost formation. The remaining areas of the rock glacier reveal less coherent patterns. The break-out zone provides a wide range of displacements from 0.51 to 3.0m, which is difficult to assess on the basis of the reference points (1.01 to 1.5m). However, with respect to additional results (e.g. Kääb et al., 2005), which yielded displacements smaller than 0.5ma^{-1} , the order of magnitude needs to be regarded as overestimated. Similarly, the area behind that zone includes displacements covering the entire range. Consulting findings in literature (Kääb et al., 2003), and the reference points (0.51 to 1.0m), the existing result is considered false. Finally, the uppermost part reveals rather large displacements, which seem to be overestimated, as the reference points represent displacements between 0.51 and 1.0m, and findings in literature yielded moderate length changes around 0.5m (Kääb et al., 2005). With respect to the last two mentioned areas, the significant amount of data voids can be of great importance. Considering the appearance of the flow direction, it is stated that overall, a reasonable down-

ward movement occurs. Furthermore, by comparing the results of the seasonal period (Figure 7.5) with the actual period (Figure 7.9), it is conspicuous that a few similar movement patterns are visible. Accordingly, the combination of those congruent outcomes and observed or measured motions in literature (e.g. Vonder Mühl, 1993; Debella-Gilo & Käab, 2011), the existing patterns are considered to be truthful and realistic.

In addition, implications of the low pass filter as well as its possible reasons are examined. As seen in the results, the low pass filter has specifically affected the region within the middle section, where a previously unordered movement pattern became a rather structured and contiguous flow movement pointing northwest. Considering the large displacements occurring within this particular area, it is suggested that low pass filtering enables the quantification of highly variable surfaces. With respect to the mentioned area beside the rock glacier, where displacements became rather less regular, a contrary finding can be stated. As low pass filtering entails smoothing of a surface by reducing the local variation (ArcGIS Resources, 2012a), it is likely that the loss of micro-topography may disable reasonable measurements in regions with small variations. Furthermore, the implications were assessed with measurements applying cell sizes of 1m as well. Here, no differences between results with common and filtered DEMs were detectable. This is assumed to be due mainly to the rasterization process, by which DEMs with a cell size of 1m are already smoothed considerably. Consequently, the effect of a further smoothing by the application of a low pass filter is negligible, compared to DEMs with a cell size of 0.5m, allowing the incorporation of highly variable surfaces.

Lastly, the result of the manually selected points shall be discussed (Figure 7.13). At first glance, it seems conspicuous that the mean value of 0.3m is exactly the same as in the previous period (Figure 7.7). Considering the standard deviation of 0.14, which is lower than in the previous result (0.17), however, the actual outcome is regarded as more reliable. The major part of the displacements ranging between 0.1 and 0.5m appears to be exact, as the lowermost point of the PERMOS network, located just in front of the first lobe, revealed a displacement of 0.3m a^{-1} (PERMOS, 2013). The slight tendency of rather smaller displacements within the eastern part to considerably larger changes within the western area was already detected in the previous periods. Similarly to before, the currently less active state of the rock glacier within the orographically right part is mentioned as a possible reason (Maurer & Hauck, 2007).

Potential problems

Considering potential sources of problems, initially, the still short time lapse needs to be mentioned. This is meant mainly in comparison with the conducted studies investigating a time span of 13 years (i.e. 1981 to 1994) (Käab & Vollmer, 2000; Käab et al., 2003). However,

the actual time lapse is only a problematic factor for the measurements applying a cell size of 1m. Considering the specific input parameters (see Formula 6.3), test area sizes of 4, 8, and 20 pixels are determined. While 8 and especially 20 pixels constitute a reliable input parameter, the size of 4 pixels remains unfeasible.

Similarly to the previous periods, the errors caused by co-registration are considered. Yet due to the higher order of magnitude of the displacements, this effect should be tolerable, as the length values smaller than 0.1m were excluded in any event. Further, the measurement-related standard deviations are constantly larger compared to that of the previous periods, except for the result including manually selected points. However, this fact is explicable by the considerably larger range of the observed displacements. Lastly, the unavoidable occurrence of data voids needs to be stated. The most strongly affected area in this regard is definitely the uppermost part of the rock glacier. Specific possible reasons here are rough surface properties, the accumulation of large debris, emerging shadows induced by surrounding rock walls, and the occurrence of individual snow patches. Considering the rasterization process, the lack of data entails strong implications mainly concerning DEMs with a cell size of 0.2 or 0.5m, respectively.

Findings

The overall reliability of the existing results has increased, compared to the findings of the previous periods. This achievement includes both the actual displacement rates and the flow movement patterns. Nevertheless, it has to be stated that the magnitude of the displacements remains quite often overestimated. This effect is especially observable in results, where cell sizes of 1m, or in some cases 0.5m, were applied. Accordingly, the coincidence of a relatively short time lapse and the comparably large cell sizes is regarded as a crucial influencing factor. That finding is confirmed by the reliable results of the manually selected points, where the magnitude of the displacements is most accurate. When comparing the actual results to findings in literature, however, the observed point in time has to be taken into account. This is meant mainly with respect to the often investigated period between 1981 to 1994 (e.g. Käab & Vollmer, 2000; Käab et al., 2003), as the permafrost conditions, and hence the displacement rates, have possibly changed since the 1990s. More recent data (i.e. reference points) and studies (e.g. PERMOS, 2013) support that outcome by yielding larger displacement rates as well.

In addition to the individual displacements, the motional direction has become more reliable and realistic. While the appearances of the seasonal movement patterns were described as partly natural, here, rather uniform flow movements are observable.

8.2 Vertical displacements

In the second part of the discussion, the calculated vertical surface changes are examined and evaluated.

The result of the monthly time period clearly reveals a tendency towards a slight height increase within the range of +0.16 to +0.30m. Yet these surface changes occur exceptionally frequently at the rock glacier front, the faces of individual lobes, the frontal part of the break-out zone, and within the area behind that zone. As these areas of the rock glacier are considered to be especially strongly influenced by mass advection processes (Kääb & Vollmer, 2000), the observed pattern appears reasonable. Furthermore, it is assumed that the result of the actual time period is strongly related to horizontal displacements, as height increases at the front and at faces of lobes generally suggest flow movement. Considering the short time lapse of the observed period, this influencing factor needs, however, to be treated with caution. Besides this pattern, the major parts of the rock glacier surface incorporate changes between -0.15 and +0.15m, which identify uncertain or stable zones. The evident height decrease at the top of the front and the related decrease in height at the bottom are due to the emergence of a distinct mass movement event. Furthermore, the mentioned appearance of rather strong height decreases easterly beside the break-out zone could be the result of disappearing snow due to melting. Overall, it is assumed that the existing patterns primarily represent the result of mass advection and small horizontal displacements.

Considering the seasonal period, the resulting tendency has a contrary appearance. Here, a general pattern of height decreases within the range of -0.16 to -0.30m occurs, which is confirmed by the mean value of -0.07m. With respect to the observed season and specific thermal properties of rock glacier Muragl, the result is explained subsequently: Initially, it is mentioned that the general thermal regime of rock glacier Muragl is primarily controlled by heat conduction (Vonder Mühll et al., 2003). Considering the relatively warm subsurface temperatures (i.e. just below 0°C), the amount of ice contained is relatively low (Vonder Mühll et al., 2003). Due to the additional considerable air-void ratio measured within the permafrost, thus, emerging flow compression can diminish the volume (Arenson et al., 2002). Furthermore, the properties of the shear zone represent an influencing factor, as Arenson et al. (2002) discovered that the major part of vertical deformation takes place within the shear zone. Considering the actual period between July and October including warm atmospheric temperatures, the aforementioned properties become crucial. Due to the warm temperatures, the shear zone moves towards the surface, and permafrost is degraded to a particular amount (Arenson et al., 2002). Thus, the occurrence of permafrost subsidence around -0.1ma^{-1} is suggested (Kääb & Vollmer, 2000), and the resulting pattern is explicable. Aside from these negative surface changes, in-

creases in height appear only at the faces of individual lobes within the area in front of the middle section. Similar to the previous period, these features are considered to be the result of horizontal flow movements. Lastly, similar mass movement events as described before are observable in the western part of the rock glacier front.

Contrary to the previous periods, no overall tendency of vertical surface changes is observable in the annual time span (i.e. mean value is 0m). Though a highly detailed representation of small-scale changes is provided and the body of rock glacier Muragl can be distinguished easily from its surroundings. This is mainly due to the fact that in the actual result considerably fewer pixels are classified within the range of -0.15 and +0.15m. In order to examine the individual patterns of height increases and decreases, the resulting surface changes of the reference points are consulted (see Figure 7.18). Beginning with the lower part of the rock glacier, the reference points indicate surface changes between -0.1 and -0.3m. Considering the actual result of the annual period, this matches quite well, as the reference points are mainly located behind faces of individual ridges. As the formation of those ridges is strongly related to longitudinal compression, a tendency of surface lowering is suggested within adjacent areas behind them (Kääb et al., 2005). Secondly, the area higher up, containing the most evident ridges and furrows, is characterized by strongly varying surface changes. Similar to before, the related reference point is located behind the front of a ridge and indicates a surface change between -0.51 to -0.70m. The area of the middle section does not reveal a general pattern, but shows a highly variable distribution of surface changes covering the entire range. In contrast, the result of the reference points reveals a clear pattern of strong surface lowering between -0.71 to -0.90m. However, when considering their exact locations, it is noticeable that the reference points are truly located within areas of strong negative changes. With respect to the aforementioned longitudinal compression, which is coupled with the formation of ridges (Kääb et al., 2005), the area of the middle section is considered to be strongly affected by surface lowering due to flow extension (Kääb et al., 2005). Considering the actual high horizontal displacement rates within this particular area, the finding is confirmed (see Figure 8.1). Another area with highly variable surface variations is the break-out zone. With respect to the reference points, which indicate surface changes between -0.31 to -0.7m, the measured variations can be considered as truthful. An evident feature is observable at the front of the break-out zone, where strong resulting height increases occur. This pattern is explainable by means of the comparatively large horizontal displacements within that particular area (Debella-Gilo & Kääb, 2011). Lastly, two regions with fuzzy appearances are discussed: the area behind the break-out zone and the uppermost area of the rock glacier. Within the first mentioned area, a slight trend of a height increase is visible. While findings in literature (e.g. Kääb et al., 2003; Kääb & Vollmer, 2000) bore an increase of around $+0.5\text{cm a}^{-1}$, the reference points indicate surface decreases

between -0.1 and -0.3m. Accordingly, a final assessment of the existing result is not possible. Furthermore, the occurrence of data voids has to be taken into account within this area. This issue is of even greater importance considering the uppermost part of the rock glacier, where the majority of the pixels appears to represent surface changes between -0.15 and +0.15 (i.e. stable or uncertain regions). The question of whether these regions are reliably regarded as stable or rather as uncertain due to data voids can be explained by consulting findings in literature. According to Kääb et al. (2003), surface variations between -0.10 and -0.20m are measured within this region, thus, it needs to be stated that data voids possibly disabled a reasonable result in that particular case. The considerable height decreases of up to -0.5ma^{-1} within the upper part of the rock glacier is explained by the distinct melting of ice patches (Kääb et al., 2005).

Comparing the outcomes of the individual periods, it is noticeable that the short time trends of overall height increases (i.e. monthly) and decreases (i.e. seasonal) are balanced during an entire year. This finding is confirmed considering the specific mean values of +0.09, -0.07, and 0m. The resulting outcome of the annual period is absolutely congruent with findings in literature, which stated that no general tendency of a surface change can be detected (e.g. Kääb & Vollmer, 2000; Kääb & Weber, 2004).

8.2.1 Synthesis

In order to put the measured point deformations into a broader context, a combined assessment of the horizontal displacements and the vertical surface changes is provided. For this purpose, vertical surface variations of the same classes are grouped and represented by ellipses. The established spatial patterns indicate the same break-values and coloring as before. For the best possible comparison, the horizontal displacements are illustrated by graduated dots, which represent the previous classes as well.

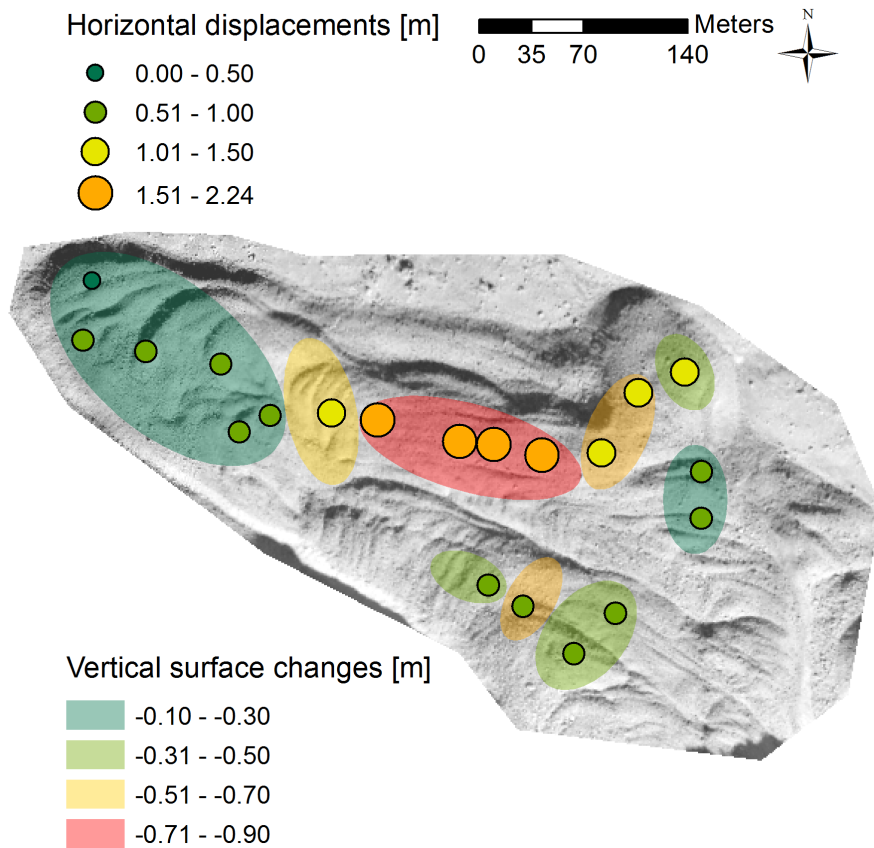


Figure 8.1: Combination of horizontal displacements and vertical surface changes, measured by terrestrial point measurements during the period of 5 July 2013 and 25 July 2014, underlying orthophoto from 2007, proceeded by I. Gärtner-Roer.

Beginning with the spatial pattern within the lowermost part of the rock glacier (i.e. dark green ellipse), the incorporated point measurements indicate horizontal displacements between 0.00 and 1.00m. With respect to the specific point locations, it is stated that the displacements between 0.51 and 1.00m are measured within areas behind individual ridges. As mentioned earlier, these areas are characterized by surface lowering (Kääb & Vollmer, 2000; Kääb & Weber, 2004) and extensive flow speeds (Haeberli et al., 2006). Additionally, the rather stable conditions concerning both, horizontal and vertical deformation, are explicable by the less active state of rock glacier Muragl within the lower part (Musil et al., 2006). The adjacent spatial pattern including vertical changes between -0.51 and -0.71m can be assessed in a similar manner; however, the magnitudes of both parameters are slightly bigger. Following this gradual increase, the spatial pattern with the largest vertical changes (i.e. -0.71 to -0.90m) and the maximum displacements (i.e. 1.51 to 2.24m) appears within the middle section. Addition-

ally to the aforementioned occurrence of extensive flow velocities, considerably steeper slopes have to be taken into account within this area (Arenson et al., 2002). The small break-out zone is characterized by varying vertical changes as well as differing horizontal displacements. This spatial pattern is congruent with the measured displacements, which showed a rather wide variation in length changes with a relatively high order of magnitude. Small vertical changes occur within the area behind the break-out zone. As the measured reference points indicate displacements within the range of 0.51 to 1.0m, this region can be regarded as rather stable. Considering the upper part of the rock glacier, medium surface lowering (i.e. -0.31 to -0.7m) is accompanied by displacements between 0.51 and 1.0m. The last two discussed outcomes are absolutely congruent with the zonal classification by Vonder Mühl (1993), mentioned in the chapter on the rock glacier appearance. Accordingly, the measured deformations represent the current states of the particular parts of rock glacier Muragl.

With respect to the aforementioned findings, it can be stated that most of the areas of rock glacier Muragl reveal contiguous and coherent spatial patterns including congruent vertical changes and horizontal displacements. However, it has to be noted that the actual grouping of vertical surface changes brings about a strong generalization. This is meant mainly with respect to the small-scale topography including ridges and furrows, where considerable height variations occur. Nevertheless, the finding that the body of rock glacier Muragl deforms as a whole with the stress transferring medium of ice (Kääb et al., 2005) can be reproduced by combining vertical changes and horizontal displacements.

9 Conclusion

In this master's thesis, the technique of terrestrial laser scanning is applied to rock glacier Muragl, situated in the Upper Engadin, Switzerland. Based on a conceptual approach, the raw data background of the acquired point clouds is assessed. Furthermore, the specific processing steps needed for the displacement measurements are evaluated regarding its suitability. Subsequently, the results are analyzed in a geomorphological view by consulting additional literature and data, and finally, the suitability of TLS for the specific feature of a rock glacier is assessed and possible improvements are discussed.

Data background

In order to represent real existing objects, the question of whether to use the field- or the object-view appears. As rock glacier Muragl can be regarded as a discrete object, the object-view seems to be more fitting; however, by partitioning the body into several sections, the question of how to merge the individual parts arises. Furthermore, the information about the variation within an object is inaccessible, as objects are homogenous (Gruver, 2014). By representing rock glacier Muragl with the field-view approach, sharp boundaries exist, no overlapping is possible, and implications of planar enforcement into several layers occur (Gruver, 2014). Though, by using field-based representations, digital elevation models can be calculated, which implies a crucial procedure in the current thesis.

Concerning the characteristics of the raw TLS data, an individual point contains specific parameters as $x[m]$, $y[m]$, and $z[m]$, as well as intensity values. Besides this information, a point does not provide any further characteristics. By enlarging the area of interest, a point cloud appears, which allows geometric information to be incurred. Accordingly, humans are enabled to detect at least structural features such as a borderline at this stage. However, in order to notice individual lobes or boulders, it is necessary to obtain large-scale information about the geometrical location and neighbourhood of the point data.

Suitability of data processing

As the exact location of the TLS device is not known during the measurement, the several point clouds have to be co-registered afterwards. Due to unavoidable imprecisions regarding the identification of the targets, this process is prone to errors within the range of centimetres. Additionally, the required georeferencing, which implies the transformation from the project coordinate system into an externally defined coordinate system, heightens the standard deviation to the range of double-digit centimetres. Regarding the process of rasterizing the point data in ArcGIS, the issue of determining reasonable cell sizes occurs. As an implication of se-

lecting cell sizes smaller than 1m, the number of data voids increases drastically. However, the alternative of interpolating the data points by applying the *Kriging* algorithm was abandoned due to the blurring effect and the increase in uncertainty of interpolated values in regions with a considerable amount of contiguous data voids.

Analysis of results

The displacement measurements of the individual time periods provide strongly differing results. Beginning with the monthly time span, it is not possible to detect and confirm distinct patterns, yet at least a few spatial tendencies are observable. The displacements are mainly out of range regarding the order of magnitude and the resulting directions do not reveal contiguous flow movements. Considering the formula for the determination of the specific test area sizes, this is hardly surprising, as the sizes of 0.6, 1.2, and 3 pixels do not represent reasonable input values. Accordingly, the observed time lapse is considered to be too short for the application of the current measurement setup. The measurements of the seasonal period yield more reliable outcomes. Reasons are the longer time lapse and its related input parameters as well as the increased displacements occurring during this period. Nevertheless, the resulting magnitudes appear to be often overestimated, although this late-summer season incorporates the largest displacement rates during the year (Kääb & Vollmer, 2000). Furthermore, the improved reliability of the movement pattern is noted, even if the occurrence of curls indicates emerging sources of problems during the measurements. Finally, most reasonable outcomes concerning both the magnitude and the direction of the displacements, are achieved within the annual period. This is mainly due to the considerably longer observation time, which results in more feasible input values. Nevertheless, existing outliers need to be mentioned, even if their occurrence is restricted mainly to measurements using DEMs with cell sizes of 1m (sometimes 0.5m). Consequently, it can be stated that the annual time span represents the lowermost limit by which the current measurement setup is adequately applicable.

Considering the vertical surface changes, the results of the monthly and the seasonal period reveal slight tendencies of height increase and decrease, respectively. The height increase is considered to be mainly a result of mass advection at the rock glacier front and the faces of individual lobes, whereas the decrease in height during the seasonal period represents a general trend of surface lowering due to permafrost subsidence. In contrast, the result of the annual period does not provide an overall tendency, but reveals a highly detailed representation of small-scale surface changes. These include especially the rock glacier front as well as strong height increases in front of individual lobes and related height decreases behind those features. By combining vertical surface changes and horizontal displacements, it is possible to distinguish contiguous spatial patterns with individual internal characteristics. When bring-

ing them into a broader context, the integrated deformation pattern of rock glacier Muragl is observable.

Suitability and limitations of TLS approach

For the purpose of investigating features in high mountain areas, TLS offers a feasible method due to its compactness, the relatively low weight, and the comparatively high cost efficiency (Lichti et al., 2005; Armesto et al., 2009). Regarding the specific case of a rock glacier, additionally the horizontal measurement perspective plays a key role. This implies, on the one hand, a considerable benefit, as some of the most obvious features of a rock glacier are its steep front and the individual lobes. On the other hand, it is not possible to avoid the occurrence of data voids. Furthermore, the prevailing weather and atmospheric conditions are of great importance. As fog or rain disables a successful scan process and snow patches deliver no data, the measurement campaign has to be planned responsibly (Prokop et al., 2008).

Reviewing the conducted approach, the most serious limitations regarding the displacement measurements are considered to be the coincidence of short observation periods and relatively large cell sizes as well as the data voids implied in the DEMs. Furthermore, the errors within the range of double-digit centimetres, caused by co-registration and georeferencing processes, have to be noted. The related implications lead to a considerable degree of uncertainty concerning displacements within the range of 0 to 0.1m. With respect to vertical surface changes, TLS provides adequate results, allowing small-scale topography to be detected. However, the limitation posed by the occurrence of data voids has to be taken into account as well.

9.1 Outlook

As terrestrial laser scanning represents a rather recent technique, future improvements regarding the technical specifications are expected. These include, among others, accuracy and resolution parameters, the maximum measurement range, and improvements regarding the beam divergence, which corresponds to an increase of 30mm per 100m distance concerning the device used here. Furthermore, a rather remote sensing-related than measurement-related issue implies improvements concerning the appliance of GPS devices in high mountain areas. This is mainly meant with respect to the co-registration of point clouds, which implicitly incorporates a considerable amount of uncertainty. With respect to the increasing number of studies carried out during the past decade, general guidelines for the best possible approach concerning specific fields of application should be established in the near future.

Considering the particular case of investigating a rock glacier surface, more specific studies are needed. This promises improvements concerning the handling of occurring data voids, which are regarded as one of the most serious limitations. Here, the appearance of no data values due to snow patches means a specific field of investigation is needed, especially concerning applications in high mountain areas. Furthermore, alternative approaches in the processing of digital elevation models are required, allowing adequate DEMs with cell sizes of 0.5m or smaller to be processed. The main challenge remains to find an agreement between small cell sizes and a minimal amount of occurring data voids.

Finally, with respect to the actual conducted measurement setup using CIAS Feature Tracking (Kääb & Vollmer, 2000), longer observation periods need to be applied in order to produce reliable input pixel sizes (i.e. reference block and test area sizes). It will be interesting to see what results future studies will bring.

Bibliography

- Abellán, A., Jaboyedoff, M., Oppikofer, T., & Vilaplana, J. M. (2009). Detection of millimetric deformation using a terrestrial laser scanner: experiment and application to a rockfall event. *Natural Hazards and Earth System Sciences*, 9, 365–372.
- Abellán, A., Oppikofer, T., Jaboyedoff, M., Rosser, N. J., Lim, M., & Lato, M. J. (2014). Terrestrial laser scanning of rock slope instabilities. *Earth Surface Processes and Landforms*, 39(1), 80–97.
- Abellán, A., Vilaplana, J. M., & Martínez, J. (2006). Application of a long-range Terrestrial Laser Scanner to a detailed rockfall study at Vall de Núria (Eastern Pyrenees, Spain). *Engineering Geology*, 88(3), 136–148.
- Arayici, Y. (2007). An approach for real world data modelling with the 3D terrestrial laser scanner for built environment. *Automation in Construction*, 16(6), 816–829.
- ArcGIS Resources (2012a). ArcGIS Help 10.1: Filter [Spatial Analyst].
URL <http://resources.arcgis.com/en/help/main/10.1/index.html#//009z000000q000000>, accessed 21.07.2014.
- ArcGIS Resources (2012b). ArcGIS Help 10.1: Hillshade [3D Analyst].
URL <http://resources.arcgis.com/en/help/main/10.1/index.html#//00q900000036000000>, accessed 15.07.2014.
- Arenson, L., Hoelzle, M., & Springman, S. (2002). Borehole Deformation Measurements and Internal Structure of Some Rock Glaciers in Switzerland. *Permafrost and Periglacial Processes*, 13(2), 117–135.
- Armesto, J., Ordóñez, C., Alejano, L., & Arias, P. (2009). Terrestrial laser scanning used to determine the geometry of a granite boulder for stability analysis purposes. *Geomorphology*, 106(3), 271–277.
- Avian, M., Kellerer-Pirklbauer, A., & Bauer, A. (2009). LiDAR for monitoring mass movements in permafrost environments at the cirque Hinteres Langtal, Austria, between 2000 and 2008. *Natural Hazards and Earth System Sciences*, 9(4), 1087–1094.
- Barsch, D. (1992). Permafrost Creep and Rockglaciers. *Permafrost and Periglacial Processes*, 3, 175–188.
- Barsch, D. (1996). *Rockglaciers: Indicators for the Present and Former Geoecology in High Mountain Environments*. Springer Series in Physical Environment. Berlin Heidelberg: Springer.
- Barsch, D., & Hell, G. (1975). Photogrammetrische Bewegungsmessungen am Blockgletscher Murtèl I, Oberengadin, Schweizer Alpen. *Zeitschrift für Gletscherkunde und Glazialgeologie*, 11(2), 111–142.

- Bauer, A., Paar, G., & Kaltenböck, A. (2005). Mass movement monitoring using terrestrial laser scanner for rock fall management. In P. van Oosterom, S. Zlatanova, & E. Fendel (Eds.), *Geo-information for Disaster Management*, Berlin Heidelberg: Springer, pp. 393–406.
- Bauer, A., Paar, G., & Kaufmann, V. (2003). Terrestrial laser scanning for rock glacier monitoring. In M. Phillips, S. Springman, & L. Arenson (Eds.), *8th International Conference on Permafrost, Proceedings*. Lisse: Swets & Zeitlinger, pp. 55–60.
- Berthling, I. (2011). Beyond confusion: Rock glaciers as cryo-conditioned landforms. *Geomorphology*, 131(3), 98–106.
- Betsill, M., & Bulkeley, H. (2007). Looking back and thinking ahead: a decade of cities and climate change research. *Local Environment*, 12(5), 447–456.
- Bian, L. (2007). Object-Oriented Representation of Environmental Phenomena: Is Everything Best Represented as an Object? *Annals of the Association of American Geographers*, 97(2), 267–281.
- Biasion, A., Bornaz, L., & Rinaudo, F. (2005). Laser scanning applications on disaster management. In P. Van Oosterom, S. Zlatanova, & E. Fendel (Eds.), *Geo-information for Disaster Management*, Berlin Heidelberg: Springer, pp. 19–33.
- Bishop, M. P., James, L. A., Shroder, J. F., & Walsh, S. J. (2012). Geospatial technologies and digital geomorphological mapping: Concepts, issues and research. *Geomorphology*, 137(1), 5–26.
- Bitelli, G., Dubbini, M., & Zanutta, A. (2004). Terrestrial laser scanning and digital photogrammetry techniques to monitor landslide bodies. *International Archives of Photogrammetry, Remote Sensing and Spatial Information Sciences*, 35, 246–251.
- Boehler, W., Bordas Vicent, M., & Marbs, A. (2003). Investigating Laser Scanner Accuracy. *The International Archives of Photogrammetry, Remote Sensing and Spatial Information Sciences*, 34, 696–701.
- Booch, G. (1991). *Object-oriented Analysis and Design: with Applications*. San Francisco: Benjamin Cummings, 2nd ed.
- Borges, K. A. V., Clodoveu, A. D. J., & Laender, A. H. F. (2001). OMT-G : An Object-Oriented Data Model for Geographic Applications. *GeoInformatica*, 5(3), 221–260.
- Bornaz, L., & Rinaudo, F. (2004). Terrestrial Laser Scanner Data Processing. In *The International Archives of the Photogrammetry, Remote Sensing and Spatial Information Science Congress*. Istanbul, pp. 514–519.
- Buckley, S. J., Howell, J., Enge, H., & Kurz, T. (2008). Terrestrial laser scanning in geology: data acquisition, processing and accuracy considerations. *Journal of the Geological Society*, 165(3), 625–638.

- Burga, C. A., Frauenfelder, R., Ruffet, J., Hoelzle, M., & Käab, A. (2004). Vegetation on Alpine rock glacier surfaces: a contribution to abundance and dynamics on extreme plant habitats. *Flora - Morphology, Distribution, Functional Ecology of Plants*, 199(6), 505–515.
- Caduff, D., & Timpf, S. (2008). On the assessment of landmark salience for human navigation. *Cognitive Processing*, 9(4), 249–267.
- Clementini, E., & Di Felice, P. (1994). Object-oriented modeling of geographic data. *Journal of the American Society for Information Science*, 45(9), 694–704.
- Congalton, R. G., & Green, K. (2008). *Assessing the accuracy of remotely sensed data: principles and practices*. Boca Raton: CRC Press, 2nd ed.
- Couclelis, H. (1992). People manipulate objects (but cultivate fields): beyond the raster-vector debate in GIS. In A. U. Frank, I. Campari, & U. Formentini (Eds.), *Theories and methods of spatio-temporal reasoning in geographic space*, Berlin Heidelberg: Springer, pp. 65–77.
- Cova, T. J., & Goodchild, M. F. (2002). Extending geographical representation to include fields of spatial objects. *International Journal of Geographical Information Science*, 16(6), 509–532.
- Debella-Gilo, M., & Käab, A. (2011). Sub-pixel precision image matching for measuring surface displacements on mass movements using normalized cross-correlation. *Remote Sensing of Environment*, 115(1), 130–142.
- Deng, Y., & Wilson, J. (2008). Multi-scale and multi-criteria mapping of mountain peaks as fuzzy entities. *International Journal of Geographical Information Science*, 22(2), 205–218.
- Dobinski, W. (2011). Permafrost. *Earth-Science Reviews*, 108(3), 158–169.
- Egenhofer, Max J and Glasgow, Janice and Gunther, Oliver and Herring, John R and Peuquet, Donna J (1999). Progress in Computational Methods for Representing Geographic Concepts. *International Journal of Geographical Information Science*, 13(8), 775–796.
- Elwood, S. (2010). Geographic information science: emerging research on the societal implications of the geospatial web. *Progress in Human Geography*, 34(3), 349–357.
- Eugster, H. (1973). *Bericht über die Untersuchungen des Blockstroms in der Val Sassa im Schweiz. Nationalpark (GR) von 1917-1971*. Ergebnisse der wissenschaftlichen Untersuchungen im Schweizerischen Nationalpark. Nationalpark-Museum.
- Frank, A. U. (1996). The Prevalence of Objects with Sharp Boundaries in GIS. In P. A. Burrough, & A. U. Frank (Eds.), *Geographic Objects with Indeterminate Boundaries*, London: Taylor & Francis, pp. 29–40.
- Frauenfelder, R., & Käab, A. (2000). Towards a palaeoclimatic model of rock-glacier formation in the Swiss Alps. *Annals of Glaciology*, 31(1), 281–286.
- Frauenfelder, R., Laustela, M., & Käab, A. (2005). Relative age dating of Alpine rockglacier surfaces. *Zeitschrift für Geomorphologie, NF*, 49(2), 145–166.

- Frauenfelder, R., & Roer, I. (2007). Was Blockgletscher bewegt (Rockglaciers and their movements). *Die Alpen/Les Alpes*, 9, 34–37.
- French, H. M. (2007). *The periglacial environment*. Chichester: John Wiley & Sons, 3rd ed.
- Fröhlich, C., & Mettenleiter, M. (2004). Terrestrial laser scanning – new perspectives in 3D surveying. *International Archives of Photogrammetry, Remote Sensing and Spatial Information Sciences*, 36(8), 7–13.
- Golledge, R. G. (1993). Geographical perspectives on spatial cognition. *Advances in Psychology*, 96, 16–46.
- Goodchild, M. F. (1992). Geographical Data Modeling. *Computers & Geosciences*, 18(4), 401–408.
- Goodchild, M. F. (1996). The application of advanced information technology in assessing environmental impacts. In D. L. Corwin and K. Loague (Ed.), *Applications of GIS to the Modeling of Non-Point Source Pollutants in the Vadose Zone*, SSSA Special Publication 48, Madison: Soil Science Society of America, pp. 1–17.
- Goodchild, M. F. (2010). Twenty years of progress: GIScience in 2010. *Journal of Spatial Information Science*, 1, 3–20.
- Goodchild, M. F. (2012). Geographic Information Systems. In A. Hastings, & L. J. Gross (Eds.), *Encyclopedia of Theoretical Ecology*, Berkeley: University of California Press, pp. 341–345.
- Goodchild, M. F., Yuan, M., & Cova, T. J. (2007). Towards a general theory of geographic representation in GIS. *International Journal of Geographical Information Science*, 21(3), 239–260.
- Gruver, A. (2014). Part VI: Objects vs. Fields (and Vector vs. Raster).
URL www.e-education.psu.edu/geog486/11_p8.html, accessed 10.08.2014.
- Haeberli, W. (1985). Creep of mountain permafrost: internal structure and flow of alpine rock glaciers. *Mitteilungen der Versuchsanstalt für Wasserbau, Hydrologie und Glaziologie an der ETH Zurich*, 77, 142.
- Haeberli, W. (1993). Possible effects of climatic change on the evolution of Alpine permafrost. *Greenhouse-Impact on Cold-Climate Ecosystems and Landscapes*, 22, 23–37.
- Haeberli, W. (2000). Modern Research Perspectives Relating to Permafrost Creep and Rock Glaciers: A Discussion. *Permafrost and Periglacial Processes*, 11(4), 290–293.
- Haeberli, W., & Beniston, M. (1998). Climate change and its impacts on glaciers and permafrost in the Alps. *Ambio*, 27(4), 258–265.
- Haeberli, W., & Burn, C. R. (2002). Natural hazards in forests: glacier and permafrost effects as related to climate change. In R. C. Sidle (Ed.), *Environmental Change and Geomorphic Hazards in Forests*, Wallingford: CABI Publishing, pp. 167–202.

- Haeberli, W., Hallet, B., Arenson, L., Elconin, R., Humlum, O., Käab, A., Kaufmann, V., Ladanyi, B., Matsuoka, N., Springman, S., & Vonder Mühll, D. S. (2006). Permafrost Creep and Rock Glacier Dynamics. *Permafrost and Periglacial Processes*, 17(3), 189–214.
- Haeberli, W., & Hoelzle, M. (1995). Application of inventory data for estimating characteristics of and regional climate-change effects on mountain glaciers: a pilot study with the European Alps. *Annals of Glaciology*, 21, 206–212.
- Henning, J. G., & Radtke, P. J. (2006). Detailed Stem Measurements of Standing Trees from Ground-Based Scanning Lidar. *Forest Science*, 52(1), 67–80.
- Hoelzle, M. (1996). Mapping and modelling of mountain permafrost distribution in the Alps. *Norsk Geografisk Tidsskrift–Norwegian Journal of Geography*, 50(1), 11–15.
- Humlum, O. (1982). Rock glacier types on Disko, central West Greenland. *Geografisk Tidsskrift–Danish Journal of Geography*, 82(1), 59–66.
- Ikedo, A., & Matsuoka, N. (2002). Degradation of talus-derived rock glaciers in the Upper Engadin, Swiss Alps. *Permafrost and Periglacial Processes*, 13(2), 145–161.
- Ingensand, H. (2006). Metrological aspects in terrestrial laser-scanning technology. In *Proceedings of the 3rd IAG/12th FIG Symposium*. Baden.
- Intergovernmental Panel on Climate Change [IPCC] (2007). Climate Change 2007: The Physical Science Basis. In S Solomon, D Qin, M Manning, Z Chen, M Marquis, K.B Averyt, M Tignor, H.L. Miller (Ed.), *Contribution of Working Group I to the Fourth Assessment Report of the Intergovernmental Panel on Climate Change*, Cambridge: Cambridge University Press.
- Jäckli, H. (1985). Blockströme, Blockgletscher. In *Zeitmaßstäbe der Erdgeschichte*, Basel: Birkhäuser, pp. 37–39.
- Johnson, P. G. (1974). Mass movement of ablation complexes and their relationship to rock glaciers. *Geografiska Annaler: Series A, Physical Geography*, 56, 93–101.
- Jones, C. B. (2014). *Geographical Information Systems and Computer Cartography*. London: Taylor & Francis.
- Jones, L. (2012). Geographic information systems. In I. A. Kreis, A. Busby, G. Leonardi, J. Meara, & V. Murray (Eds.), *Essentials of Environmental Epidemiology for Health Protection: A handbook for field professionals*, Oxford: Oxford University Press.
- Käab, A. (2002). Monitoring high-mountain terrain deformation from repeated air- and spaceborne optical data: examples using digital aerial imagery and ASTER data. *ISPRS Journal of Photogrammetry and Remote Sensing*, 57(1), 39–52.
- Käab, A. (2013a). Image correlation software CIAS.
URL www.mn.uio.no/geo/english/research/projects/icemass/cias/, accessed 12.08.2014.

- Kääb, A. (2013b). Permafrost and Periglacial Features: Rock Glaciers and Protalus Forms. In S. A. Elias, & C. J. Mock (Eds.), *Encyclopedia of Quaternary Science*, Amsterdam: Elsevier, pp. 535–541. 2nd ed.
- Kääb, A., Frauenfelder, R., & Roer, I. (2007). On the response of rockglacier creep to surface temperature increase. *Global and Planetary Change*, 56(1), 172–187.
- Kääb, A., Huggel, C., Fischer, L., Guex, S., Paul, F., Roer, I., Salzmann, N., Schlaefli, S., Schmutz, K., Schneider, D., Strozzi, T., & Weidmann, Y. (2005). Remote sensing of glacier- and permafrost-related hazards in high mountains: an overview. *Natural Hazards and Earth System Sciences*, 5(4), 527–554.
- Kääb, A., Kaufmann, V., Ladstädter, R., & Eiken, T. (2003). Rock glacier dynamics: implications from high-resolution measurements of surface velocity fields. In M. Phillips, S. Springman, & L. Arenson (Eds.), *8th International Conference on Permafrost, Proceedings*. Lisse: Swets & Zeitlinger, pp. 501–506.
- Kääb, A., & Kneisel, C. (2006). Permafrost creep within a recently deglaciated glacier forefield: Muragl, Swiss Alps. *Permafrost and Periglacial Processes*, 17(1), 79–85.
- Kääb, A., & Vollmer, M. (2000). Surface Geometry, Thickness Changes and Flow Fields on Creeping Mountain Permafrost: Automatic Extraction by Digital Image Analysis. *Permafrost and Periglacial Processes*, 11(4), 315–326.
- Kääb, A., & Weber, M. (2004). Development of transverse ridges on rock glaciers: field measurements and laboratory experiments. *Permafrost and Periglacial Processes*, 15(4), 379–391.
- Kaufmann, V., & Ladstädter, R. (2010). Documentation and visualization of the morphodynamics of Hinteres Langtalkar rock glacier (Hohe Tauern range, Austrian Alps) based on aerial photographs (1954-2006) and geodetic measurements (1999-2007). *Grazer Schriften der Geographie und Raumforschung*, 45, 103–116.
- Kenner, R., Bühler, Y., Delaloye, R., Ginzler, C., & Phillips, M. (2014). Monitoring of high alpine mass movements combining laser scanning with digital airborne photogrammetry. *Geomorphology*, 206, 492–504.
- Kenner, R., Phillips, M., Danioth, C., Denier, C., Thee, P., & Zraggen, A. (2011). Investigation of rock and ice loss in a recently deglaciated mountain rock wall using terrestrial laser scanning: Gemsstock, Swiss Alps. *Cold Regions Science and Technology*, 67(3), 157–164.
- Kenyi, L. W., & Kaufmann, V. (2003). Estimation of rock glacier surface deformation using SAR interferometry data. *IEEE Transactions on Geoscience and Remote Sensing*, 41(6), 1512–1515.
- Kneisel, C. (2010). The nature and dynamics of frozen ground in alpine and subarctic periglacial environments. *The Holocene*, 20(3), 423–445.

- Kneisel, C., & Käab, A. (2007). Mountain permafrost dynamics within a recently exposed glacier forefield inferred by a combined geomorphological, geophysical and photogrammetrical approach. *Earth Surface Processes and Landforms*, 32(12), 1797–1810.
- Kociuba, W., Kubisz, W., & Zagórski, P. (2013). Use of terrestrial laser scanning (TLS) for monitoring and modelling of geomorphic processes and phenomena at a small and medium spatial scale in Polar environment (Scott River– Spitsbergen). *Geomorphology*, 212, 84–96.
- Kotur, P. B. (2012). *Object Oriented Programming with C++*. Bangalore: Sapna Book House.
- Lam, N. S.-N. (1983). Spatial interpolation methods: a review. *The American Cartographer*, 10(2), 129–150.
- Lambiel, C., & Delaloye, R. (2004). Contribution of real-time kinematic GPS in the study of creeping mountain permafrost: Examples from the Western Swiss Alps. *Permafrost and Periglacial Processes*, 15(3), 229–241.
- Langran, G. (1992). *Time in geographic information systems*. London: Taylor & Francis.
- Lichti, D. D., Gordon, S. J., & Tipdecho, T. (2005). Error models and propagation in directly georeferenced terrestrial laser scanner networks. *Journal of Surveying Engineering*, 131(4), 135–142.
- Liu, H., Wang, L., Sherman, D., Gao, Y., & Wu, Q. (2010). An object-based conceptual framework and computational method for representing and analyzing coastal morphological changes. *International Journal of Geographical Information Science*, 24(7), 1015–1041.
- Livingstone, D., & Raper, J. (1994). Modelling environmental systems with GIS: theoretical barriers to progress. *Innovations in GIS*, 1, 229–240.
- Maisch, M., Haeberli, W., Frauenfelder, R., & Käab, A. (2003). Lateglacial and Holocene evolution of glaciers and permafrost in the Val Muragl, Upper Engadin, Swiss Alps. In M. Phillips, S. M. Springman, & L. Arenson (Eds.), *8th International Conference on Permafrost, Proceedings*. Lisse: Swets & Zeitlinger, pp. 717–722.
- Mark, D. M. (1989). *Languages of Spatial Relations: Researchable Questions & NCGIA Research Agenda*. Tech. rep., National Center for Geographic Information and Analysis, Santa Barbara. University of California.
- Mark, D. M., & Smith, B. (2004). A Science of Topography: Bridging the Qualitative-Quantitative Divide. In M. P. Bishop, & J. F. Shroder (Eds.), *Geographic Information Science and Mountain Geomorphology*, Chichester: Springer-Praxis, pp. 75–100.
- Maurer, H., & Hauck, C. (2007). Geophysical imaging of alpine rock glaciers. *Journal of Glaciology*, 53(180), 110–120.

- Mennis, J. L., & Peuquet, D. J. (2000). A conceptual framework for incorporating cognitive principles into geographical database representation. *International Journal of Geographical Information Science*, 14(6), 501–520.
- Monserrat, O., & Crosetto, M. (2008). Deformation measurement using terrestrial laser scanning data and least squares 3D surface matching. *ISPRS Journal of Photogrammetry and Remote Sensing Remote Sensing*, 63(1), 142–154.
- Montello, D. R. (2009). Cognitive Research in GIScience: Recent Achievements and Future Prospects. *Geography Compass*, 3(5), 1824–1840.
- Montello, D. R., & Friendschuh, S. (2005). Cognition of Geographic Information. In R. B. McMaster, & E. L. Usery (Eds.), *A research agenda for geographic information science*, Boca Raton: CRC Press, pp. 61–91.
- Musil, M. (2002). *Inverting Seismic and Georadar Data with Applications to the Muragl Rock Glacier*. Ph.d thesis, Swiss Federal Institute of Technology, Zurich.
- Musil, M., Maurer, H., Hollinger, K., & Green, A. G. (2006). Internal structure of an alpine rock glacier based on crosshole georadar traveltimes and amplitudes. *Geophysical Prospecting*, 54(3), 273–285.
- Oppikofer, T., Jaboyedoff, M., Blikra, L., Derron, M.-H., & Metzger, R. (2009). Characterization and monitoring of the Åknes rockslide using terrestrial laser scanning. *Natural Hazards and Earth System Sciences*, 9(3), 1003–1019.
- PERMOS (2013). Permafrost in Switzerland 2008/2009 and 2009/2010. In J. Noetzi (Ed.), *Glaciological Report Permafrost No. 10/11 of the Cryospheric Commission of the Swiss Academy of Sciences*, p. 80.
- Pesci, A., Teza, G., & Bonali, E. (2011). Terrestrial Laser Scanner Resolution: Numerical Simulations and Experiments on Spatial Sampling Optimization. *Remote Sensing*, 3(1), 167–184.
- Pfeifer, N., & Briese, C. (2007). Geometrical aspects of airborne laser scanning and terrestrial laser scanning. *International Archives of Photogrammetry, Remote Sensing and Spatial Information Sciences*, 36(3), 311–319.
- Pillewizer, W. (1957). Untersuchungen an Blockströmen der Ötztaler Alpen. *Geomorphologische Abhandlungen des Geographischen Institutes der FU Berlin (Otto-Maull-Festschrift)*, 5, 37–50.
- Potter, J. N. (1972). Ice-Cored Rock Glacier, Galena Creek, Northern Absaroka Mountains, Wyoming. *Geological Society of America Bulletin*, 83(10), 3025–3058.
- Prokop, A., & Panholzer, H. (2009). Assessing the capability of terrestrial laser scanning for monitoring slow moving landslides. *Natural Hazards and Earth System Sciences*, 9(6), 1921–1928.

- Prokop, A., Schirmer, M., Rub, M., Lehning, M., & Stocker, M. (2008). A comparison of measurement methods: terrestrial laser scanning, tachymetry and snow probing for the determination of the spatial snow-depth distribution on slopes. *Annals of Glaciology*, 49(1), 210–216.
- Pu, S., & Vosselman, G. (2006). Automatic extraction of building features from terrestrial laser scanning. *International Archives of Photogrammetry, Remote Sensing and Spatial Information Sciences*, 36(5), 25–27.
- Rabatel, A., Deline, P., Jaillet, S., & Ravelin, L. (2008). Rock falls in high-alpine rock walls quantified by terrestrial lidar measurements: A case study in the Mont Blanc area. *Geophysical Research Letters*, 35(10).
- Raper, J. (2000). *Multidimensional Geographic Information Science*. Boca Raton: CRC Press.
- Raper, J., & Livingstone, D. (1995). Development of a geomorphological spatial model using object-oriented design. *International Journal of Geographical Information Systems*, 9(4), 359–383.
- Rasemann, S. (2003). *Geomorphometrische Struktur eines mesoskaligen alpinen Geosystems*. Ph.d. thesis, Rheinische Friedrich-Wilhelms-Universität, Bonn.
- Reshetyuk, Y. (2006). *Investigation and calibration of pulsed time-of-flight terrestrial laser scanners*. Ph.d. thesis, Royal Institute of Technology (KTH), Stockholm.
- RIEGL Laser Measurement Systems GmbH (2012a). Manuals Pdf: RiSCAN PRO (personal communication Johann Müller).
- RIEGL Laser Measurement Systems GmbH (2012b). Manuals Powerpoint Presentation: 03_TLS-Training_Data_Registration_v1 (personal communication Johann Müller).
- RIEGL Laser Measurement Systems GmbH (2014). RIEGL VZ-1000.
URL <http://www.riegl.com/nc/products/terrestrial-scanning/produktdetail/product/scanner/27/>, accessed 19.07.2014.
- Rödler, T., & Kneisel, C. (2012). Influence of snow cover and grain size on the ground thermal regime in the discontinuous permafrost zone, Swiss Alps. *Geomorphology*, 175, 176–189.
- Roer, I. (2005). *Rockglacier Kinematics in a High Mountain Geosystem*. Ph.d thesis, Rheinische Friedrich-Wilhelms-Universität, Bonn.
- Roer, I., Haeberli, W., Avian, M., Kaufmann, V., Delaloye, R., Lambiel, C., & Käab, A. (2008). Observations and Considerations on Destabilizing Active Rock Glaciers in the European Alps. In D. Kane, & K. Hinkel (Eds.), *9th International Conference on Permafrost*. Institute of Northern Engineering, University of Alaska at Fairbanks, 4, pp. 1505–1510.
- Roer, I., Käab, A., & Dikau, R. (2005). Rockglacier acceleration in the Turtmann valley (Swiss Alps): Probable controls. *Norsk Geografisk Tidsskrift–Norwegian Journal of Geography*, 59(2), 157–163.

- Rub, M., & Zogg, H.-M. (2008). Terrestrisches Long-Range Laserscanning–Überblick und Anwendungen. In *Geomatik Schweiz, Géomatique Suisse*, Scherz: SIGImedia AG, pp. 104–108.
- Schulz, T., & Ingensand, H. (2004). Terrestrial Laser Scanning–Investigations and Applications for High Precision Scanning. In *Proceedings of the 'FIG Working Week–The Olympic Spirit in Surveying'*. Athens, pp. 1–15.
- Shan, J., & Toth, C. K. (2009). *Topographic Laser Ranging and Scanning: Principles and Processing*. Boca Raton: CRC Press.
- Smith, B., & Mark, D. M. (2003). Do mountains exist? Towards an ontology of landforms. *Environment and Planning B: Planning and Design*, 30(3), 411–427.
- Springman, S. M., Arenson, L. U., Yamamoto, Y., Maurer, H., Kos, A., Buchli, T., & Derungs, G. (2012). Multidisciplinary Investigations on Three Rock Glaciers in the Swiss Alps: Legacies and Future Perspectives. *Geografiska Annaler: Series A, Physical Geography*, 94(2), 215–243.
- Strozzi, T., Kääb, A., & Frauenfelder, R. (2004). Detecting and quantifying mountain permafrost creep from in situ inventory, space-borne radar interferometry and airborne digital photogrammetry. *International Journal of Remote Sensing*, 25(15), 2919–2931.
- Tarolli, P., Arrowsmith, J. R., & Vivoni, E. R. (2009). Understanding earth surface processes from remotely sensed digital terrain models. *Geomorphology*, 113(1), 1–3.
- Vollmer, M. (1999). *Kriechen alpinen Permafrostes: Grundlagen zur digitalen photogrammetrischen Bewegungsmessung*. Master's thesis, University of Zurich.
- Vonder Mühll, D. S. (1993). Geophysikalische Untersuchungen im Permafrost des Oberengadins. *Mitteilungen der Versuchsanstalt für Wasserbau, Hydrologie und Glaziologie an der Eidgenössischen Technischen Hochschule Zurich*, (122), 1–222.
- Vonder Mühll, D. S., Arenson, L., & Springman, S. (2003). Temperature conditions in two Alpine rock glaciers. In M. Phillips, S. M. Springman, & L. Arenson (Eds.), *8th International Conference on Permafrost, Proceedings*. Lisse: Swets & Zeitlinger, pp. 1195–1200.
- Vosselman, G., Gorte, B. G. H., Sithole, G., & Rabbani, T. (2004). Recognising Structure in Laser Scanner Point Clouds. *International Archives of the Photogrammetry, Remote Sensing and Spatial Information Sciences*, 46(8), 33–38.
- Vosselman, G., & Maas, H. G. (2010). *Airborne and Terrestrial Laser Scanning*. Dunbeath: Whitlles Publishing.
- Wang, J., & Shan, J. (2009). Segmentation of LiDAR point clouds for building extraction. In *American Society for Photogrammetry and Remote Sensing, Annual Conference*. Baltimore, pp. 9–13.

- Watt, P. J., & Donoghue, D. N. M. (2005). Measuring forest structure with terrestrial laser scanning. *International Journal of Remote Sensing*, 26(7), 1437–1446.
- Yuan, M. (2001). Representing Complex Geographic Phenomena in GIS. *Cartography and Geographic Information Science*, 28(2), 83–96.
- Zeibak, R., & Filin, S. (2009). Object Extraction from Terrestrial Laser Scanning Data. In *FIG Working Week*. Eilat.
- Zogg, H.-M., & Grimm, D. (2008). Kinematic Surface Analysis by Terrestrial Laser Scanning. In *1st International Conference on Machine Control & Guidance*. Zurich.
- Zogg, H.-M., & Ingensand, H. (2008). Terrestrial Laser Scanning for Deformation Monitoring—Load Tests on the Felsenau Viaduct (CH). *International Archives of Photogrammetry and Remote Sensing*, 37, 555–562.

Appendix

A.1 The total of all acquired scans

The following tables show the total of all scans, acquired at the several measurement campaigns between 4 July 2013 and 25 July 2014. For all scans, the measurement program was determined to 70kHz, which equals a range of 1400m.

Table A.1: All scans acquired at measurement campaign from 4th of July 2013

Name	Coverage	MB	Tiepoints (auto.)	Tiepoints (man.)
73434	Whole rock glacier, rock wall, headwall	32	TP Forefield, TP Behind	No TP found
74445	Whole rock glacier, rock wall, headwall	32	TP Behind	No TP found
80452	Whole rock glacier, rock wall, headwall	33	No TP found	TP Forefield, TP Headwall
82130	Rock glacier without upper-most part, rock wall, headwall partly	32	TP Headwall	TP Forefield, TP Catchment
82845	Whole rock glacier, rock wall	36	No TP found	TP Catchment, TP Headwall
84002	Whole rock glacier, rock wall, headwall partly	260	TP Catchment, TP Forefield	No TP found
90831	Whole rock glacier, rock wall, headwall, behind	32	TP Behind	TP Catchment, TP Headwall & TP Forefield (not clear)

Table A.2: All scans acquired at measurement campaign from 5th of July 2013

Name	Coverage	MB	Tiepoints (auto.)	Tiepoints (man.)
111815	Whole rock glacier, rock wall, headwall, behind	27	No TP found	TP Catchment, TP Headwall, TP Behind, TP Forefield (not clear)
112847	Whole rock glacier, rock wall, headwall, behind partly	388	TP Forefield, TP Headwall, TP Behind (not clear)	TP Catchment
121146	Whole rock glacier, rock wall, headwall partly	529	TP Catchment, TP Forefield, TP Headwall	No TP found

Table A.3: All scans acquired at measurement campaign from 23rd of August 2013

Name	Coverage	MB	Tiepoints (auto.)	Tiepoints (man.)
104428	Only lower part of glacier, headwall, behind	32	No TP found	TP Headwall, TP Behind
105244	Only small band	55	No TP found	No TP found
110056	Whole rock glacier, rock wall, headwall	900	TP Headwall, TP Forefield	TP Catchment
123804	Whole rock glacier, rock wall, headwall, behind	520	TP Headwall, TP Behind	TP Forefield, TP Catchment

Table A.4: All scans acquired at measurement campaign from 7th of October 2013

Name	Coverage	MB	Tiepoints (auto.)	Tiepoints (man.)
131908	Whole rock glacier, lower part of rock wall, headwall, behind	32	No TP found	manually difficult
133236	Whole rock glacier, rock wall, headwall	700	TP Catchment, TP Forefield, TP Headwall	Already all TP found
153749	Whole rock glacier, lower part of rock wall, headwall, Behind	130	TP Behind	TP Catchment, TP Forefield, TP Headwall
155345	Only small band	65	No TP found	No TP found
160310	Only small band	23	No TP found	No TP found
160748	Only small band	55	No TP found	No TP found
173119	Very coarse resolution	1	No TP found	No TP found
181340	Very coarse resolution	1	No TP found	No TP found
181530	Very coarse, poor resolution, only front, poor quality	0.5	No TP found	No TP found
181939	Only left part of front	330	No TP found	No TP found

Table A.5: All scans acquired at measurement campaign from 25th of July 2014

Name	Coverage	MB	Tiepoints (auto.)	Tiepoints (man.)
101935	Only small band	47	No TP found	No TP found
102732	Entire rock glacier, rock wall, headwall	570	TP Catchment, TP Forefield, TP Headwall	Already all TP found
113034	Only small band	13	No TP found	No TP found
113419	Only small band	7	No TP found	No TP found
113645	Entire rock glacier, rock wall, headwall	485	TP Catchment, TP Forefield, TP Headwall	Already all TP found

A.2 MATLAB scripts

Scale matrices

```

1 w = waitbar(0, 'Listing files');
  files = dir('H:\FeatureTracking\27Juni\*.tif');
3 for(i=1:length(files))
    waitbar(i/length(files), w, 'Reading matrix');
5     info = geotiffinfo(['H:\FeatureTracking\27Juni\' files(i).name]);
    [matrix,R] = geotiffread(['H:\FeatureTracking\27Juni\' files(i).name]);
7     matrix = double(matrix);
    scaledMatrix = (matrix - min(matrix(:))) ./ (max(matrix(:) - min(matrix(:))));
9     scaledMatrix = scaledMatrix * 255;
    scaledMatrix = uint8(scaledMatrix);
11    geotiffwrite(['H:\FeatureTracking\27Juni\ScaledMatrices\' strrep(files(i).name,
        '.tif', '_0_255.tif')], scaledMatrix, R, 'GeoKeyDirectoryTag', info.GeoTIFFTags.
        GeoKeyDirectoryTag);
    clearvars info matrix scaledMatrix;
13 end
  close(w);
15 clearvars w files i;

```

Listing 1: Matlab script to stretch the Tiff-files in order to obtain the full grey scale range from 0 to 255

Define control points

```

1 function defineControlPoints(inputFileName, outputFileName, numberOfPoints,
    randomOrSystematical)
  info = geotiffinfo(inputFileName);
3 matrix = geotiffread(inputFileName);
  xaxis = info.SpatialRef.XLimWorld(1) : info.SpatialRef.DeltaX : info.SpatialRef.
    XLimWorld(2) - info.SpatialRef.DeltaX;
5 yaxis = info.SpatialRef.YLimWorld(2) + info.SpatialRef.DeltaY : info.SpatialRef.DeltaY :
    info.SpatialRef.YLimWorld(1);
  left = info.BoundingBox(1,1);
7 right = info.BoundingBox(2,1);
  upper = info.BoundingBox(2,2);
9 lower = info.BoundingBox(1,2);
  if(strcmpi(randomOrSystematical, 'r'))
11     for(i=1:numberOfPoints)
        noData = 1;
13     while(noData == 1)
            samplePoints(i,1) = (rand(1) * (right - left)) + left;

```

```

15     samplePoints(i,2) = (rand(1)*(upper-lower))+lower;
16     [~,xindex] = min(abs(samplePoints(i,1)-xaxis));
17     [~,yindex] = min(abs(samplePoints(i,2)-yaxis));
18     if (matrix(yindex, xindex)~=255)
19         noData = 0;
20     end
21 end
22 end
23 elseif(strcmpi(randomOrSystematical, 's'))
24     if(mod(sqrt(numberOfPoints),1)~=0)
25         disp(['Achtung: Anzahl Punkte kann nicht gleichmaessig in x- und y-Richtung
26             verteilt werden. Anstelle von ' num2str(numberOfPoints) ' werden '
27             num2str(power(round(sqrt(numberOfPoints)),2)) ' Punkte ausgegeben.']);
28         numberOfPoints = power(round(sqrt(numberOfPoints)),2);
29     end
30     counter = 0;
31     for(i=1:sqrt(numberOfPoints))
32         for(j=1:sqrt(numberOfPoints))
33             counter = counter + 1;
34             samplePoints(counter,1) = (((right-left)/(sqrt(numberOfPoints)+1))*i)+
35                 left;
36             samplePoints(counter,2) = (((upper-lower)/(sqrt(numberOfPoints)+1))*j)+
37                 lower;
38         end
39     end
40 else
41     disp('Es gibt zwei Moeglichkeiten: "r" und „s“');
42     return;
43 end
44 xlsxwrite(outputFileName, samplePoints);
45 clearvars info left right lower upper numberOfPoints ;
46 end

```

Listing 2: Matlab script to define the specific measurement points

A.3 Detailed process of CIAS Feature Tracking

The final section includes a detailed description of the individual process steps implied when using CIAS Feature Tracking software (Kääb & Vollmer, 2000). In the following example, the data sets of 5 July 2013 and 25 July 2014 with DEMs possessing a cell size of 1m are used. Furthermore, the Helmert transformation was applied and the measurement points were determined by a drawn polygon.

IDL software

The requirement of running CIAS Feature Tracking software (Kääb & Vollmer, 2000) is the IDL software. IDL stands for Interactive Data Language. In this thesis the IDL virtual machine, which is available on the GIUZ server, was used.



Figure A.1: IDL virtual machine for IDL applications.

Running CIAS Feature Tracking

- Input of image of time 1
 - Select image of the first point in time (see figure A.2)
 - Specify format of input file: *GeoTIFF* or *TIFF World* (see figure A.3)

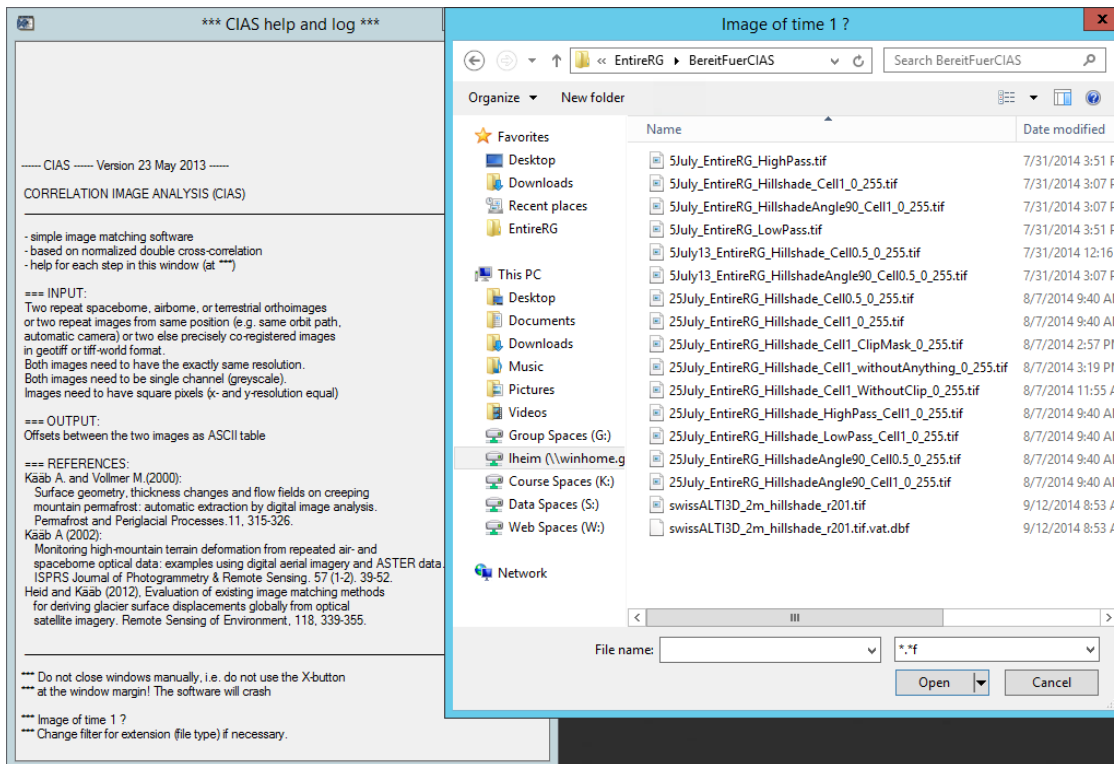


Figure A.2: Selection of image of time 1.

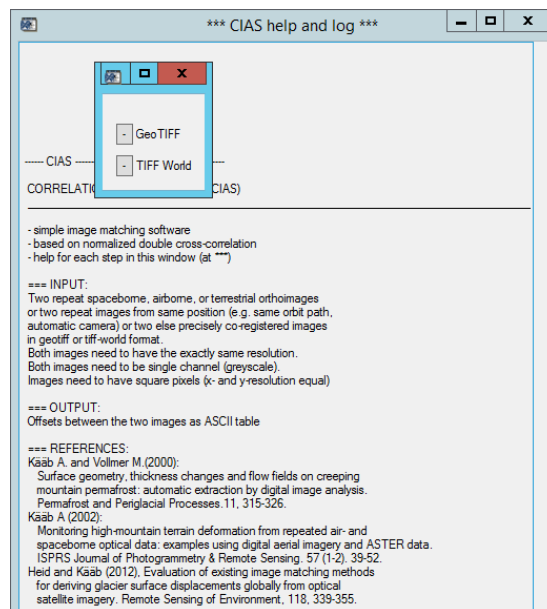


Figure A.3: Specification of format of input file 1.

- Input of image of time 2
 - Select image of the second point in time (see figure A.4)
 - Specify format of input file: *GeoTIFF* or *TIFF World* (similar to figure A.3)

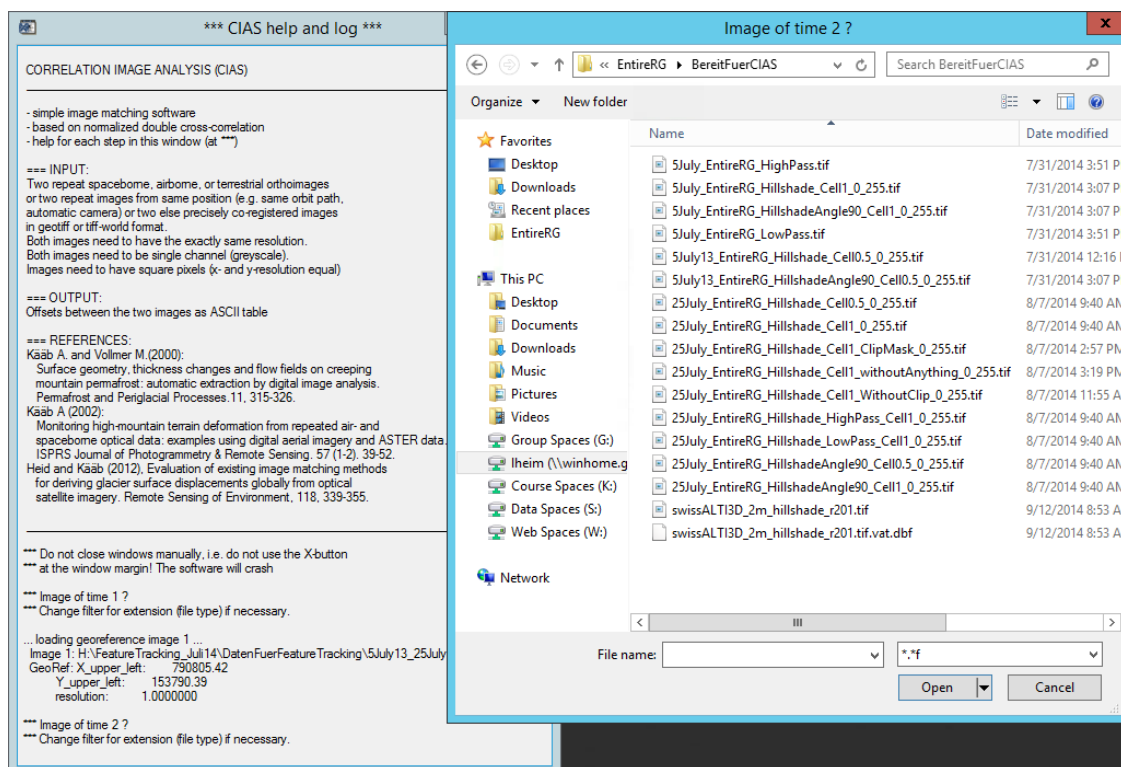


Figure A.4: Selection of image of time 2.

- Including/excluding Helmert transformation (see figure A.5)
 - Choosing *Without co-registration*: displacement measurement will directly start.
 - Choosing *With co-registration*: matching of features on stable ground, compute a shift, scale and rotation between the two images, then start the displacement measurement.

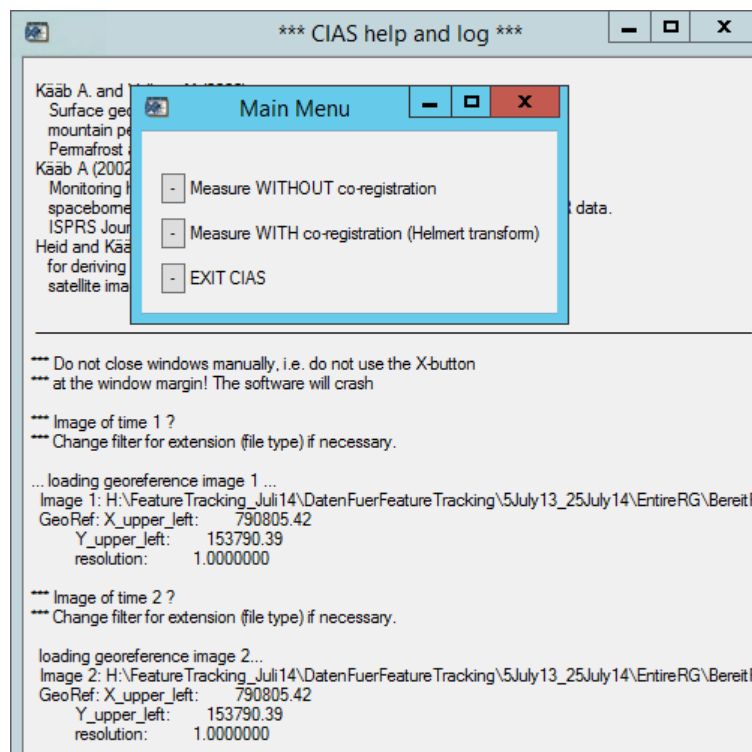


Figure A.5: Including/excluding Helmert transformation.

- Selection of correlation algorithm (see figure A.6)
 - *NCC Normalized Cross-Correlation*: typical cross-correlation approach as described in Formula 6.2.
 - *NCC-O Orientation Correlation*: is useful for low-contrast images and images with data voids, might not be useful for very noisy images, NCC-O requires more memory.

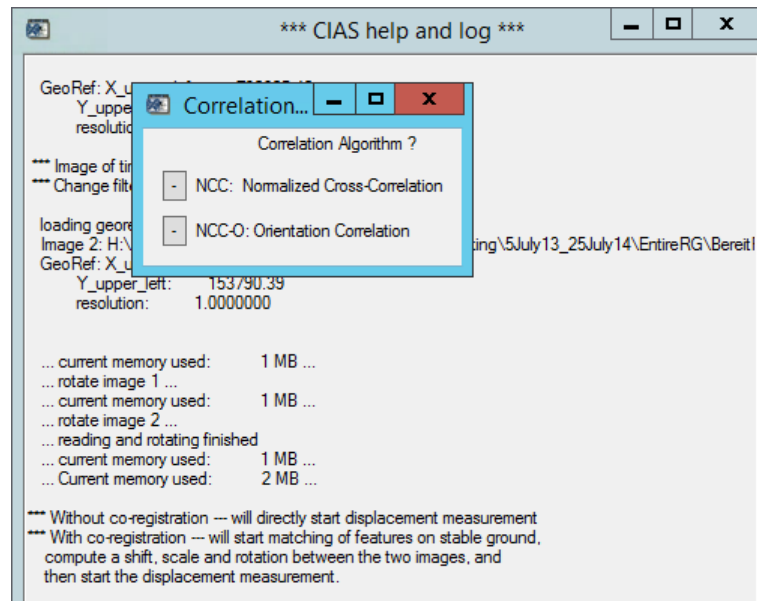


Figure A.6: Specification of the correlation algorithm.

- Specification of reference block size and test area size (pixels) for the Helmert transformation (see figure A.7)
 - Reference block size: determining the reference block size; here specified as 5 pixels.
 - Test area size: determining the test area size; here specified as 10 pixels.

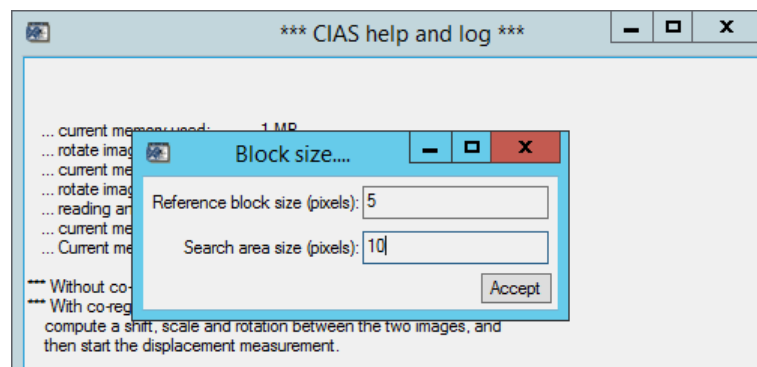


Figure A.7: Specification of reference block size and test area size (pixels) for Helmert transformation.

- Specification of matching speed concerning the Helmert transformation (see figure A.8)
 - *Normal*: 1st matching iteration at full image resolution.
 - *Fast*: 1st matching iteration at 25% reduced resolution.
 - 2nd iteration in both cases to $\sim 10\%$ of a original pixel (Debella-Gilo & Käab, 2011).

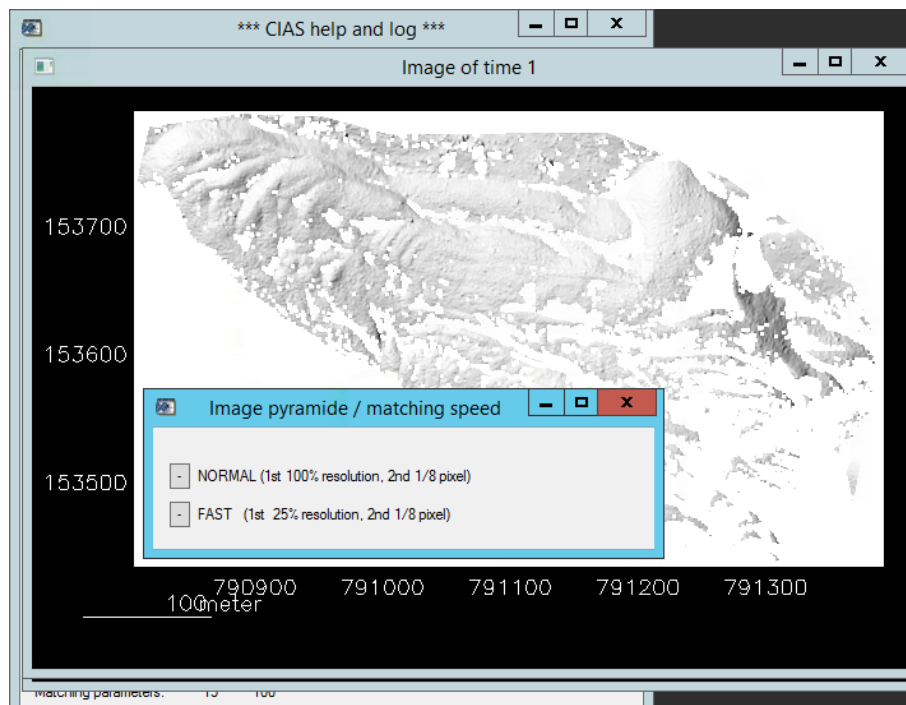


Figure A.8: Specification of matching speed concerning the Helmert transformation.

- Determination of corresponding points for Helmert transformation (see figure A.9)
 - *Select on image (with zoom)*: selecting points manually.
 - *Read XY file*: determination of corresponding points by input of txt-file.

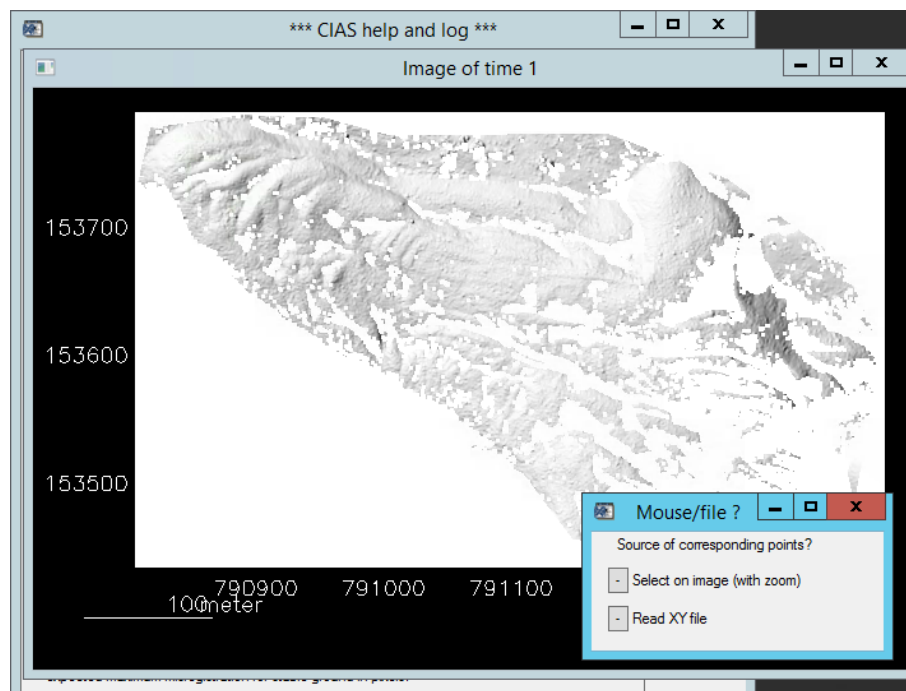


Figure A.9: Determination of corresponding points for the Helmert transformation.

- Example for Helmert transformation with txt-file as input file (see figure A.10)
 - The prepared txt-file including 10 possibly stable points is used.

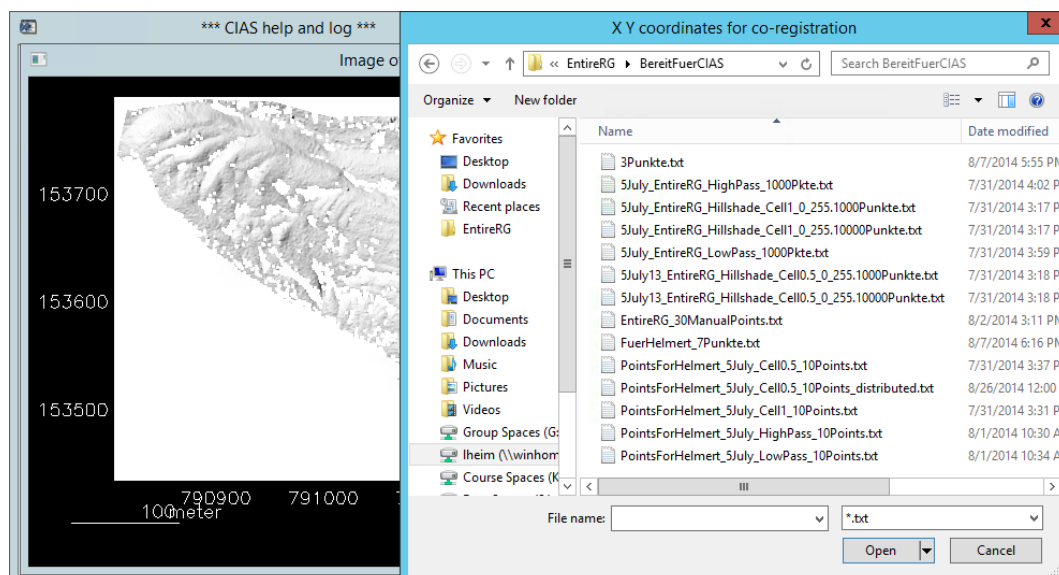


Figure A.10: Helmert transformation with txt-file as input.

- Helmert transformation (see figure A.11)
 - The resulting parameters of the Helmert transformation are represented.
 - An optimal zoom is provided including the used corresponding points for the Helmert transformation
 - Subsequent options are available: *Delete selected transformation points*, *Add points for transformation*, *Continue to displacement measurement*, and *End CIAS Feature Tracking*

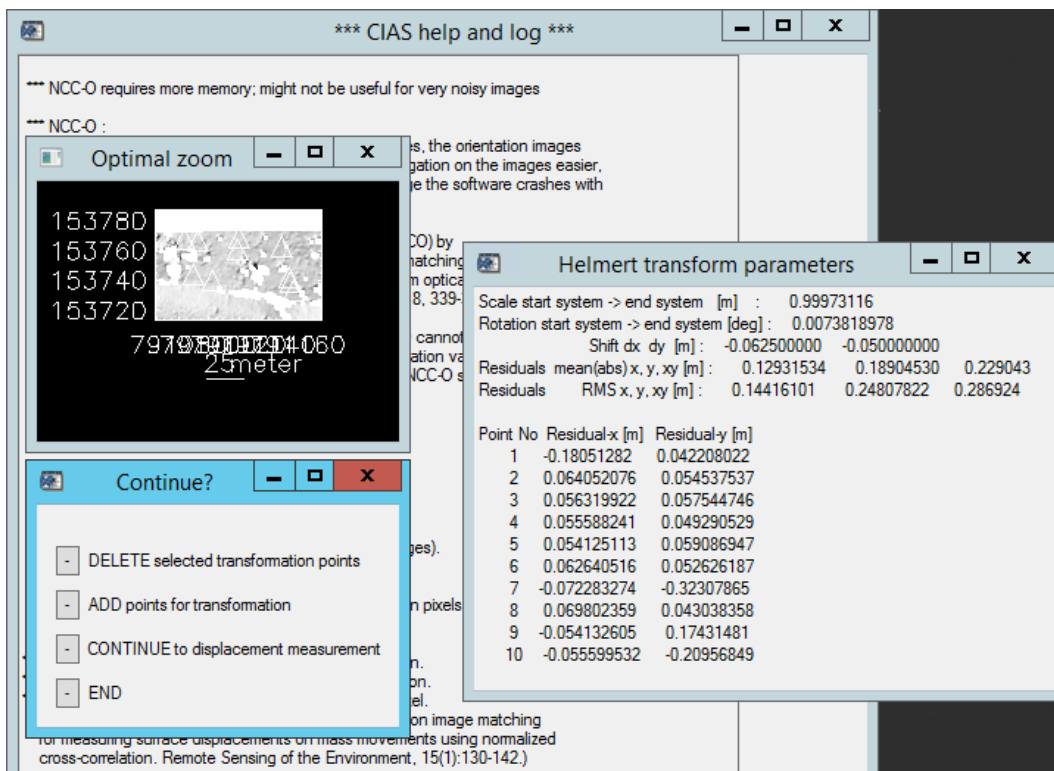


Figure A.11: Representation of resulting parameters of the Helmert transformation.

- Specification of the measurement points (see figure A.12)
 - *Single points*: selecting the points manually.
 - *Polygon*: drawing a polygon in order to select the incorporated points.
 - *XY file*: using the previously determined *control points* by MATLAB script as input for the measurement points.

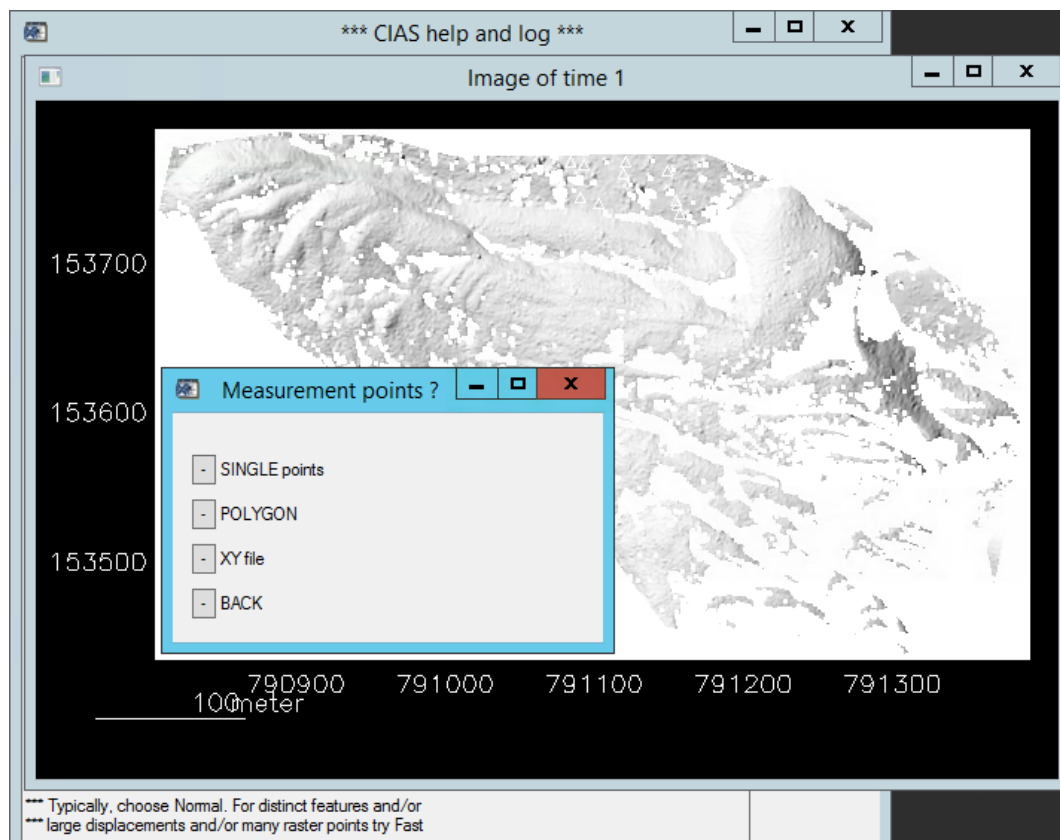


Figure A.12: Specification of the measurement points.

- Specification of parameters needed for the measurement by drawn polygon (see figure A.13)
 - *Reference block size (pixels)*: specifying the reference block size; here determined as 5 pixels.
 - *Test area size (pixels)*: specifying the test area size; here determined as 10 pixels.
 - *Grid distance (metres)*: specifying the grid distance within the drawn polygon; here determined as 2m.

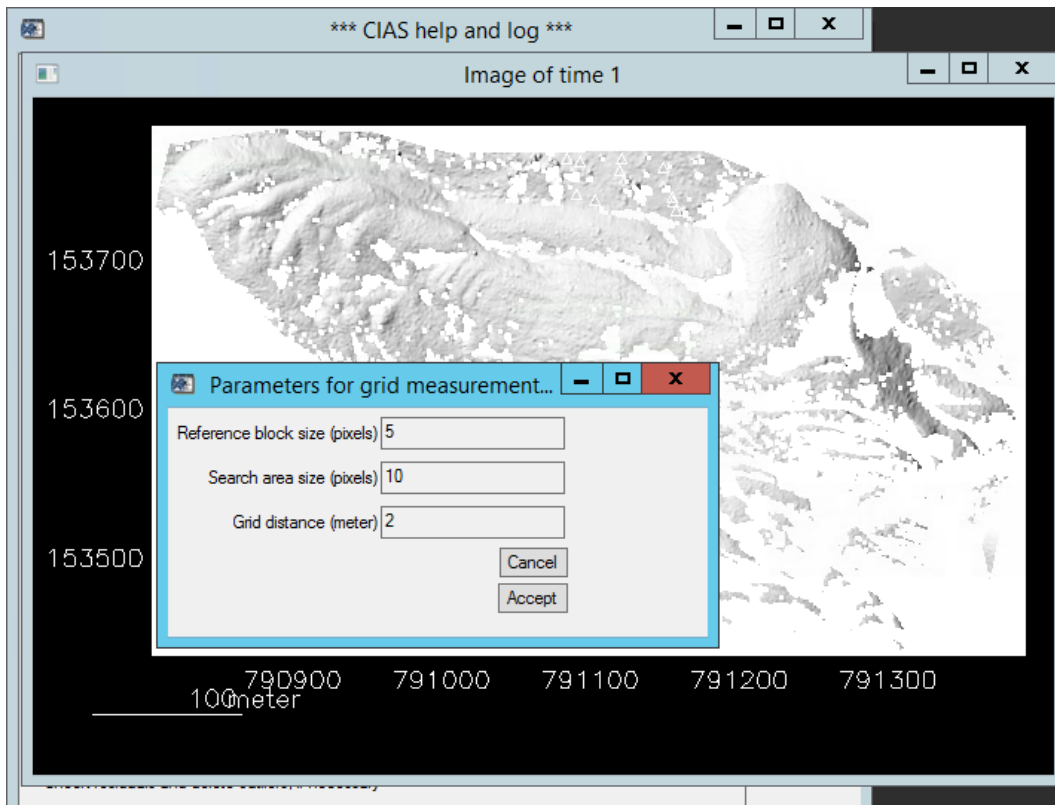


Figure A.13: Specification of parameters needed for the measurement by polygon.

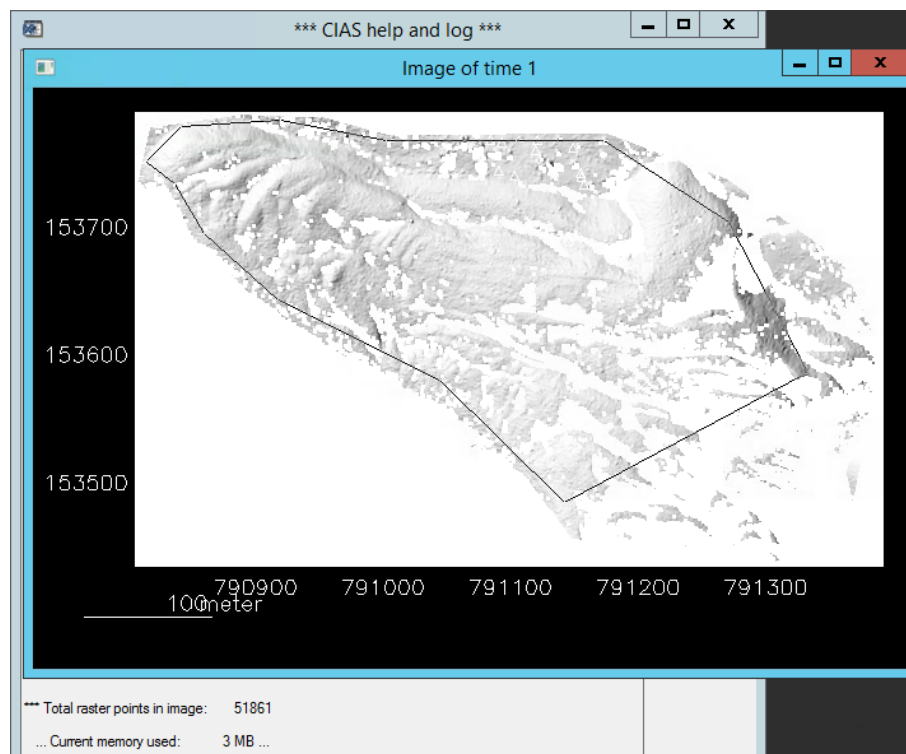


Figure A.14: Example of a digitized polygon.

- Determination of matching speed concerning the displacement measurement, similar to matching speed concerning the Helmert transformation (see figure A.15)
 - *Normal*: 1st matching iteration at full image resolution.
 - *Fast*: 1st matching iteration at 25% reduced resolution.
 - 2nd iteration in both cases to $\sim 10\%$ of a original pixel (Debella-Gilo & Käab, 2011).

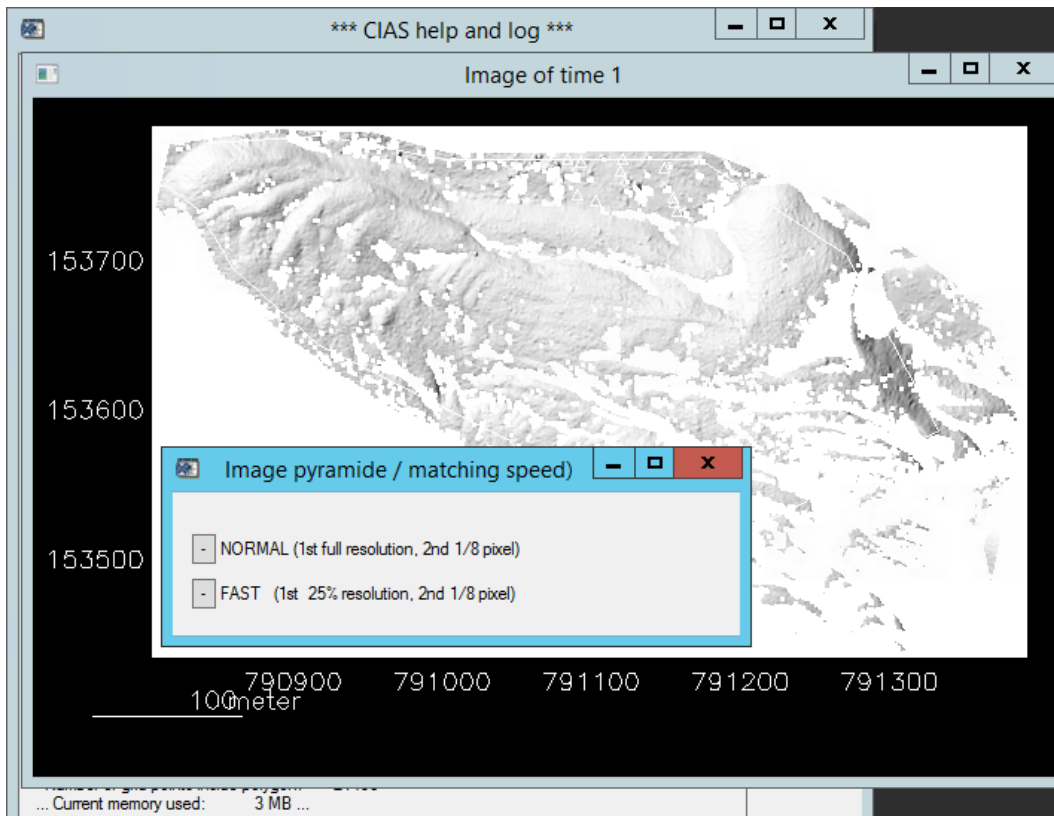


Figure A.15: Determination of matching speed concerning the displacement measurement.

- Available possibilities after the displacement measurement has ended (see figure A.16)
 - *Show result*: resulting displacements can be shown directly in CIAS Feature Tracking.
 - *Add points*: additional points can be added to the subsequent displacement measurement.
 - *Save results*: resulting output file can be saved as txt-file. It is recommended to specify the applied reference and test area sizes and algorithm used in the file name, as this information is not stored in the output file.
 - *Back*: start again at the beginning, unsaved results will be lost.

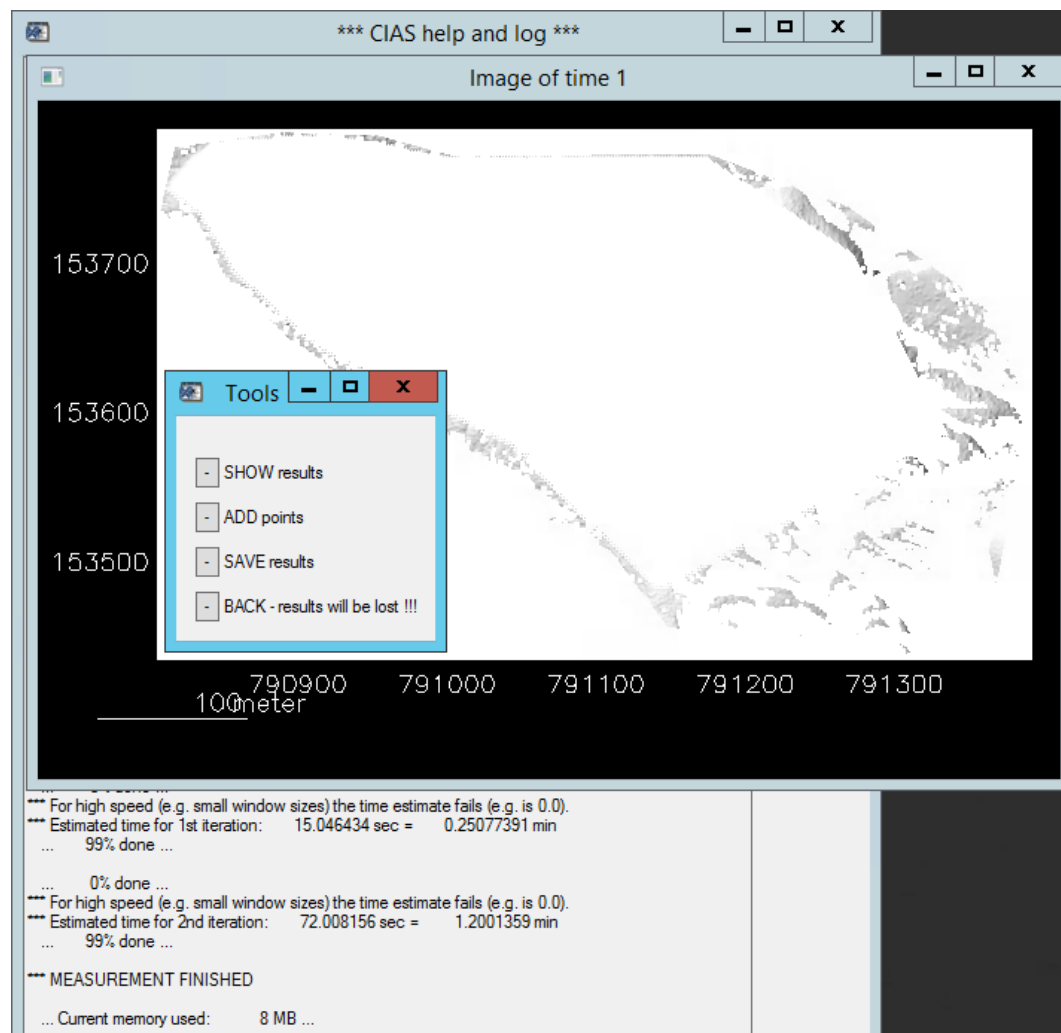


Figure A.16: Available possibilities after the displacement measurement has ended.

Personal declaration

Personal declaration: I hereby declare that the submitted thesis is the result of my own, independent work. All external sources are explicitly acknowledged in the thesis.